Università
degli Studi
di Ferrara

DOTTORATO DI RICERCA IN

" Scienze Biomediche e Biotecnologiche"

CICLO **XXXIII**

COORDINATORE

Prof. PINTON Paolo

In vitro assessment of the impact of CS on skin

Settore Scientifico Disciplinare BIO/09

Dottoranda

Dott. PRIEUX Roxane

Tutore

Prof. VALACCHI Giuseppe

Anni 2017/2020

« The pursuit of PhD is enduring daring adventure. » Lailah Gifty Akita

« It is not the strongest or the most intelligent who will survive but those who can best manage change. » Charles Darwin

« Accept challenges and adversity with the spirit of adventure and opportunity. This is an opportunity for growth and learning. » Ariann Thomas

« I am among those who think that science has great beauty. » Marie Sklodowska Curie

« Develop a passion for learning and you'll never cease to grow. » Anthony J. D'Angelo

ACKNOWLEDGMENTS

First of all, I would like to thank the whole CITYCARE team members, the Belgian team, Benedetta, Marc, Isabelle, Stuart, Agnès and the Swiss team, Irini, Barbara R. and Barbara D.

Many thanks to my dear Italian team from UNIFE, Prof. Giuseppe Valacchi, Mascia, Franco, Francesca, Anna, Erika, Alessandra and Valeria for their patience, natural communicative cheerfulness and for their inspiring enthusiasm for Science. This is only thanks to them that I could learn and practice Italian in the most pleasant way. Special thanks to my mentor Mascia for her exceptional patience, cheerfulness and spirit that kept my head up all along. Anna and Francesca, chance made us co-researchers but the good times we shared made us friends.

A big thank you to the CITYCARE project coordinator Dr. Marc Eeman without who I would not have had this PhD opportunity. I would also like to thank my academic tutor Prof. Giuseppe Valacchi for accepting me in his laboratory and giving the opportunity to become an independent researcher in Cell Biology. I am grateful to both of them for their valuable guidance and for giving the chance to share a life between two beautiful cities Bologna and Brussels. *"Home doesn't have just one address"*.

I am also grateful to have got to know and closely worked with two wonderful co-PhD researchers Irini and Benedetta and I thank them for the beautiful flowers.

I would also like very much to thank my Brussels roommates from Cohabs Marlow 933 that have been the source of many laughs even during times of stress. I believe their good spirit and goodness mainly contributed to this achievement. "*Happiness inspires Productivity*".

I am deeply grateful for the support of my family and friends that always believed in me during all along this three-year project.

I must also thank the center of electron microscopy from UNIFE for the TEM and SEM tissue processing and imaging and Dhanya Puthenmadom from the Analytical Department of Dow Silicones Belgium for her contribution in the Raman analysis and data interpretation.

Finally, this PhD project would not have been possible without the financial support from the European Union's Horizon 2020 research and innovation program under the Marie Skłodowska-Curie grant agreement No 765602.

TABLE OF CONTENT

ABSTRACT

CS (CS) stands among the most toxic environmental pollutants and is composed of thousands of chemicals including polycyclic aromatic hydrocarbons (PAHs). Despite restrict cigarette smoking bans in indoor or some outdoor locations, the risk of non-smokers being exposed to environmental CS is not yet eliminated. Besides the well-known effects of CS on the respiratory and cardiovascular systems, a growing literature has shown during the last three decades its noxious effects also on cutaneous tissues. Being the largest organ as well as the interface between the outer environment and the body, human skin acts as a natural shield that is continuously exposed to harmful exogenous agents. Thus, a prolonged and/or repetitive exposure to significant levels of toxic smoke pollutants may have detrimental effects on the cutaneous tissue by disrupting the epidermal barrier function and by exacerbating inflammatory skin disorders (i.e. psoriasis, atopic dermatitis). With the development of very complex skin tissue models and sophisticated CS exposure systems, it has become important to better understand the toxicity pathways induced by smoke pollutants in more realistic laboratory conditions to find solutions for counteracting their effects. This doctoral thesis provides first a state of art on the skin models currently available to study CS exposure, the reported deleterious effects induced by CS in the skin, as well as the inflammatory skin pathologies potentially induced and/or exacerbated by CS exposure.

This study consists of investigating and providing further insight into the mechanical pathways involved in CS-induced toxicity in a 3D *in vitro* skin models, a well-characterized reconstructed human epidermis (RHE). As a first stage of the study, the RHE model will be fully characterized and validated as the main *in vitro* biological target, secondly, it will focus on the implementation and optimization of the exposure conditions of CS. Once both the skin model and the exposure conditions have been validated, markers of oxidative stress and inflammation can be assessed to relate pathways activated by the skin epithelial cells as a defense strategy against CS exposure. With this knowledge, therapeutic solutions may be developed targeting the altered markers, hence counteracting the detrimental impact. Finally, the reconstructed skin model was used to screen protective solutions against air pollutants such as CS.

A. LITERATURE STUDY

The content in the literature study section was reprinted from two accepted review articles:

"**Prieux R**. et al, *Mimicking CS exposure to assess cutaneous toxicity*. Toxicology *in vitro* 62, 104664, Copyright (2020), with permission from Elsevier."

"Ferrara. F/**Prieux. R** et al, *Inflammasome activation in pollution-induced skin conditions*. Plastic and Reconstructive Surgery, Science of Aging, to be published with the January 2021 issue"

I. The skin barrier as a first target of the external environment

1. The Skin physiology

The human skin is a highly dynamic interface as well as the largest organ. The skin can be divided into two main layers: the epidermis, which is the upper layer mainly constituted of keratinocytes, and the underlying dermis with a fibroblast-populated collagen matrix.[1] The epidermis is the outermost layer at the direct interface between the organism and the external environment, its main functions are to provide protection, repair, and renewal.[2] It can be subdivided into 4-5 layers. From the inside to the outside, epidermal skin layers start from the viable epidermis, i.e. the stratum basale (SB), the stratum spinosum (SS), and the stratum granulosum (SG) to the non-viable layer represented by the stratum corneum (SC) (see **Figure A-I-1**). The basal layer is mainly composed of proliferating keratinocytes with keratin enriched nucleus which starts differentiating to migrate through the stratum spinosum. During their maturation, various changes in protein and lipid structure occur. Keratinocytes become connected through desmosomes and initiate the generation of lamellar bodies enriched in polar lipids such as glycosphingolipids, free sterols, phospholipids. In the stratum granulosum, keratinocytes tend to lose their nuclei releasing keratohyalin granules spread in the cytoplasm. A lipidic barrier made of non-polar lipids such as ceramides, cholesterol, and free fatty acids is subsequently formed from the discharge of lamellar bodies lipids arranged to the surface of the cells. Finally, the outermost skin layer corresponding to the stratum corneum is made of anuclear corneocytes filled with keratin filaments and water and enveloped by crosslinked protein layers which are surrounded by stacked bilayers of non-polar lipids in the extracellular space. [3,4]

The resulting multi-layered stratified epithelium is continually renewed from stem cells, with a turnover time of approximately a month.

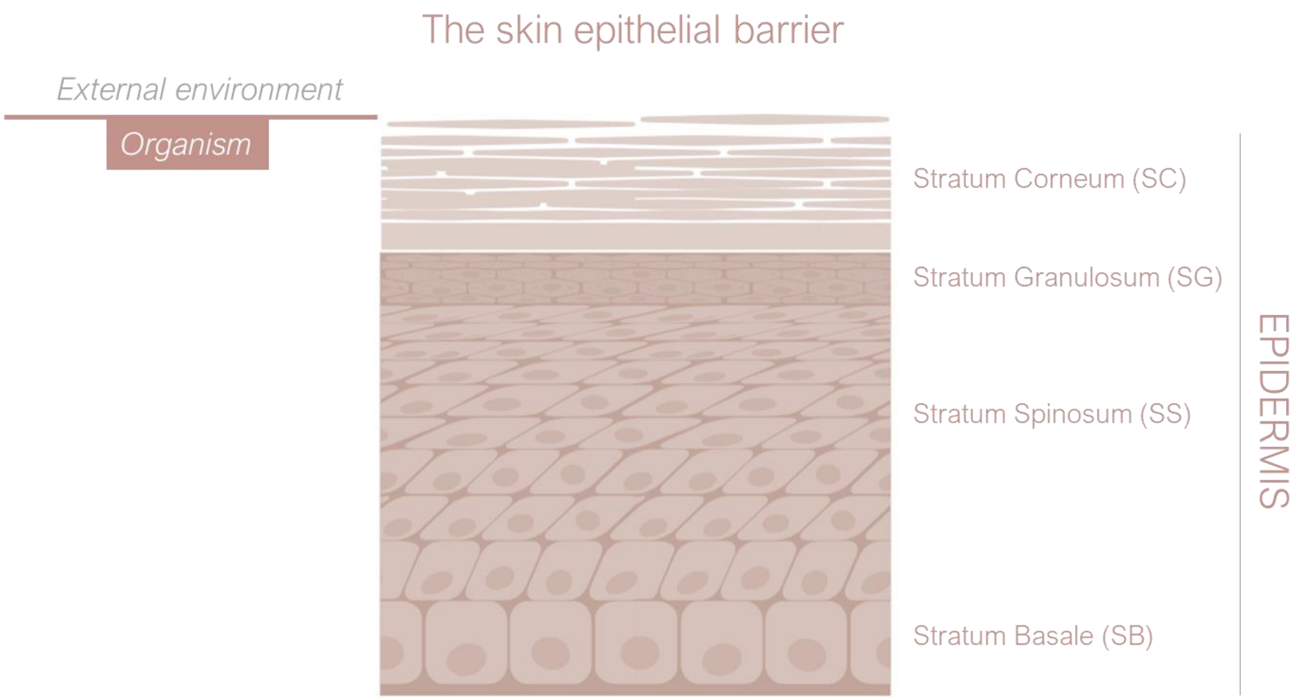

Figure A-I-1. Schematic representation of the distinct epidermal layers. From the inside to the outside, skin layers start from the viable epidermis, i.e. the stratum basale, the stratum spinosum, and the stratum granulosum to the non-viable layer represented by the stratum corneum.

2. State of the Art of skin models (*in vitro, in vivo, ex vivo*)

Various skin models have been described to assess possible hazards and risks resulting from contact or exposure to chemical compounds. Nowadays, greater effort is put into the development of *in vitro* models based on human cells to replace animal testing. Indeed, besides having a limited predictive capacity for human toxicity, they generate ethical issues. *In vitro* skin models are simple and promising tools for a wide field of applications such as cosmetology and regenerative medicine.

From the inside to the outside, skin strata start from the subcutaneous tissue, the dermis, and finally the outermost layer, the epidermis. The epidermis consists of four or five layers of keratinocytes which synthesize protective proteins such as keratin and a lipidic matrix crucial for the skin barrier function.[5,4]

2D cell models

Cell lines are more homogenous populations in comparison to primary cells and show reduced donor to donor variability. Immortalized cell lines are readily available, stable, and easy to handle whereas primary cells have some passage number limitations. Therefore cell lines appear to be appropriate as an *in vitro* cell model for the rapid assessment of acute toxicity induced by pollutants.[6]

HaCaT cells, the first spontaneously immortalized human keratinocyte line exhibiting normal differentiation, is the most used 2D skin model consisting mostly of keratinocytes.[7,8]

Their use for skin irritancy studies was found relevant for their ability to respond to injurious stimuli, however, they have dysregulated molecular mechanisms related to carcinogenesis which might compromise their use for chemoprevention studies.[9,10]

Alternative cell lines exist such as A431, a human epidermoid carcinoma cell line, and JB6, a mouse epidermal cell model. Both of them have been mainly used to study tumor promotion and progression.[11–13]

As fibroblasts are responsible for secreting substances of the extracellular matrix essential for keratinocyte growth, co-culturing keratinocytes with fibroblasts allow reproducing cellular crosstalk, especially of interest when studying wound healing mechanisms.[14,15] The main fibroblast cell line is known as the 3T3 cell line.[16]

Primary cell cultures are explanted directly from either healthy donors or subjects with pathologies and are considered more biologically relevant. Primary fibroblasts are an ideal model for studying skin aging *in vitro*. In comparison to primary keratinocytes that can only grow for about 7 passages, human primary fibroblasts can generally be grown in a culture medium for up to 40-50 passages and become especially relevant for prolonged senescent studies. However, primary cells may be damaged during isolation resulting in poor purity and yield.

Although easy, fast, and inexpensive, a major shortcoming with the 2D cell culture system is the sensitivity to pollutant exposure since it lacks the protective physiological cutaneous structure. Therefore, the use of a 3D skin model with a closer morphology to real skin combined with an exposure scenario is recommended to better understand some of the biological mechanisms linking pollution toxicity to skin structure disruptions.

3D skin models

The RHE is one of the most reliable *in vitro* models to investigate cutaneous stress responses. RHE closely mimics the morphological, biochemical, and physiological properties of the human epidermis, and can be created in laboratories or commercially purchased.[17] 3D models allow the reproduction of exposure scenarios closer to a real-life situation, for instance by topically applying components on the epidermis. The main shortcomings of RHE are the poor barrier properties, the lack of vascularization, sweat glands and hair, the lack of representation of the physiologically-relevant desquamation process, and the lack of immune system even though several efforts have been put to create immune-competent skin models with the integration of T cells.[18]

The 3D full-thickness (FT) skin model contains both dermal and epidermal parts separated by a basement membrane. A fully stratified keratinocyte-populated epidermis associated with a fibroblast-populated dermis permits intercellular signaling. Cell interactions between keratinocytes and dermal fibroblasts can affect the expression of proteins and are vital in skin homeostasis. Whereas such models are commercially available, they are less commonly used than reconstructed epidermis models, which are easier to handle, less complex, and less costly.

To obtain increased longevity of *in vitro* skin equivalents, adjustment and implementation into miniaturized conditions as found in chip technologies or into the environment of a perfused bioreactor is now feasible.[19–21]

In vivo models

The most common animal species used to date as skin models have been pigs mainly for the structural resemblance with human skin.[22,23] Nonetheless, pigs exhibit poor vascularization, a thicker skin epidermis, and an increased amount of fat components compared to humans.[24]

Furthermore, animal testing has numerous drawbacks such as strict regulation, excessive costs, high variability i.e. Local node lymph (LNA) assay as well as ethical concerns.[25] Complying with the commitment of replacing animal testing in industrial toxicology laboratories, the validation of alternative *in vitro* test methods has become a crucial need. Today, non-invasive clinical methods involving small groups of human volunteers have also been used to evaluate the biological responses induced by CS in contact with reduced skin areas. However, this controlled clinical method also generates pollution stress on 'living skin'.[26]

Ex vivo skin tissue

Ex vivo human skin is usually obtained from plastic surgeries either directly from hospitals or distributed by tissue banks. For dermal absorption studies, skin explant is the preferred model since the barrier properties are well preserved after excision with controlled conditions. However, the donor dependency of skin explants is disadvantageous as it complicates the comparison of different studies. Restricted access and excessive costs are among limitations to the use of native human skin.[27–29]

In comparison to *ex vivo* skin tissue and *in vivo* testing, *in vitro* studies offer several advantages including more flexibility, better reproducibility, investigation of cellular components, and cost-effectiveness. *In vitro* models have however some limitations. It is well demonstrated that the permeation of exogenous agents through *in vitro*-based skin models overestimate the *in vivo* data, as a consequence of a thinner stratum corneum and a less complex structure missing hair follicles, sebaceous glands, and sweat glands.[30] Culturing mammalian cells outside of their physiological environment, i.e. in an environment lacking protective and detoxifying element such as the microbiota, skin metabolism, and the immune system, is also a drawback of the *in vitro* models and makes *in vitro* cultures more sensitive and vulnerable than *in vivo* / *ex vivo* models.

In conclusion, it can be stated that there is no perfect model to study the cutaneous responses to exogenous challenges such as CS and that new insights concerning the toxicity pathways induced by CS must be obtained using different experimental approaches from 2D cell culture to 3D skin models.

3. The Skin exposome

Major skin environmental stressors

The term "exposome" was first described by American cancer epidemiologist Christopher Wild and is defined as "*the totality of exposures to which an individual is subjected from conception to death, including both external and internal factors as well as the human body's response to these factors*".[31] The skin external exposome is characterized by all environmental physical, chemical, and mechanical stressors to which the cutaneous barrier is exposed.

Viruses, bacteria, fungi, or parasites can also enter the skin via an insect bite resulting in injurious skin infections.[32] In contrast, the skin houses a vital ecosystem of microbes constantly interacting, referred to as the skin microbiota, which is fundamental to maintain skin homeostasis.[33] Physical stressors include ionizing and non-ionizing radiations. While some sources of radiation might be anthropogenic such as nuclear irradiation, infra-red (IR), and electromagnetic, some are naturally present in the environment, for instance, natural radiation from cosmic and solar rays.[34] Strong variations in temperature and humidity may seriously affect the equilibrium state of the skin.[35,36]

Among all stressors, UV rays coming from solar radiation are known to be the most detrimental to human skin.[37] The UV rays can be divided into three categories based on their range of wavelength in decreasing order of energy: UVC (100-280 nm), UVB (280-320 nm), and UVA (320-400 nm). All the UVC and a major part of the UVB are being absorbed by the ozone layer in the stratosphere, therefore the UVA represents the most predominant range reaching Earth with a varying intensity according to the daytime, season, geographic latitude, altitude as well as atmospheric aerosols.[38,39] The few UVB rays penetrating the stratosphere are called the "burning rays" due to their higher intensity, hence toxic effect on skin cells. Being less intense than UVB, UVA has been qualified as "aging rays" due to its involvement in premature skin aging.[40,41] Indeed, they can reach and induce "photoaging" through alteration of the dermis layer while UVB essentially alters the epidermis.[42] UVA are a source of reactive oxygen species (ROS) interacting directly with the skin cell components, thus indirectly induce DNA damages.[43–46] Exposure to UV increases the risk of developing many skin disorders and skin cancers such as melanoma.[37,47,48] Besides UV exposure, air pollution comes as the second most damaging skin aggressor.[49] Environmental scientists found air pollution can act as a protective shield from UV radiation penetration into the stratosphere.[50,51] Anthropogenic emissions increase the concentration of atmospheric aerosols which can scatter and absorb a part of the solar rays, hence attenuate the UV direct incidence.[52,53] Although this contribution can appear beneficial, many deleterious components are generated through UV radiation interaction with atmospheric pollutants. Primary pollutants such as PAHs can absorb photons in the UVA and visible range, subsequently generate ROS via photo-oxidation and result in cell damages.[54,55] Soeur et al. have demonstrated a synergistic effect in 2D and 3D skin models when combining a systemic exposure to PAHs and direct exposure to UVA.[56]

There are four pathways of skin penetration, including mechanical delivery, an intracellular route, a transcellular route, and a transfollicular route.[57,58] It has been suggested that toxins present on PM, such as PAHs, can enter systemic circulation through hair follicles or transepidermal absorption.[56,59,60]

Air pollution

Air pollution kills an estimated seven million people worldwide every year; 9 out of 10 people breathe air containing high levels of pollutants.[61] The adverse health effects of exposure to air pollutants have been subjected to intense research in the last few decades.[62,63] Beyond the strong correlation to cardiovascular and respiratory diseases, exposure to air pollutants is also involved in the development/exacerbation of numerous skin disorders.[63,64] Air pollution consists of chemical, physical, or biological agents that can cause harmful effects on humans, animals, and plants.[65] Air pollutants originate from indoor and outdoor sources in developing and developed countries, making air pollution a worldwide concern.[66] The Environmental Protection Agency (EPA) has defined national ambient air quality standards for six common air pollutants or "criteria air pollutants," which include ground-level ozone (O_3), particulate matter (PM), carbon monoxide (CO), sulfur dioxide (SO_2) and nitrogen dioxide (NO_2).[67] Interaction between air pollutants and sunlight can result in the formation of pro-oxidants, including O_3.[68,54] The major source of anthropogenic emissions of oxide gases and PM is the combustion of fossil fuels from stationary sources and motor vehicles.[68,69] PM is a mixture of liquid, solid, or liquid and solid particles suspended in the air that is composed of organic, such as PAHs, and inorganic components, including transition metals. Based on diameter, PM can be divided into three categories: PM10 (less than 10 μm), PM2.5 (less than 2.5 μm), and UFPs (less than 100 nm).[70,71] Environmental tobacco smoke (ETS) is a complex mixture of thousands of chemicals coming from the burning of a cigarette and smoke exhaled from smokers; therefore, it represents a major contaminant of indoor air.[72]

4. Skin defense mechanisms against air pollution

Skin redox response in inflammation

Being the primary interface between our body and the external environment, the skin's most critical role is to provide a strong physiological barrier. Pollutant exposure results in the induction of an oxidative stress/inflammatory status in cutaneous tissues, which is exacerbated when pollutants act synergistically.[73–75] However, the mechanism of action of single pollutants varies. For instance, O_3 does not penetrate the skin; it instantaneously interacts with lipids in the upper layers of the epithelium, generating a cascade of ozonation products that drive the production of ROS and aldehydes, such as 4-hydroxy-2-nonenal (4-HNE).[76–80] Other pollutants, such as PM and CS, also alter skin redox homeostasis by inducing lipid peroxidation, albeit in different manners. For instance, particles have been suggested to eventually penetrate the skin, triggering ROS production and lipid peroxidation, although this idea is controversial.[81–84] Transition metals in PM can undergo Fenton or Fenton-like chemistry, resulting in the production of the hydroxyl radical[85]. Furthermore, PAHs can be converted into redox-active quinones that stimulate ROS production in keratinocytes.[85] Moreover, water-soluble PAHs of CS increase NAPDH oxidase activity within the skin, inducing oxidative stress.[85,86] Therefore, the effects of these various stressors all result in increased ROS, which are key mediators of cellular signaling pathways, inducing activation of redox-sensitive factors, such as proinflammatory nuclear factor kappa-light-chain-enhancer of activated B cells (NF-κB), activator protein-1 (AP-1), Nuclear factor (erythroid-derived 2)-like 2 (Nrf2), and heat shock proteins (HSPs). Moreover, 4-HNE, a product of lipid peroxidation, can interact with DNA and proteins, forming adducts which damage DNA and alter protein conformations.[87,88,97,98,89–96]

In the skin, pollutant exposure results in inflammation, cellular apoptosis, and DNA and mitochondrial damage.[81–83] Increased oxidative stress in the skin also stimulates activation of matrix metalloproteinases (MMPs), which breakdown collagen and elastin, contributing to skin aging.[99] Indeed, the involvement of pollutant exposure in skin aging is believed to be due to pollutant-induced activation of the aryl hydrocarbon receptor (AhR), promoting skin inflammaging.[100–106] Thus, it is no surprise that both inflammation and oxidative stress are displayed in several skin conditions [108–110], and cross-talk between these two conditions results in skin inflammaging.[107–114]

Skin as an immune sensor

The skin is not only a physical barrier against exogenous substances, it also acts as an immune sensor upon pathogen agent exposure. The skin can trigger innate and adaptive immune responses. Keratinocytes are the first line of defense; hence they can create immune signaling in response to external threats. These signals include the secretion of cytokines, chemokines, and antimicrobial peptides, which subsequently initiate a local inflammation in the skin. As they cover most of the epidermal surface, skin keratinocytes express a wide variety of danger sensors, including Toll-like receptors (TLR) and NOD-like receptors (NLR). Inflammasomes are cytosolic multiprotein oligomer complexes of the innate immune system that become activated as a consequence of exposure to harmful stimuli (infectious pathogens, irritants, dead cells) and modulate immune responses in various tissues.[115,116]

The most well-characterized inflammasomes belong to the Nod-like receptor (NLR) and Aim2-like receptors (ALR) families, such as NLRP1, NLRP3, NLRC4, and AIM2, which are mainly present in immune cells, although they are also found in keratinocytes.[117–119] These receptors all display a similar mechanism of activation and are induced by a variety of stimuli including Lipopolysaccharide (LPS), Adenosine triphosphate (ATP), cytosolic DNA, ROS, pathogens, etc.[120]

NLRP1 has been reported to be strongly expressed in keratinocytes and represents a crucial skin immune sensor.[121–123] Genetic mutations in NLRP1 were associated with hyperplasia and skin autoimmune disease like vitiligo accompanied with high levels of IL-1b, IL-18 detected in the serum of patients.[121,124,125]

Several studies have also demonstrated that pollutants can induce inflammasome activation. For instance, several cardio-pulmonary diseases are associated with NLRP3 inflammasome modulation by PM, CS, and O_3.[126,127,136,128–135] However, although skin is constantly exposed to environmental stressors, very few studies have demonstrated whether pollutant exposure triggers inflammasome activation in the skin. Thus, only the role of ultraviolet (UV) light has been appreciated; activation of NLRP1, NLRP3, AIM2, and NLRC4 inflammasomes can be induced by UVB exposure in human keratinocytes.[137–141] A recent study also demonstrated that the NLRP1 inflammasome can be activated by O_3 exposure in different human skin models via redox regulation.[142] Thus, environmental stressors may promote the development/exacerbation of skin conditions by inducing inflammasome activation and opening a new area of research in preventing stressor-induced skin damage and inflammation. **Figure A-I-2** summarizes all the inflammasome that are activated by specific pollutants.

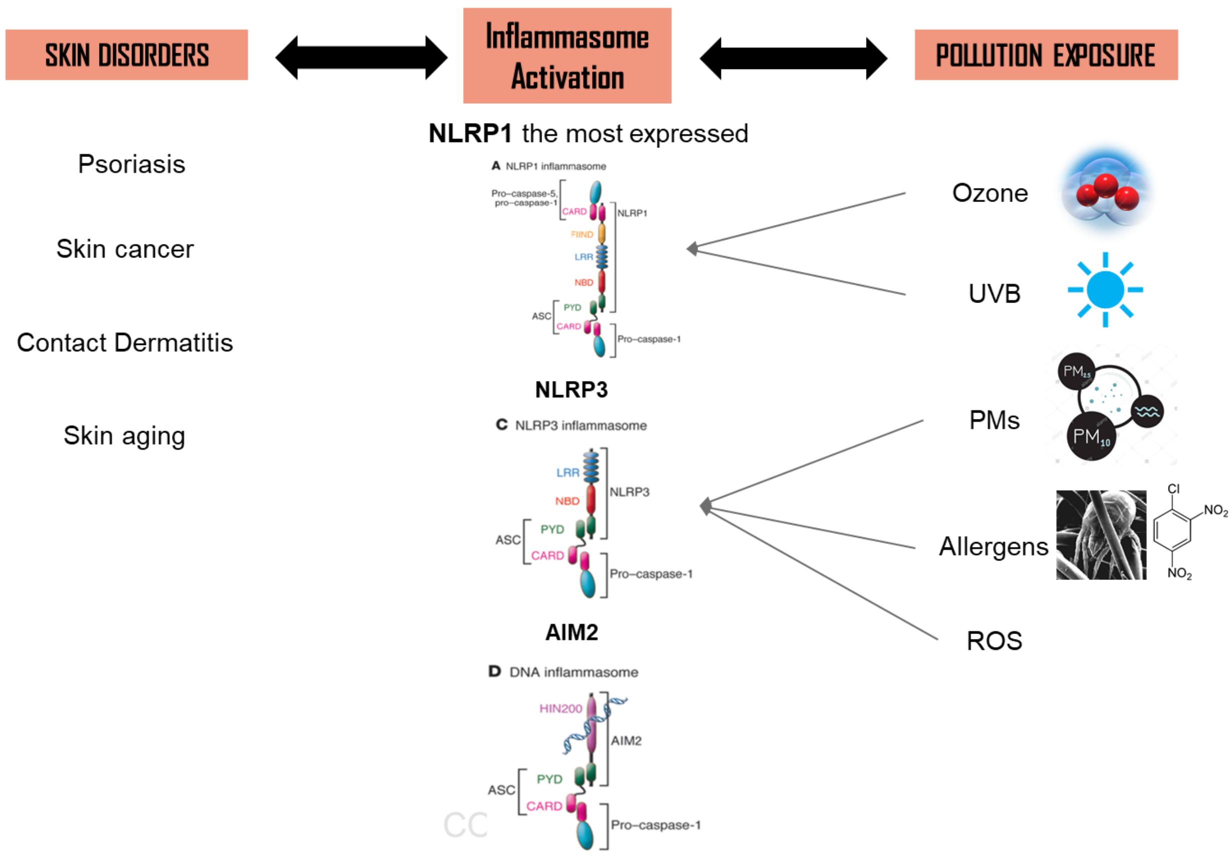

Figure A-I-2. Scheme of the known inflammasome expressed in the skin that is induced by certain pollutants and linked to skin disorders.

5. Air pollution-related skin disorders

Exposure of skin to air pollutants alters the functions of epidermal proteins and damages lipids and DNA, leading to a range of skin disorders.[143] The most prevalent skin disease associated with failure of the skin barrier is atopic dermatitis (AD); defects in barrier function can lead to increased vulnerability to air pollutants.[144] A large range of environmental stressors are involved in the development or aggravation of AD, such as ETS, volatile organic compounds (VOCs), nitrogen dioxide, and PM.[145–149] There is clear evidence that individuals living in urban areas with higher exposure to vehicle exhaust are more likely to develop AD.[150–153] Furthermore, childhood exposure to ETS is a major risk factor for AD.[154] Also, O_3 exposure has been correlated with urticaria, AD, and contact dermatitis.[155]

Skin exposure to environmental stressors is also associated with the development/exacerbation of psoriasis, aging, cancer, and acne. For instance, tobacco smoke is an independent risk factor for psoriasis development.[156,157] PM is one of the main pollutants that contribute to extrinsic skin aging, based on cohort studies using the SCINEXA aging score.[158] Characteristics of aging, such as wrinkles and pigmented spots, are more frequently observed in subjects living in urban areas.[159] Premature skin aging is also observed in smokers, independently of age, sex, and sun exposure, which is known as “smoker’s face”.[160,161] Additionally, PM contains PAHs, which are involved in the development of skin cancer.[70,162–164] Other studies have demonstrated a link between acne vulgaris and air pollution.[165,166] Exposure to PAHs can lead to acneiform eruptions and chloracne.[167] Some studies have also shown a correlation between acne severity and the number of smoked cigarettes.[168,169] In addition, CS has been associated with androgenetic alopecia (AGA).[170] In conclusion, exposure to environmental stressors contributes to the development/exacerbation of inflammatory skin diseases and premature aging.

Some individuals may present a compromised skin barrier, due to intrinsic factors, including aging[186] or genetic predispositions, or due to extrinsic factors, such as repeated exposure to external insults, leading to chronic diseases.[171–176] Impaired barrier function results in an increased risk of absorption and penetration of air pollutants. Therefore, individuals with altered barrier function are particularly sensitive to pollution-induced skin disorders.[177]

II. Impact of CS on skin

1. Mimicking CS exposure *in vitro* to assess cutaneous toxicity

Among the main sources of environmental pollutants, CS is of important concern for its deleterious effects on health, being considered as the world's leading preventable cause of death.[178–181] Despite policy-based interventions such as tax increases on tobacco, health care prevention campaigns, enforcing bans on advertising, cigarette consumption is still increasing in many countries and the epidemic is shifting towards the developing world.[182,183] As a presented alternative to the traditional cigarette, recently developed vaporizers have helped to remove the risks coming from combustion derived components. However, they have not been reported as harmless since their liquid composition includes a large variety of chemicals directly in contact with epithelial barriers and for which long term effects are currently under investigation.[184–186]

The Chemistry behind CS

The CS aerosol is produced by incomplete combustion when burning a cigarette and can be divided into two phases: a particulate and a gas phase (see **Figure A-II-1**). The particulate phase is the minor fraction and constitutes 4-9% of the total smoke by weight whereas the gas phase is the major fraction with 91-96%.[187] The most harmful CS components are products of combustion contained in the gas phase, hence the importance of performing any assessment using both the particulate and gas-phase to better simulate real-life exposure. In addition, combining both CS phases takes into consideration the potential interactions that could occur between components from the gas and particulate phase. Gas-phase chemicals include small and reactive aldehydes (formaldehyde, acrolein), reactive oxygen species (H_2O_2, O_2, $OH^{\cdot}$), reactive nitrogen species (RNS), and hydrogen cyanide whereas the particulate phase includes PAHs and tobacco-specific nitrosamines (TSNAs).

CS is associated with pulmonary and cardiovascular diseases. Many shreds of evidence have also shown detrimental effects of CS on the skin.[178–181,188] More specifically, the oxidative compounds derived from incomplete combustion of the cigarette can affect the cutaneous tissue.[189] Inhaled sidestream CS is approximately four times more toxic per gram of total PM than mainstream CS.[190]

Cigarette smoking has been linked to various dermatological conditions and pathologies: poor wound healing, squamous cell carcinoma, melanoma, acne, psoriasis, eczema, and hair loss.[191] Moreover, an epidemiologic study has shown that CS is one of the numerous factors contributing to premature skin aging, independent of age, sex, pigmentation, sun exposure history, alcohol consumption, and other factors.[192] A study on twin pairs has demonstrated the obvious relationship between cigarette smoking and premature skin aging[208] and a British doctor, Douglas Model, defined the term “smoker’s face” in 1985 to describe the wrinkling and premature aging associated with smoking.[193,194] Besides affecting cellular redox homeostasis, CS components can provoke inflammatory skin responses. Numerous chemicals, especially PAHs, can penetrate the epidermal barrier and enter the systemic circulation through the capillaries in the dermis causing systemic effects.[56] Indeed, many skin disorders are related to a chronic inflammation response, for instance in both atopic dermatitis and psoriasis, where the immune activation by the release of cytokines influences keratinocyte proliferation and differentiation.[195]

The use of an appropriate CS exposure system has become fundamental to study and identify the CS-induced cutaneous toxicity pathways as realistic as possible.

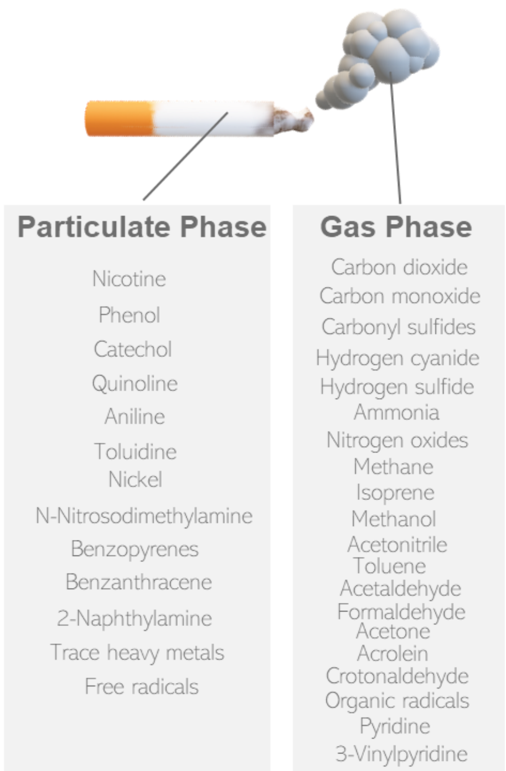

Figure A-II-1. Main characterized particulate and gas-phase components originating from CS.[183]

CS exposure from life to bench

In the field of CS toxicity testing, many studies have developed relevant and appropriate CS exposure methods trying to mimic real-life conditions (see **Figure A-II-2**). However, the lack of important information such as types of cigarette, exposure time, smoking machine characteristics, etc. makes it difficult to compare among different studies.

Cigarette type

Whereas some researchers have used commercial cigarettes for their studies, the typical cigarettes used for experimental purposes are "reference 3R4F cigarettes" which have a standardized composition.[196–198] The cutaneous toxicity of those cigarettes is usually evaluated by exposing a skin model to the smoke of a cigarette either extracted into a culture medium or delivered into an exposure chamber.

Cigarette smoke extract (CSE)

CSE is collected via a trapping system and is then usually dissolved in a cell culture medium or buffer. Typically, CSE is prepared at a concentration of 1 cigarette/25mL in a serum-free cell culture medium.[199–201] The resulting solution which is always at saturation is defined as the highest concentration (100% CSE) and is then diluted to various concentrations. CSE is used after adjusting the dispersion to pH 7.4 using sodium bicarbonate and filtering through a 0.22 µm filter.[201,202] Depending on the solvent used, CSE composition can vary. It can be either aqueous using PBS or organic using hexane.[203] The generation of CSE in aqueous solutions is mainly performed for the larger number of CS water-soluble components from both the particulate and gas phase, representing approximately 90 weight % of CS. An organic solvent is mainly used to collect a large amount of PAHs which are slightly soluble in water.[204] In the case of internal organs exposure, it is more relevant to use CSE since CS likely interacts and solubilizes into biological fluids during inhalation to further interact with the cells from the trachea and bronchial tubes. CSE is more relevant for lung exposure studies as it can mimic the interaction of components inhaled by smokers The main weakness of CSE relies on its composition as it mainly contains the particulate phase and excludes the volatile compounds such as aldehydes (acrolein and acetaldehyde) that are major contributors of CS-induced toxicity.[205] Also, CSE solution should be prepared immediately before being applied to avoid any aging effect of the extract. Fresh CSE is very different from aged CSE due to the presence of short-lived reactive species that are no longer present in old CSE.[206–208] The CS extract has been used to study the effects of CS on skin pathology *in vivo* and *in vitro*. For instance, in fibroblasts, approximately 20% of the cells survived in 100% CSE, and at 10% CSE, approximately 80% of the cells survived.[199] Chronic effects of CS on the skin can be simulated by dosing CSE concentrations, for instance using a low concentration for 20 days to minimize toxicity.[209]

Cigarette smoke chamber (CSC)

CS can be simply generated using small devices such as a vacuum pump or an electrical fan. However, to achieve better repeatability and reproducibility in terms of smoke composition and volume, it is recommended to use specific smoking machines that generate smoke at a standardized rate. Those smoking machines are often connected to an exposure chamber where small fans provide a homogeneous distribution of the smoke over the skin models under investigation. Several smoking machines with different settings and designs are commercially available.[210–213]

The use of smoking machines allows exposing the model of interest to the so-called ETS which includes on the one hand both the mainstream and second-hand smoke, and on the other hand both the particulate and gas phase. Furthermore, it is possible to filter the particulate phase at the opening of the exposure chamber to expose the skin models to the gas phase only. By providing a better quantification of the exposure dose (time, airflow, ratio aerosol/air, puff number, the yield of delivered smoke), these smoking systems will be particularly useful for cross-platform comparisons.

To conclude, these well-developed exposure chamber systems address the need for a standardized and reproducible method for skin exposure to CS. **Tables A-II-1 and A-II-2** summarize the skin models used over time to assess the adverse effects of CS exposure on the skin using the two main routes of exposure set up in laboratories: CSE (**Table A-II-1**) and CSC (**Table A-II-2**).

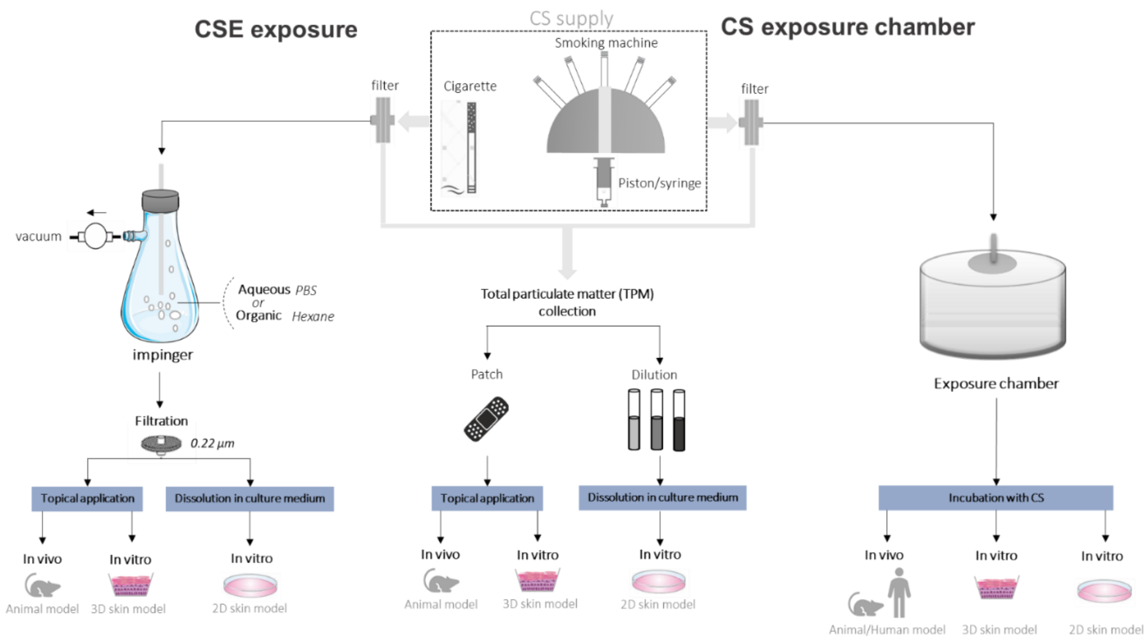

Figure A-II-2. Overview of predominant CS routes of exposure: CSE and CSC.

E-cigarettes

Electronic cigarettes have become extremely popular in a short period, being presented as a safe alternative to cigarettes. While the toxins from CS are caused primarily by burning the tar, e-cigarettes generally contain cartridges filled with nicotine and other chemicals turning into a vapor or steam that is inhaled by the smoker. Although more research needs to be done to truly determine the effect of e-cigarettes on individual health, there seems to be some evidence that points to its harmful effects on health.[186,214] A recent case in the U.S has accounted for the fifth patient who died of lung dysfunction after significant e-cigarette consumption.[215] In fact, e-cigarettes contain harmful substances as well, including propylene glycol, glycerol, a variety of flavoring substances, and a similar dose of nicotine to cigarettes known to delay wound healing and accelerate skin aging.[184,216] A review of studies found that levels of toxins and metals in e-cigarette aerosol varied considerably within and between brands.[217] In addition, previous work has demonstrated that the flavoring substances from e-cigarettes were the most toxic in embryonal and adult cells and epithelial cells such as HaCaT cells.[218–220] Studies have also shown that the only mechanical action of puckering your lips causes deep lines and wrinkles around the mouth.[221]

Despite several studies introducing electronic cigarettes as a safer alternative to cigarettes because of their lack of tobacco, tar, and combustion, they have still not proven to be safe and have not been approved by Food and Drug Administration (FDA) as a cessation aid.[222,223] Since vaporizers are a new technology, the long-term effects are still unknown.

Skin models used to assess CS-induced toxicity

To assess CS toxicity, toxicologists have relied mainly on animal testing. Nonetheless, besides having a limited predictive capacity for human toxicity, they generate ethical issues.

Data from *in vivo* human studies have been limited by the small number of subjects, however, *ex-vivo* approaches have gained importance and allowed researchers to compare the biopsies of smokers and non-smokers. As already mentioned previously, biopsies cannot be easily accessible to all researchers, therefore the design of *in vitro* skin models appears justified. Therefore, creating human exposure data became now a requirement in the process of risk and hazard assessment. Several efforts were made to develop alternative test methods based on *in vitro* technologies or *in silico* models.[224] As a starting point, *in vitro* studies certainly help to identify possible mechanical pathways involved in the CS-induced toxicity or CS-induced human disease. Nonetheless, cell studies might have the risk to overestimate the real impact of CS due to the lack of physiological barriers that render them more vulnerable or the harsh CS exposure conditions used experimentally. Furthermore, to assess the effect of CS, numerous *in vitro* studies on cells use CSE or individual CS components like Acrolein, whereas human skin cells are exposed to the whole CS. The dynamics and interactions between the different CS components might lead to a more complex biological response than those observed from single component exposure. Despite their constraints, *in vitro* studies provide valuable insight and knowledge in the investigation of the impact of CS on the skin. However, a correlation between the *in vitro* and *in vivo* human studies in smokers must exist to be clinically approved to further proceed in the treatment of CS-induced diseases. In conclusion, each given skin model has limitations and strengths. However if cautiously interpreted and correlated, every data may offer useful information towards understanding and progress.

Table A-II-1. Types of skin models exposed to CSE to investigate the cutaneous toxicity induced by CS.

Model type	*Model description*	*References*
In vitro **(2D cell model)**	Human keratinocyte cell line (HaCaT)	[225,226]
	Murine keratinocyte cell line (PAM212)	[227]
	Normal human epidermal keratinocytes (NHEK)	[209]
	Normal human dermal fibroblasts (NHDF)	[199,203,228,229]
	Normal human gingival fibroblasts (NHGF)	[205]
	Normal human epidermal melanocytes (NHEM)	[230]
In vitro **(3D cell model)**	Reconstituted human epidermis model derived from primary keratinocytes (StratiCELL RHE/001 model)	[231]
In vivo	Mice (SENCAR)	[232]
	Chicken	[233]
Ex vivo	Rat	[234]

Table A-II-2. Types of skin models exposed to CSC to investigate the cutaneous toxicity induced by CS.

Model type	*Model description*	*References*
***In vitro* (2D cell model)**	Human keratinocyte cell line (HaCaT)	220,235–238
	Normal human dermal fibroblasts (NHDF)	239
	Coculture of HaCaT cell line and human fibroblast cell line (HFF-1)	240
	Coculture of HaCaT cell line and human sebocytes cell line (SZ95)	200
***In vitro* (3D cell model)**	Reconstituted human epidermis (RHE) model derived from primary keratinocytes (SkinEthic™ model)	196
	Reconstituted human epidermis (RHE) model derived from primary keratinocytes (EpiDerm™ model)	241
	Full-thickness (FT) skin model derived from NIKS cells seeded onto dermal equivalents comprised of normal human dermal fibroblasts embedded in type I collagen (StrataTest® model)	242
In vivo	Mice (C57BL/6)	243,244
	Mice (SKH1)	245
	Rats	246
Ex vivo	Human full-thickness skin	239

2. Reported effects of CS in skin

CS induces an inflammatory response in the skin

CS exposure is known to increase pro-inflammatory mediators and oxidative stress markers in many organs such as the lung, cardiovascular, intestine, and skin. Skin is one of the most direct targets of CS exposure and many studies have shown the ability of CS to affect skin homeostasis. Oxidants contained in CS induce adverse effects on the cutaneous tissue through oxidative modifications of key biological structures as well as inflammatory responses.

Inflammation is a tissue response to damage that involves a sequence of activated cells able to secrete inflammatory mediators like cytokines and chemokines.[247] Overproduction of pro-inflammatory cytokines such as interleukins IL-1α, IL-6, and IL-18 have been widely used as inflammatory biomarkers for assessing the adverse effects of CS in skin models.[196,220,240,245,248]

IL-1α is one of the key cytokines playing a pivotal role in the development of an acute and chronic response by initiating a cascade of signaling molecules that subsequently induces the gene expression and production of secondary mediators.[249,250] Among the primary cytokines, IL-1α is predominantly produced by skin keratinocytes and its overexpression is associated with the progression and exacerbation of various inflammatory skin diseases such as psoriasis, atopic dermatitis, and skin cancer.[251,252] Since IL-1α production in keratinocytes is increased upon exposure to environmental aggressors such as UV-B irradiation, it represents a valuable marker to investigate the molecular mechanisms involved in the CS-induced cutaneous inflammatory response and its potential link with the progression of inflammatory skin disease.[249,253] Nowadays, *in vitro* extracellular IL-1α release from RHEs is one of the common markers used to assess the potency of irritation of skin sensitizers. It represents a useful endpoint to predict *in vivo* skin sensitization data.[254–256]

Tumor necrosis factor-α (TNF-α) is another cell-signaling cytokine often found in studies investigating the noxious effects of CS. TNF-α is involved in disease pathologies such as psoriasis, contact dermatitis, drug eruptions, and cutaneous T-cell lymphoma.[257–259] TNF-α regulates gene expression in response to environmental damage and induces inflammation both locally and systemically. A low level of TNF-α is present in the upper layer of the healthy epidermis, but its synthesis and release from keratinocytes are significantly increased after exposure to CS as shown in several studies performed with HaCaT cell lines[216,235] and mice skin tissues.[201,220,260,261] Thus, low levels of TNF-α are essential to perform key homeostatic functions but an overproduction of TNF-α and other pro-inflammatory markers weakens the host defense against pollution and contributes to the development of inflammatory skin diseases.

IL-8 represents one of the major cytokines involved in an inflammatory response. This chemokine mediates the recruitment and activation of neutrophils via signaling mechanisms and extracellular adhesion molecules.[262] The pathogenetic role of IL-8 has been suggested in inflammation-related skin diseases such as psoriasis, palmoplantar pustulosis, and acne where *Propionibacterium acnes* induces its production in various cell types including primary keratinocytes.[263–266] The secretion of IL-8 is stimulated when the skin is exposed to environmental stressors such as CS as shown by several studies on primary keratinocytes and reconstructed human epidermis.[196,267] **Table A-II-3** gives an overview of the inflammatory biomarkers used to assess the cutaneous responses to CS exposure *in vitro* and *in vivo*.

Table A-II-3: Review of inflammatory biomarkers reported in studies assessing the cutaneous toxicity induced by CS.

Model type	***Cell type***	***Exposure condition***	***Biomarkers***	***Main observations***	***Reference (Year)***
In vitro **(2D cell model)**	HaCaT	CSE	EGR-1, MAPKs, TNF-α, p-ERK1/2, p38 kinase, p-JNK1/2	Increase of EGR-1 protein and TNF-α in a dose-dependent manner Increase of p-ERK1⁄2, p-JNK1⁄2, and p38 kinase in a time-dependent manner	[201] (2010)
		CSC	NF-κB-aldehydes adducts formation	A drastic increase in Acrolein (ACR) Increase of 4-HNE-p65 and ACR-p65 adducts	[236] (2010)
			Various cytokines	Increased release of IL-1α, IL-6, IL-10, G-CSF, IFN-c, RANTES, TNF-α, and VEGF	[220] (2014)
			IL-1α, IL-8	Increased release of IL-1α and IL-8	[240] (2017)
	PAM212	CSE	NF-κB, TSLP, p-IKβ-α, IKβ-α, p-AMPK, p-ERK1/2	Suppression of NF-κB activation through the α7 nAChR–PI3K–AMPK signaling pathway. Decreased release of TSLP	[227] (2016)
	NHDF	CSE	TβR-II, p-ERK1/2, EGR-1	Decreased expression of TβR-II mRNA Increase of p-ERK1⁄2 in a time-dependent manner Increase of EGR-1 in time- and dose-dependent manners	[229] (2010)
			EGR-1	Increase of EGR-1 in a time-dependent manner	[199] (2011)
	NHEM	CSE	AhR, MITF, β-catenin	Increased activation of AhR	[230] (2013)

				Increased expression of MITF and β-catenin in a dose-dependent manner	
In vitro **(3D cell model)**	RHE	CSC	IL-1α, IL-8, IL-18	Increased release of IL-1a, IL-8, and IL-18	[196] (2016)
In vivo	SKH1 mice	CSC	IL-6 and IL-8 p-ERK1/2, p22phox, p47phox, p66Shc	Increase of IL-6 and IL-8, p-ERK1/2, p22phox, p47phox, and p66Shc	[245] (2012)
	C57BL/6	CSC	MPO TNF-α, IL-1β, IL-6, NF-κB p65 subunit	Increased activity of MPO Increased release of TNF-α, IL-1β, IL-6 Increased expression of NF-κB p65 subunit	[261] (2016)

CS alters skin redox homeostasis

Skin redox balance is an equilibrium between the generation and the scavenging of ROS. ROS can derive from exogenous sources such as CS as well as from endogenous sources such as NADPH oxidase, xanthine oxidase, and myeloperoxidase (MPO). Failure to maintain the physiological redox steady state is defined as oxidative stress and has been linked to premature skin aging, chronic inflammation, and skin diseases.[46,268,269]

As demonstrated in many studies, upon exposure to CS oxidant species an increase of intracellular ROS and protein carbonyls levels has been observed in cutaneous tissues, *in vitro,* and *in vivo*.[197,202,241,242,245] This leads to the generation of reactive electrophilic molecules, such as reactive aldehydes (e.g. 4-HNE and malondialdehyde (MDA) that can induce irreversible damage, as displayed in **Figure A-II-3**.[196,200,234,245,261,270,271] CS has been shown to promote 4-HNE production in many cell types by increasing ROS levels in many cell types.[272] Previous studies have demonstrated that skin exposure to CS and PM induces the production of 4-HNE in several 2D and 3D commercialized skin models.[272–275]

Due to the close interaction between lipids and proteins in tissues, these lipid peroxidation products can cause protein-adduct formation and crosslinking, progressively leading to impaired protein function and ultimately to cell dysfunction, inflammatory response, and apoptosis.[276] An increase in lipid peroxidation correlates as well with a diminution of the skin antioxidant capacity as both antioxidant compounds (e.g. vitamin C, vitamin E, uric acid, and glutathione aka GSH) and enzymes, e.g. superoxide dismutase (SOD), glutathione peroxidase (GPX), and catalase (CAT) are depleted or inactivated after exposure to environmental stressors such as CS.[197,202,209] Cytoprotective enzyme heme oxygenase (HO-1), which plays an important role in cellular protection and oxidative stress reduction, is rapidly upregulated in response to CS in skin and lung models.[245,277] **Table A-II-4** lists all the predominant biomarkers of oxidative stress studied to assess CS toxicity *in vitro* and *in vivo*.

Table A-II-4: Review of oxidative stress biomarkers reported in studies assessing the cutaneous toxicity induced by CS

Model type	*Cell type*	*Exposure condition*	*Biomarkers*	*Main observations*	*Reference (Year)*
In vitro **(2D cell model)**	HaCaT	CSC	GSH, ROS, protein carbonyls	Increase of protein carbonyls in a dose-dependent manner Increased levels of GSH and ROS	[197] (2014)
	HaCaT + SZ95	CSC	4-HNE	Increased levels of 4-HNE/SRB1 adducts	[200] (2017)
	NHDF	CSE	GPX, SOD, ROS	Decrease of GPX and SOD activity Increased levels of ROS	[202] (2013)
	NHEK	CSE	SOD	Decrease of SOD activity	[209] (2016)
In vitro **(3D cell model)**	RHE	CSC	4-HNE	Increased levels of 4-HNE	[196] (2016)
			Protein carbonyls	Increased levels of protein carbonyls	[241] (2017)
	FT	CSC	ROS	Increased levels of intracellular ROS	[242] (2010)
In vivo	SKH1 mice	CSC	4-HNE, HO-1 Protein carbonyls	Increased levels of 4-HNE, HO-1, and protein carbonyls, more importantly in young (vs. old) mice	[245] (2012)

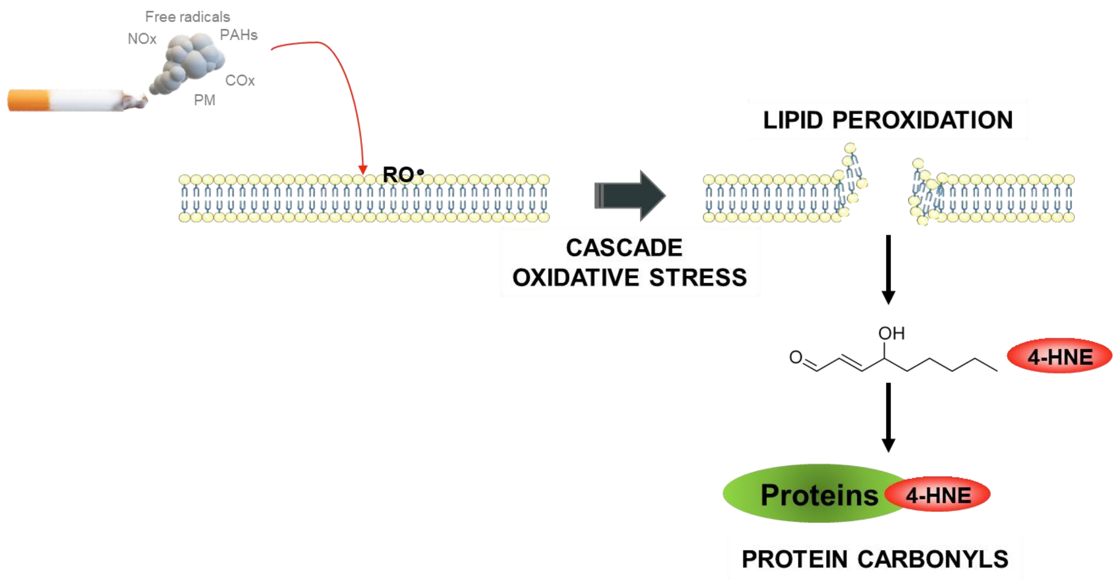

Figure A-II-3. CS components inducing a free radical cascade reaction with the cell lipids leading to excessive oxidative stress that may lead to deleterious lipid peroxidation and protein carbonylation.

Cross talk inflammation and oxidative stress in skin

Exogenous factors like CS can affect cutaneous homeostasis by inducing a pro-inflammatory status and modifying tissue redox homeostasis.[268,278] Failure to control oxidative stress can stimulate the skin to possibly develop inflammatory-related skin conditions.[247] CS exposure activates a series of transcription factors, such as AhR, NF-κB, and AP-1 that, in turn, can induce a combination of inflammatory mediators and contribute to immune dysfunction and an altered cytokine profile.

The AhR is a cytosolic ligand-activated transcription factor found in various types of skin cells and widely expressed in the skin response to external environmental signals.[279–281] It plays a crucial role in skin detoxification and inflammation regulation but is also involved in epidermal differentiation and attachment.[282,283] After exposure to CS, an inflammatory cascade of cytokines and chemokines has been observed following AhR activation *in vitro* and *in vivo*.[225,261] Xenobiotic molecules such as PAHs, contained in CS, transdermally permeate the skin and form a complex with AhR.[284] Activation of AhR results in its translocation from the cytosol to the nucleus, where it forms a heterodimer with the AhR nuclear translocator (ARNT) and binds to specific DNA consensus sites known as xenobiotic response element (XRE). DNA binding of AhR in keratinocytes induces the generation of cytochrome P450 1A1 (CYP1A1) and ROS, the production of 8-hydroxydeoxyguanosine (8-OHdG), a well-known DNA damage marker, and inflammatory cytokines.[267]

NF-κB redox-sensitive transcription factor has been reported to be the common pathway for the conversion of environmental insults into inflammation in the skin. Perturbations in its activity such as overactivation or inhibition are linked to the development of skin defects, inflammatory skin disease, and skin cancer.[285–288] NF-κB acts in immune and non-immune cells to control the maintenance of tissue immune homeostasis which is maintained by an extensive cross-talk between epidermal keratinocytes and immune cells.[289] NF-κB inhibition disturbs the response of the epidermis to environmental challenges and compromises the communication between the epidermis and the dermis, triggering an inflammatory response that resembles a wound-healing reaction[290,291] Exposure to CS have been shown to induce NF-κB activation in keratinocytes via the activation of endogenous sources of ROS.[236]

It has been demonstrated that the activation of the NADPH oxidases (NOX) is involved in both migration and proliferation in extensive cell types such as epithelial cells, fibroblasts, and vascular endothelial cells, therefore, playing a critical role in skin physiology.[292] NOX also contributes to the pathogenesis associated with impaired immune responses due to environmental factors.[293] Once activated by an exogenous stimulus, cytoplasmic NOX components, p67 phox, and p47 phox, translocate to the membrane to form the NOX complex (NOX2) and induce H_2O_2 production via the generation of superoxide (O2–).[235]

Also, ERK1/2 activity in keratinocytes takes part in a homeostatic mechanism regulating inflammatory responses[309] and its phosphorylation is stimulated by CS in fibroblasts,[244] keratinocytes[216,] and mice skin.[201,229,245,294]

In the imbalanced state of oxidative stress, specific transcription factors (i.e. AP-1 and Nrf2) are known to be activated.[295–297] The AP-1 transcription factor, mainly composed of Jun and Fos protein dimers, is a key regulator of epidermal keratinocyte survival and differentiation and an important driver of cancer development.[298] The Nrf2 transcription factor plays an essential role in maintaining skin redox balance by regulating numerous genes involved in the defense against environmental stressors. Nrf2 activation promotes repair of a deficient epidermis and its activation has detrimental effects on the skin, therefore its dysfunction can be associated with various human skin diseases.[296] Although mostly demonstrated on lung models, both AP-1 and Nrf2 transcription factors are stimulated after CS exposure.[299,300] It has been demonstrated that CS exposure alters the Nrf2 pathway in a variety of cells and tissues.[277,301–306] CS-dependent Nrf2 activation is assumed to be based on the interaction of electrophilic molecules with the cysteine residues of Keap1.[307] **Figure A-II-4** presents a summary of the mechanisms involved in the CS-induced toxicity.

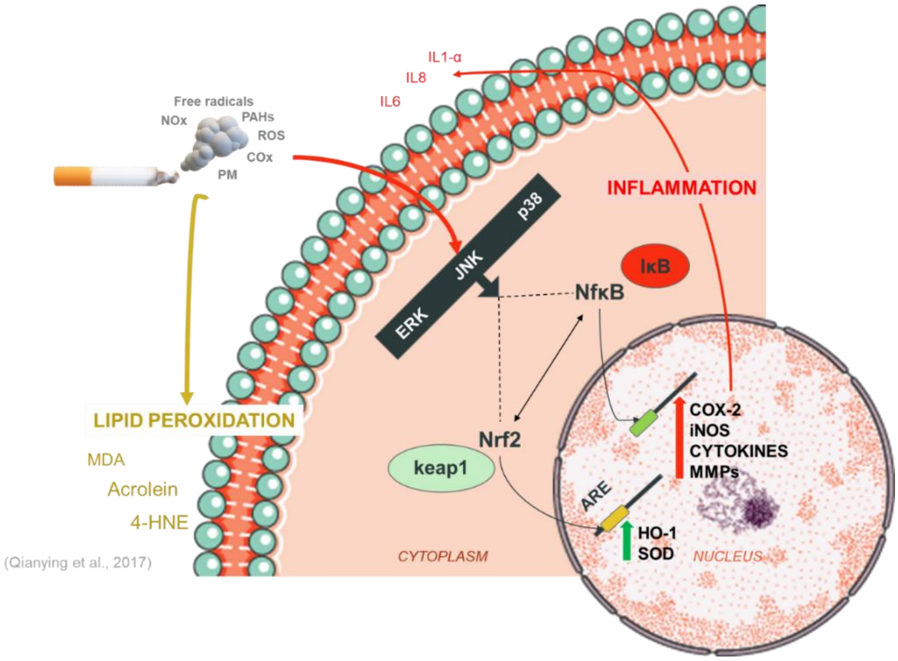

Figure A-II-5. CS induces lipid peroxidation and alters Nrf2 and Nfkb signaling pathways in cells resulting in a cell antioxidant and inflammation response.

Although CS has been shown to alter inflammasome in other tissues, its impact still needs to be investigated in the skin.[308–311] We assume that CS could be also be involved in the inflammasome activation in the skin via a ROS-production-dependent mechanism similar to other air pollutants. [142]

3. CS in the pathogenesis of inflammatory skin diseases

As seen in the previous sections, CS exposure imbalances skin homeostasis through the generation of oxidative damage and inflammatory responses leading to the pathogenesis of several skin disorders. Although the exact mechanism is not identified because of a large variety of toxins in cigarettes, CS exposure stands as a potential environmental risk factor for the development or exacerbation of inflammatory skin pathologies. **Figure A-II-5** illustrates the general mechanism of CS as a risk factor for the development or aggravation of inflammatory skin conditions such as psoriasis and atopic dermatitis.

Psoriasis

Psoriasis is a multifactorial inflammatory skin disease affecting 3% of the population.[312] The most common form is chronic plaque psoriasis, accounting for 90% of cases and presenting with monomorphic lesions that are erythematous and scaly. In the pathogenesis of psoriasis, there is an interplay between immune cells and keratinocytes.[313] Psoriasis skin pathology is mainly associated with excessive secretion of inflammatory cytokines by T-cell populations, infiltration of neutrophils and T cells as well as hyperactivation of the transcription factor Signal Transducer and Activator of Transcription 3 (STAT3), which is associated with hyperplasia.[314,315] Cells of the innate immune system such as dendritic cells and macrophages facilitate the differentiation of Th17 cells through the production of IL-23 and IL-6, leading to a Th17-skewed adaptive immunity. Consequently, Th17 cells secrete IL-17A and IL-22 that stimulate epidermal keratinocytes which in turn produce pro-inflammatory cytokines (e.g. IL-1, IL-6, and TNF-α) and chemokines (e.g. IL-8 aka CXCL8, interferon-inducible protein 10 aka CXCL10, and macrophage inflammatory protein-3 alpha aka CCL20) that will further interact with the innate immune system. This crosstalk results in an inflammatory loop or "vicious circle" involving resident epidermal cells, as well as innate and adaptive immune cells.[316]

In respect to the abnormal epidermal barrier formation, the activation of keratinocytes leads to an excessive and atypical epidermal differentiation and proliferation (hyperkeratosis and parakeratosis), the neutrophil influx into the epidermal compartment, production of antimicrobial peptides (AMPs) including LL-37, β-defensins, and psoriasin (S100A7) as well as a deficient synthesis of intercellular lipids in the extracellular space.[317,318] In addition, in psoriatic skin, the components of the stratum corneum (SC) are prematurely synthesized in the stratum spinosum and the expression of the early differentiation markers such as involucrin (INV) and corneodesmosin (CDSN) is upregulated, while the expression of the late differentiation markers like loricrin (LOR) and filaggrin (FLG) is downregulated.[319] These constituting proteins covalently linked together by transglutaminases and located on the inside of the plasma membrane of terminally differentiated keratinocytes, called corneocytes, form the so-called cornified envelope and have an important protective role against trauma, ultraviolet irradiation, and infections.[173] An altered formation of the cornified envelope, as in the case of psoriatic lesions, significantly affects the barrier capacity to retain water leading to the formation of scales or flakes arising from the shedding of SC fragments.[320,321] Keratinocytes of psoriatic skin have an epidermal turnover of 6-8 days compared to approximately 45 days in normal skin.[322] In psoriasis lesions, the SC is thicker and disorganized, the granular layer is almost nonexistent and the hyper-proliferative basal layer appears as a finger-like projection known as the dermal papillae.

Besides a genetic predisposition and its autoimmunity, psoriasis can also be exacerbated or triggered by environmental factors such as traumatic injury to the skin, physical and psychological stress, cold weather, excessive alcohol, and drug intake, nutrition, and smoking.[323–326] The altered physical barrier and weakened defense mechanism make psoriatic skin more vulnerable to external aggressors such as CS. Ozden et *al.* evaluated risk factors associated with the development of pediatric psoriasis and observed that maternal and environmental tobacco smoke exposure may influence the development of pediatric psoriasis.[156] Although mostly demonstrated in lung models, CS plays a role in the exacerbation of psoriasis by enhancing the differentiation of Th17 cells, which play a predominant role in pathogenesis and production of pro-inflammatory cytokines.[201,327–332]

Atopic dermatitis (AD)

AD is an intensely pruritic, chronic, inflammatory skin disease affecting 10–20% of children and 3–5% of adults, therefore representing a growing health concern. AD is clinically characterized by intense pruritus and erythema and, in its chronic form, by thin scaling, focal parakeratosis, and lichenification (i.e. thickening of the epidermis).[333] Similarly to psoriasis, the cause of AD is multifactorial, with genetic and environmental factors.[144,145,334] Both diseases share common pathogenetic processes involving an impaired immune response, a T-cell mediated skin barrier function deficiency, and a similar STAT3 hyperactivation involved in hyperplasia. However, AD epidermal disruption is not only driven by the secretion of IL-17, IL-22, and interferon-gamma (IFNγ) proteins, which are produced by Th17, Th22, and Th1 cells, respectively. It is also induced by the secretion of IL-4 and IL-13 following Th2 activation.[195] These two cytokines can suppress FLG expression resulting in a reduced keratinocyte terminal differentiation and epidermal barrier defect.[335] Recently, loss-of-function mutations in the FLG gene have been identified in AD patients, therefore suggesting skin barrier deficiency as a major cause of the disease.[336–338] As a consequence, the prevalence of the null allele for the FLG gene has been correlated with a decreased levels of natural moisturizing factor (NMF) molecules and a dry skin phenotype.[339,340] AD is also characterized by an overproduction of immunoglobulin E (IgE) by B-cells, allergies, and asthma-associated features as well as a distinguishable overexpression of the thymic stromal lymphopoietin (TSLP) receptor.[341,342] The role of TSLP was found to induce itch by acting directly on nerve fibers.[343] Itching and pruritus provoke in turn scratching and hence aggravate barrier disruption. This vicious cycle is called the “itch-scratch cycle”.[344] Chronic itching and subsequent dysbiosis with predominant colonization by Staphylococcus aureus contribute to the maintenance of AD.[345] AD affect differently the populations according to their racial skin type; for instance, the disease is more prevalent in Black and mixed-race individuals compared to Whites.[346] Furthermore, Asian AD demonstrates closer patterns to psoriasis than European-American such as more epidermal acanthosis, neutrophil infiltration, and co-expression of IL-17 and IFNγ.[195,347]

An incomplete skin barrier repair after an injury might facilitate the penetration of environmental antigens or stimuli and as a result, trigger an enhanced inflammatory process. Exposure to CS has been associated with AD symptoms, acting as risk factors for its development or aggravation.[348] Indeed, AD was significantly associated with active and passive smoking in Korean adolescents and children and adults, and even dogs according to recent studies.[349–351] A study involving 7030 children aged between 6 to 13 years demonstrated a positive correlation between AD and maternal smoking during pregnancy and/or in the first year after birth.[352] Prenatal exposure to CS is likely to be linked to the development of AD through immune dysregulation.[145]

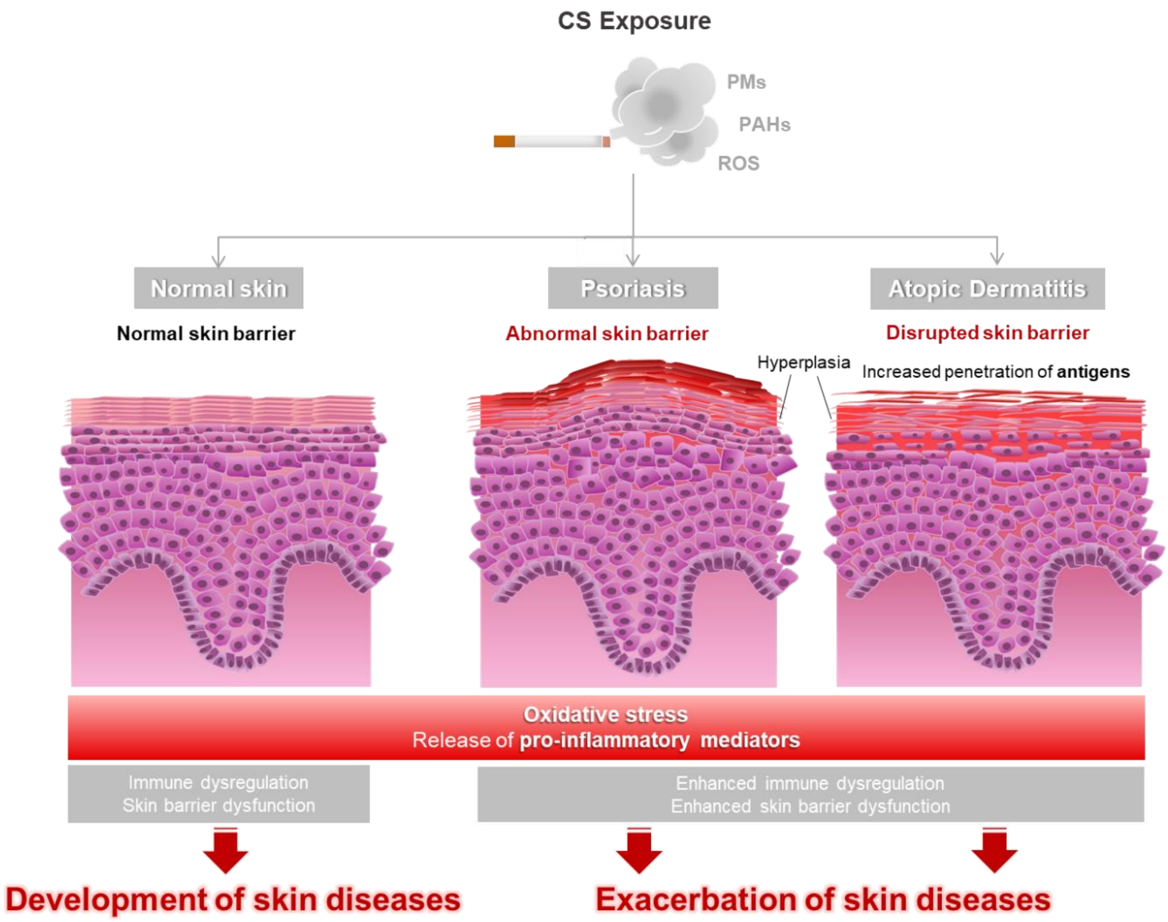

Figure A-II-5. CS acts as a potential environmental trigger of oxidative stress and inflammation in normal, psoriatic, and AD skin, negatively impacting the skin barrier function. PMs: Particulate Matters; PAHs: Polycyclic Aromatic Hydrocarbons; ROS: Reactive Oxygen Species.

Other skin disorders

Vitiligo is a depigmenting disorder in which epidermal melanocytes are destroyed. While the pathogenesis of vitiligo remains unclear, oxidative stress has been considered to be one predominant factor in the initiation of the disease through melanocyte destruction caused by ROS accumulation.[353,354] In vitiligo, melanocytes are particularly vulnerable to oxidative stress due to the pro-oxidant state generated during melanin synthesis and to the genetic antioxidant defects. This could suggest a potential role of CS exposure as a trigger of the disease.[355]

Acne vulgaris, a chronic inflammatory disorder involving sebaceous glands, ducts, and hair follicles, is caused by a combination of genetic, environmental, and hormonal factors. Acne affects mostly children and adolescents and is clinically characterized by comedones, papules, pustules, and cysts.[356] CS is a potential environmental risk factor in the development or exacerbation of acne vulgaris. Epidemiological studies on the German population by Schäfer et al. showed that smoking was a clinically important contributory factor to acne prevalence and severity.[168] In addition, Capitanio et al. reported a positive correlation between cigarette smoking habits and adult women with acne. Nicotine, an agonist of acetylcholine (ACh) is suspected of inducing hyperkeratinization and comedogenesis via the stimulation of nicotinic acetylcholine receptors (nAChRs) on epidermal keratinocytes.[357]

CS exposure impacts the closure of cutaneous wounds via upregulation of genes involved in cell migration and downregulation of genes involved in inflammatory and immune responses, as demonstrated *in vivo* in dorsum excisional wound assay.[233,358] Nicotine was shown to promote wound healing, to induce angiogenesis, and to increase cutaneous blood flow by activating nAChRs.[359–362] Obviously, the risk of developing poor wound healing properties is not only limited to smokers but also to the non-smokers exposed to secondhand smoke.[239,246]

Finally, CS has been associated with increased incidence and production of basal and squamous cell carcinomas. Due to its high content in PAHs, CS may cause DNA damage, DNA repair system damage, as well as an upregulation of cell proliferation via AhR binding activation, generation of ROS, and pro-inflammatory cytokines.[363]

Figure A-II-6 highlights the deleterious effects of cigarette smoking on the skin when comparing two individuals with the same genetic background, i.e. twins.

Figure A-II-6. Clinical observations between smoker and non-smoker twins. The so-called “smoker's face” is characterized by signs of premature skin aging and pigmentation.[193,364]

B. RESULTS AND DISCUSSION

I. Mimicking CS exposure to assess cutaneous responses

1. Development and characterization of an in-house reconstructed skin model

Objective

As a first approach, the establishment and characterization of the 3D *in vitro* skin model of interest remains crucial. To allow cross-comparison studies between different laboratories, it is important to establish a reliable and standardized procedure. We selected the reconstructed human epidermis as a biological target for its physiological relevance and simplicity based on the air-liquid culture of a single cell type, foreskin human neonatal primary keratinocytes. 3D models based on cells of human origin mimic more closely the native human skin and its response to exogenous chemicals. To validate our in-house reconstructed human epidermal (RHE) model, important parameters such as cytotoxic responses, barrier permeability and resistance, morphology, ultrastructure, and biomolecular composition will be assessed and compared with commercialized RHE models such as EpiDerm™ (MatTek Corporation) or EpiSkin™ (L'Oréal).

Evaluation of the RHE response to cytotoxicity

As an essential prerequisite, cytotoxicity response was checked by evaluating lactate dehydrogenase (LDH) release in the supernatant upon topical application of a common toxic substance, Triton-X 100, on top of the reconstructed human epidermal (RHE) model. The cytotoxicity response was then internally compared with RHE commercialized models.

LDH results presented in **Figure B-I-1** demonstrate that the size of the insert did not affect the LDH release significantly. Triton X-100 treatments, either topical at 0.1% or systemic at 0.2%, appear as good positive controls to define a threshold of cytotoxicity with a similar response to commercialized RHE models (data are provided in our manuscript, Dijkhoff I. et al., "A Reliable Procedure to Cultivate Three-dimensional Human Epidermal Equivalents at Large Scale", JoVE journal). To run mechanistic studies, CS exposure must not induce more than 30% cytotoxicity in our reconstructed human epidermal (RHE) model.

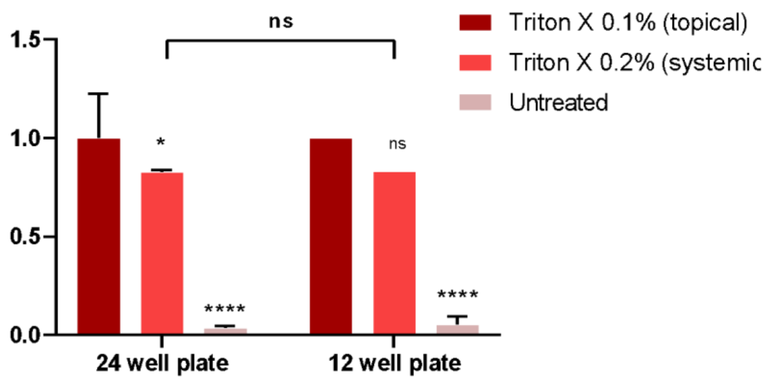

Figure B-I-1. LDH release in the culture medium of untreated RHE and RHE treated with Triton X-100 for 24h. In the 24-well plate, twelve tissues of 0.47 cm^2 were used as untreated and three tissues per positive controls. In the 12-well plate, four tissues of 1.13 cm^2 were used as untreated controls and one sample per positive control. Data are presented as mean ± SEM relatively to the most cytotoxic positive control (0.1% Triton X-100 topical treatment). Statistical analysis was carried out using GraphPad 8.0 (GraphPad Software Inc., San Diego, CA, USA) by two-way analysis of variance (ANOVA) and Turkey's multiple comparison test to compare the 24-well versus 12-well plate; ns = non-significant, *$p < 0.05$ vs control; **** $p<0.0001$.

Evaluation of the RHE barrier integrity

One of the most important criteria for evaluating the performance of any *in vitro* skin culture system is the formation of a competent permeability barrier since the stratum corneum (SC), the uppermost layer of the epidermis, is directly exposed to pollutants before affecting the viable cells. To monitor the formation of the skin barrier (related to the tightness of cell layers), the trans epidermal electrical resistance (TEER) was determined. TEER values around 4000-6000 Ohm.cm^2 translate to a strong barrier function. As a comparison, commercial models such as EpiDerm™ (MatTek Corporation's Reconstructed Human Epidermal model) have a barrier function around 3000-5000 Ohm.cm^2.[21,365] Kandarova *et al.* have demonstrated that high content of water in the *in vitro* 3D skin model increases the ion exchange and thus decreases the overall TEER value.[366] TEER is temperature dependent, therefore it is recommended to wait for an equilibration time of 30 minutes before TEER measurement.[367] Our preliminary studies showed a "plate effect": tissues cultured at the edges of the plate exhibiting lower TEER values than tissues located in the center of the plate. Those results were attributed to an uneven temperature distribution over the plate. To counteract this effect, a special configuration was used with the tissues centered in the plate and PBS dispensed in the wells at the plate periphery. Despite this precaution, the tissues in the center of the plate still exhibited higher TEER values than those from the surrounding area (data not shown).

TEER was measured at different stages of the air-liquid interface (ALI) culture of the RHE tissues: at days 7, 10, and 13. As shown in **Figure B-I-2**, TEER values increase with the age of the RHE tissues with a rise from 1000 Ohm.cm^2 at day 7 to 6000 Ohm.cm^2 at day 13 and translate an increased differentiation of the tissues over time and the formation of a permeability barrier and a functional multilayered epithelium.

Using the same protocol and culture conditions, the reconstruction of epidermal tissue in a large insert (1.13 cm^2) in a 12-well plate was found to be more challenging than in the smaller insert (0.47 cm^2) in the 24-well plate using the same seeding density. Indeed, the TEER values measured for the larger tissues were very low translating a defect in the epidermal barrier formation (**Figure B-I-3**) that would require adjustments in the protocol. For this reason, it has been decided to focus our research activities only on 0.47cm^2 RHE tissues.

To conclude, TEER measurement is a rapid and reliable indicator to characterize the barrier function of the reconstructed human skin models. These TEER data demonstrate normal overall barrier integrity of our in-house RHE models, similar to commercial skin models.

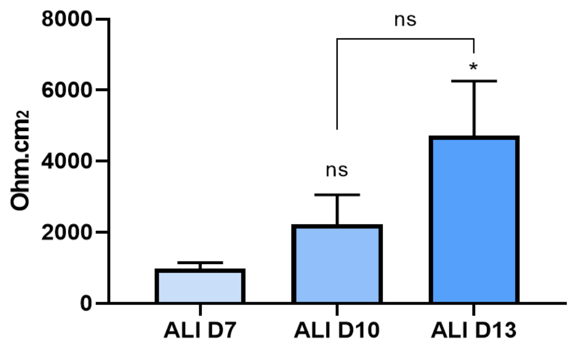

Figure B-I-2. TEER measured at different stages of the air-liquid culture of the reconstructed human epidermis at air-liquid days 7, 10, and 13. Data are presented as mean TEER ± SEM; ALI D7 n=2; ALI D10 n=2; ALI D13 n=5. Statistical analysis was carried out using GraphPad 8.0 (GraphPad Software Inc., San Diego, CA, USA). Data were analyzed by one-way analysis of variance (ANOVA); * $p<0.05$.

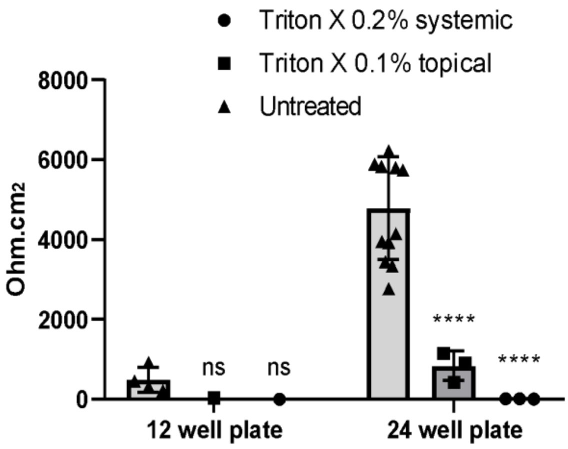

Figure B-I-2. TEER values were compared between two different insert sizes (1.13 cm^2 vs. 0.47 cm^2). In the 24-well plate, twelve tissues of 0.47 cm^2 were used as untreated and three as positive controls. In the 12-well plate, four tissues of 1.13 cm^2 were used as untreated controls and one sample per positive control. Data are presented as mean TEER ± SEM. Tissues treated with Triton X-100 values are compared vs. untreated tissues. Statistical analysis was carried out using GraphPad 8.0 (GraphPad Software Inc., San Diego, CA, USA). Data were analyzed by two-way analysis of variance (ANOVA) and Turkey's multiple comparison test to compare the 24-well versus 12-well plate; ns= non-significant, **** $p<0.0001$.

Evaluation of the RHE barrier permeability

Our data showed that the Lucifer yellow fluorescent dye is not able to penetrate the RHE barrier from Day 7 (**Figure B-I-4**) confirming the existence of an impermeable layer of corneocytes. These results are consistent with previous TEER measurements (**Figure B-I-2**).

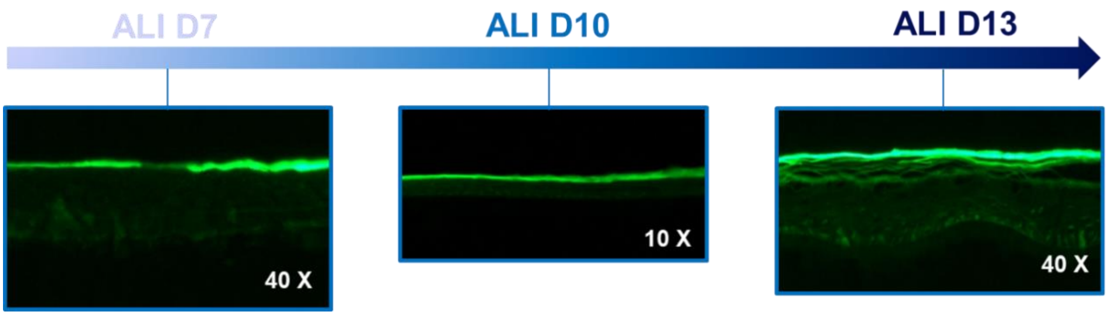

Figure B-I-4. Visual analysis of the barrier permeability using Lucifer fluorescent yellow dye at ALI days 7, 10, and 13. Magnification 10x and 40x; Nikon Microphot FXA microscope (Nikon Instruments).

Morphology evaluation of the RHE

Tissue morphology was analyzed for the cell shape, the number of both viable and non-viable cell layers, and associated thickness. As shown in **Figure B-I-5**, the Hematoxylin & Eosin (H&E) staining presents all epidermal layers: the stratum basale, stratum spinosum, stratum granulosum, and anuclear stratum corneum. In addition, the transition from perpendicular oriented basal cells to flattened granular cells is observed in the histology image. The comparison of the morphology of the in-house RHE model, the EpiDerm™ model (MatTek Corporation), and the native human skin is displayed in **Table B-I-1**.

Basal cells of cubical shape migrate to the stratum spinosum. The stratum granulosum is clearly observed by the flattened cells and visible keratohyalin granules stained in purple hematoxylin, but appear thinner than for the EpiDerm™ model.[366] The SC is relatively thin (12-15 µm) and presents well organized and packed corneocyte layers. The number of viable cell layers is estimated to 6-7 in the RHE model, which is lower than for the EpiDerm™ model (8-12) and human skin (7-14).[368] Intercellular space is more predominant in the *in vitro* 3D models than in native human skin.

Overall, the RHE model demonstrates a similar architecture to that of the native human epidermis.

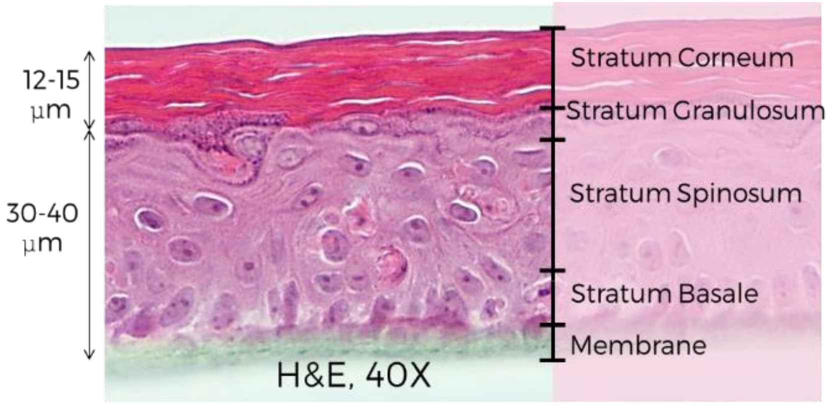

Figure B-I-5. The tissue morphology of the RHE was evaluated by H&E staining. Basal, spinous, granular, and cornified epidermal layers are represented. Magnification 40x; Nikon Microphot FXA microscope (Nikon Instruments)

Table B-I-1. Tissue morphology comparison between the RHE model, the EpiDerm™ model and native human skin.[368]

		In-house RHE model	EpiDerm™ model	Human Skin
Epidermis	Number of viable cell layers	6-7	8-12	7-14
Stratum basale	Cell shape	1-2 layers of cubical cells	Columnar to round cells	Columnar to round cells
Stratum Spinosum	Number of layers	5-6	5-6	5-6
Stratum Granulosum	Keratohyalin granules	Visible	Visible	Visible
Stratum Corneum	thickness	12-15 um	15-30 um	10-12 um

As a next approach, our in-house RHE was compared to the epidermal compartment of an in-house full-thickness (FT) skin model represented in **Figure B-I-6**. The FT skin model development consists of adding the dermal compartment, a fibroblast embedded matrix with keratinocytes seeded on top and cultured at ALI to form the epidermis. The presence of a dermal matrix influences the epidermal morphogenesis and barrier due to additional fibroblast-keratinocyte interactions making them more relevant skin models.

To compare with our well-characterized RHE, the tissue morphology of the FT skin model was analyzed by H&E staining for the cell shape, the number of both viable and non-viable cell layers, and associated thickness.

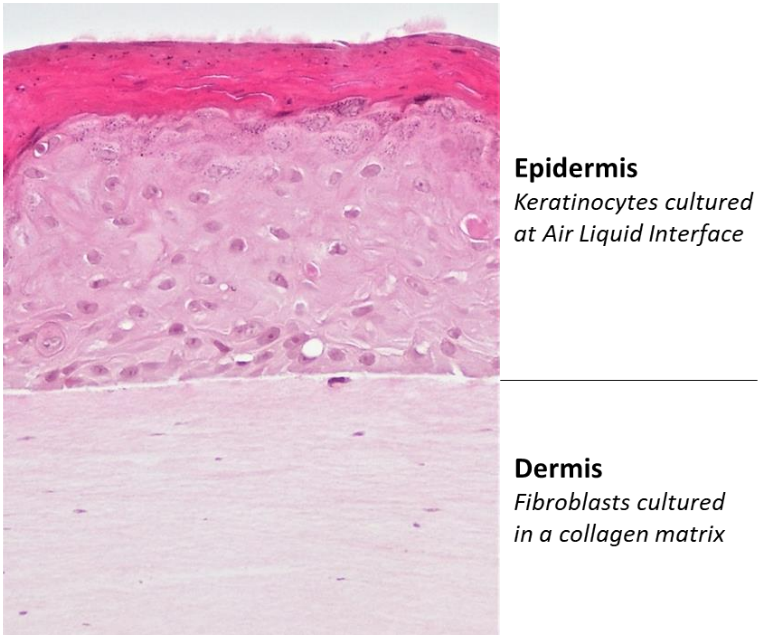

Figure B-I-6. The tissue morphology of the FT skin model was evaluated by H&E staining. Basal, spinous, granular, and cornified epidermal layers are represented. Magnification 40x; Nikon Microphot FXA microscope (Nikon Instruments).

A comparison between the morphology of the RHE model and the FT model is displayed in **Table B-I-2.** As shown in **Figure B-I-7**, the FT model presents a comparable SC thickness (around 15 μm) made of well-organized and packed corneocyte layers to the RHE as well as all epidermal layers: the stratum basale, stratum spinosum, stratum granulosum, and anuclear stratum corneum. However, the transition from perpendicular oriented basal cells to flattened granular cells is not clearly observed on the FT model. This might be explained by the different strengths in cell attachment between the polycarbonate membrane in the RHE and the dermal collagen matrix in the FT model. The FT model shows more visible keratohyalin granules stained in purple hematoxylin in the stratum granulosum and a higher number of viable cell layers estimated to 8-10 compared to the RHE model.

Overall, the RHE model demonstrates a similar architecture to the epidermal compartment of the FT model.

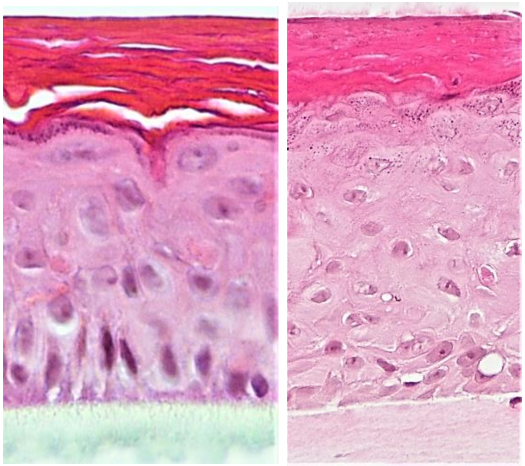

Figure B-I-7. H&E staining of both RHE and FT model tissue morphology. Basal, spinous, granular, and cornified epidermal layers are represented. Magnification 40x; Nikon Microphot FXA microscope (Nikon Instruments).

Table B-I-2 Tissue morphology comparison between the RHE model and the FT model.

		RHE model	FT model
Epidermis	Number of viable cell layers	6-7	8-10
Stratum basale	Cell shape	1-2 layers of cubical cells	round cells
Stratum Spinosum	Number of layers	5-6	5-6
Stratum Granulosum	Keratohyalin granules	Visible	Visible
Stratum Corneum	thickness	12-15 µm	15-20 µm

Evaluation of the localization and expression of typical epidermal proteins in my in-house RHE

Figure B-I-8 presents the immunostaining pictures for filaggrin, loricrin, involucrin, and cytokeratin 10 stainings. The expression of involucrin and filaggrin, which are considered as later markers of epidermal differentiation, is observed within the upper layers of the RHE. Involucrin staining appears more predominant in the stratum granulosum since its expression is initiated earlier during the differentiation process, whereas the expression of filaggrin and loricrin is found only in the upper layers. To conclude, all three markers are expressed in the appropriate epidermal layers and translate into a normal epidermal differentiation process.

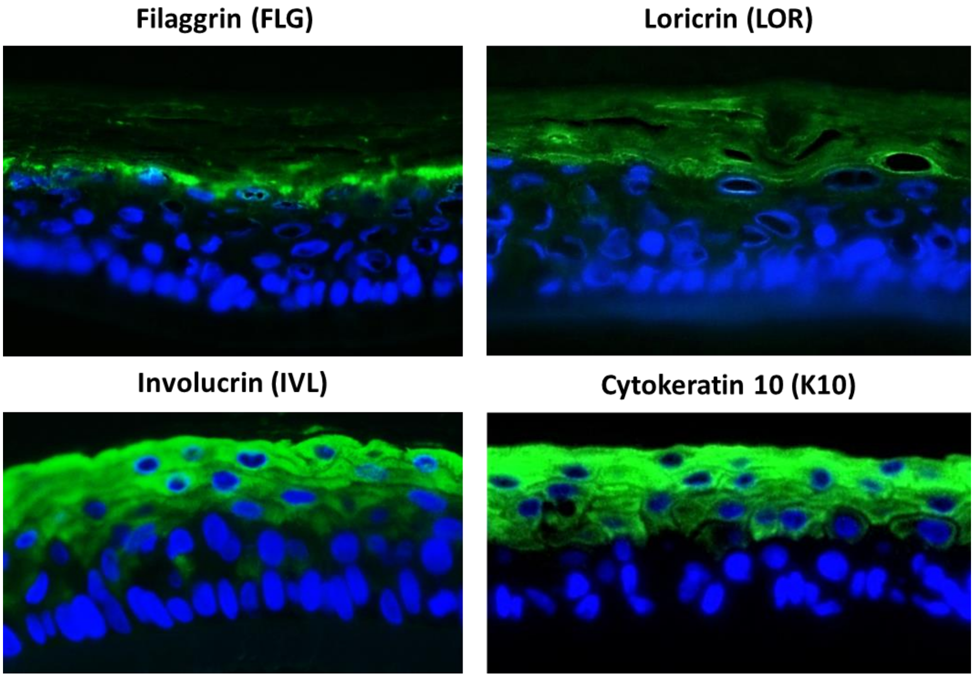

Figure B-I-8. Analysis of localization of differentiation markers via immunofluorescent staining of histological sections: filaggrin (top left), loricrin (top right), involucrin (bottom left), and cytokeratin 10 (bottom right). Nuclei (blue) were stained with DAPI. Magnification 40x; Nikon Microphot FXA microscope (Nikon Instruments).

Evaluation of the RHE ultrastructure and surface

The RHE model was further characterized using the transmission electron microscopy (TEM) and the scanning electron microscopy (SEM) techniques. The following analysis has been done in analogy with the work published by Ponec *et al.* on commercial models.[368] In the electron micrographs in **Figure B-I-9**, the SC is clearly visible and made from approximately 15 densely packed layers of corneocytes. As seen also for the EpiDerm™ model, the SC of the RHE model exhibits the normal basket-weave pattern. The stratum granulosum exhibits round and stellar-shaped keratohyalin granules (KG) (as depicted by the white arrows in **Figure B-I-9**.

Characteristic features of the basal cell layer such as nuclei chromatin clumping (N), vacuoles (V), and tonofilaments (T) are shown in **Figure B-I-10**. Intracellular lipid droplets were seen in the stratum basale and cells appear rounder with less intercellular space over time cultured at the air-liquid interface (**Figure B-I-9**). Visible hemidesmosomes appear to have fine anchoring filaments on polycarbonate membranes.

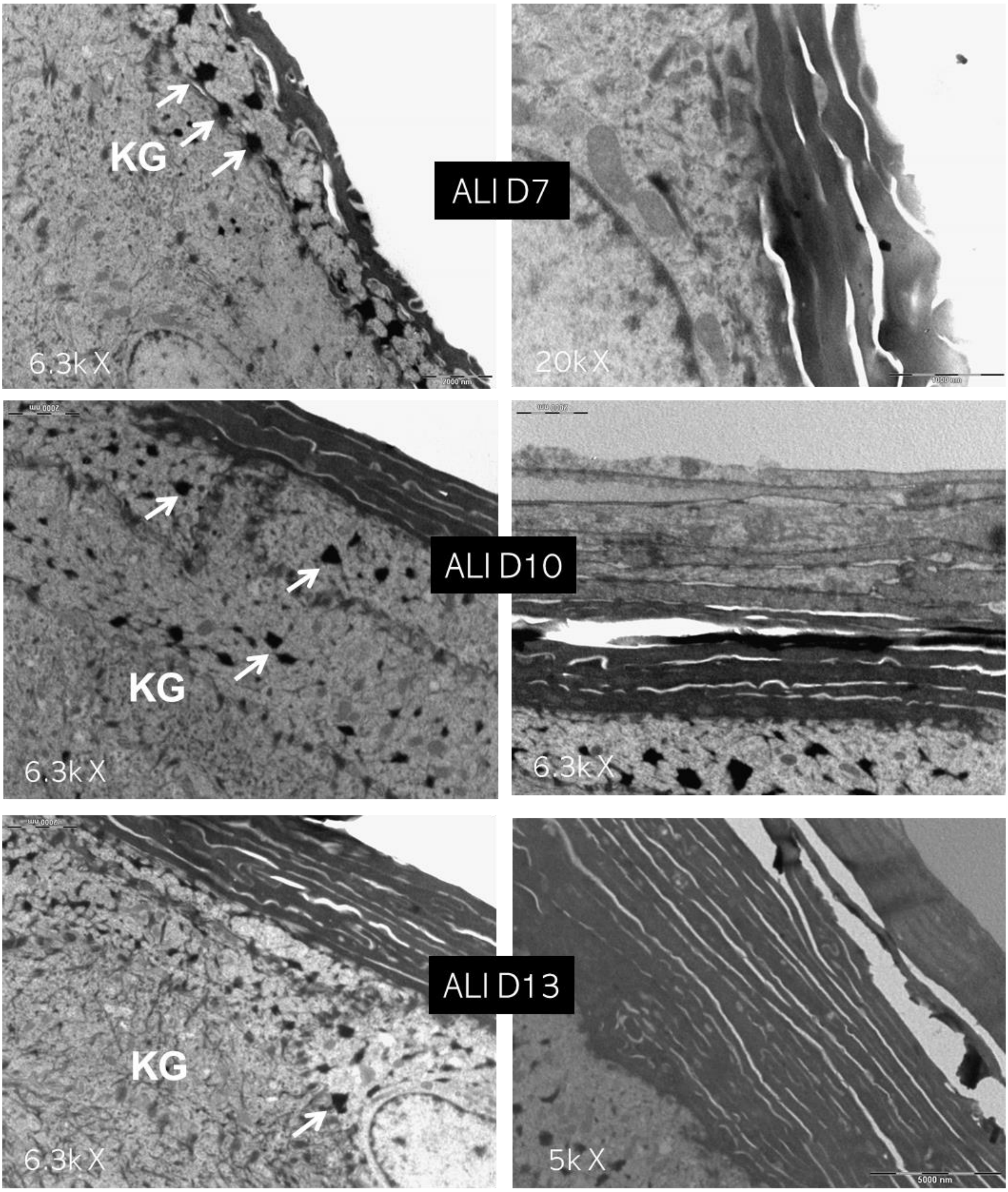

Figure B-I-3. Transmission electron micrographs showing the ultrastructure of the RHE model at different stages of differentiation (Day 7, 10, and 13) with an increased number of layers for the SC and a typical SG layer with keratohyalin granules (KG; white arrows). Hitachi H100 transmission electron microscope, magnification used as indicated on each picture (5k, 6.3k, and 20k x). The scale bar is 2000 nm for the images on the left column and 1000, 2000, and 5000 nm for the images on the right column respectively from the top to the bottom.

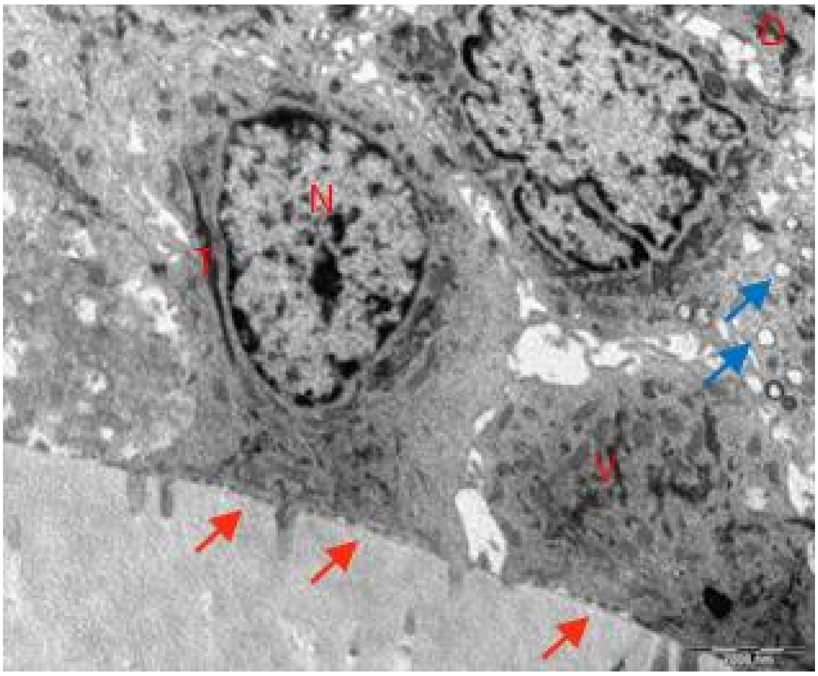

Figure B-I-4. Transmission electron micrograph of RHE at ALI D13 showing normal stratum basale cells containing a nucleus (N), tonofilaments (T), desmosomes (D), vacuoles (V), lipid droplets (blue arrows), and numerous hemidesmosomes (red arrows) along the basement membrane. Hitachi H100 transmission electron microscope, magnification used 5k x. Scale bar corresponds to 2000 nm.

Table B-I-3 summarizes all ultrastructural features of the RHE model at different stages of differentiation in comparison with the EpiDerm™ model (MatTek Corporation) and native human skin. In general, the overall ultrastructure of the RHE model is similar to that of the EpiDerm™ commercial model. All major epidermal strata, including stratum basale, stratum spinosum, stratum granulosum, and stratum corneum, were present (**Table I-3**). Differences to the native human skin include the presence of lipid droplets in basal cells.[369]

Table B-I-3. Morphological epidermal characteristics of the RHE model at different stages of the differentiation process (Day 7, 10, and 13), the EpiDerm™ model (MatTek Corporation), and the native human skin.

		ALI D7	ALI D10	ALI D13	EpiDerm, MatTek	Native skin
Stratum corneum	*Number of corneocytes layers*	7-8	9-10	12-15	16-25	15-20
	SC thickness	1.3 µm	6.7 µm	10.9 µm	12-28 µm	10-12 µm
	Arrangement of SC layers	Loosely packed	Loosely packed	Loosely packed	Loosely packed	Loosely packed
	Lamellar body extrusion at SG/SC interface	Non visible	Non visible	Non visible	Complete, rapid	Complete, rapid
	Transformation of KCs at SG/SC interface	Incomplete (cytoplasmic organelles present)	Incomplete (cytoplasmic organelles present)	Complete	Complete, rapid	Complete
	Transformation of desmosomes in lower SC	Desmosome-like structures persist	Abrupt	Anrupt	Abrupt	Abrupt
	Intracorneocyte lipid droplets	Absent	Absent	Absent	Present in low numbers	Absent
	Intercellular lipid organization	Regular lamellar	Regular lamellar	Regular lamellar	Regular lamellar	Regular lamellar
	Repeat distance of lamellar phase				Only long 12 nm phase present	6.4 and 13.4 nm
	Lateral packing	Mainly hexagonal	Mainly hexagonal	Mainly hexagonal	Mainly hexagonal. Orthorombic rarely	
Basement membrane	*Hemidesmosomes*	Patchy	Patchy	Patchy	Patchy	Continuous
	Lamina densa/Lucida	Present	Present	Present	Present in about 50% cultures	Present
Stratum basale	*Cell shape*	Columnar to round	Columnar to round	Columnar to round	Columnar to round	Columnar
	Intracellular lipid droplets	Present	Present	Present	Present	Absent
Stratum spinosum	*Cell shape*	Upper layers: cell flattening	Upper layers: cell flattening	Upper layers: cell flattening	Upper layers: cell flattening	Upper layers: cell flattening
	Intracellular lipid droplets	Occasionally present	Occasionally present	Occasionally present	Occasionally present	Absent
Stratum granulosum	*Lammelar bodies*	Normal, numerous	Normal, numerous	Normal, numerous	Normal, numerous	Normal, numerous
	Keratohyalin granules	Stellate and rounded	Stellate and rounded	Stellate and rounded	Stellate and rounded	Stellate

Figure B-I-11 consists of a scanning electron micrograph where the flat and packed layers of corneocytes are clearly observable on top of the viable layers. The thickness of the SC and overall epidermis was evaluated to around 15µm and 40µm, respectively.

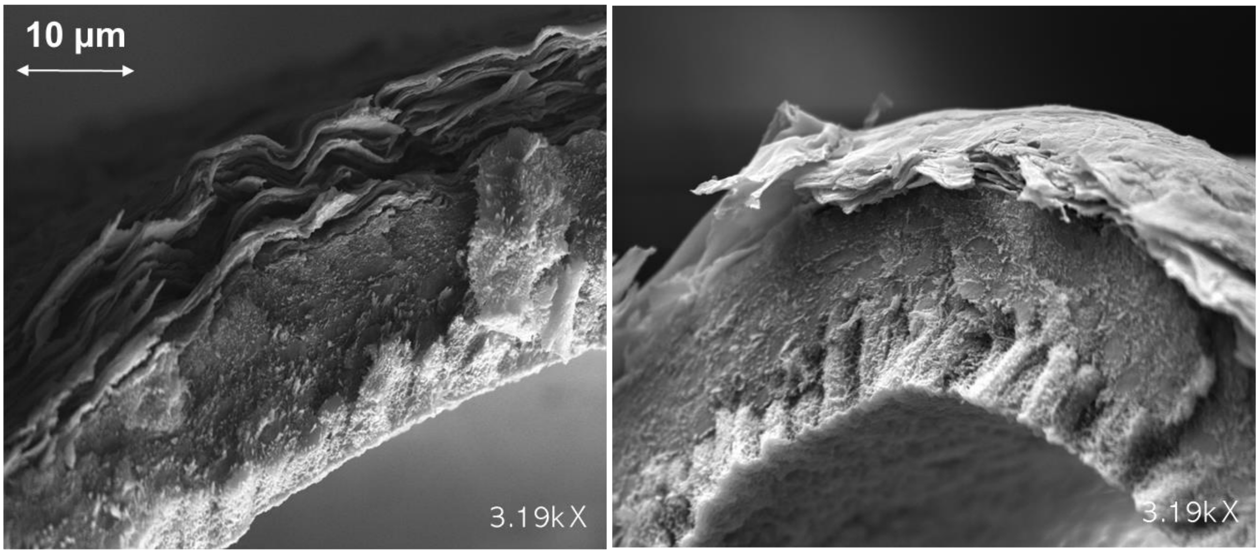

Figure B-I-5. Scanning electron micrograph of a section of the RHE model showing the packed flat layers of corneocytes and the overall arrangement of the epidermis. Hitachi H100 transmission electron microscope, magnification used was 3.19k x. The scale bar is 10 µm.

Evaluation of biomolecular structure of the RHE

The characterization of the RHE model was performed by comparing its Raman spectrum with data generated on the EpiSkin™ RHE model and published by Tfaily *et al*. (**Table B-I-4**).[370] As shown in **Figure B-I-12**, the Raman spectrum of the RHE model closely resembles the EpiSkin™ RHE model.

Identification of epidermal amino acids

The Raman spectrum gives some information about the amino acid composition in the reconstructed skin epidermis. Amino acids are essential molecules, involved in protein synthesis and can serve as biomarkers of skin homeostasis.[371] The presence of Phenylalanine (Phe), Tryptophan (Trp), Tyrosine (Tyr), and Cysteine (Cys) is confirmed in the RHE model.

Phenylalanine (Phe) is a precursor of Tyrosine (Tyr) and plays a role in skin protection and skin hydration.[371,372] Its vibrational bands (*highlighted in purple on spectrum*) are identified at 619 cm^{-1} (ring breathing), 1003 cm^{-1} (ring breathing), 1032 cm^{-1} (C-H), 1175 cm^{-1} (C-H) and 1340 cm^{-1} (C-C).

Tyrosine (Tyr) is a stimulator of melanin synthesis in the skin.[373] This amino acid is characterized by the 643 cm^{-1} bands (ring breathing) and the Raman doublet at 829 and 851 cm^{-1} (*highlighted in red on the spectrum*). It has been demonstrated that this Fermi doublet can indicate the conformation of Tyrosine whether it "exposed" or not to the environment. A positive ratio of 851/829 cm^{-1} has been associated with weak H bonding between the COO^- group and the phenolic hydroxyl in the molecule.[374–376] It will be interesting to compare the intensity of this Fermi doublet in the RHE model after CS exposure.

Tryptophan metabolic pathway plays a regulatory role in skin microbiota[392] and skin disease.[377,378] Its characteristic vibrational bands (*highlighted in light blue*) are present at 758, 1340, and 1555 cm^{-1}.

Cysteine (*highlighted in light blue*) is the amino acid providing strength and rigidity in keratin fibers via the disulfide bonds.[379] Cysteine also plays a role in melanogenesis.[380] Its characteristic Raman bands are all affiliated with the disulfide vibration at 671, 699, and 721 cm^{-1} (stretching C-S).

Identification of epidermal protein structure

The Raman spectrum of the RHE model reveals the secondary structure of proteins. Raman vibrational bands at 1650 cm^{-1} (Amide I, keratin), 1283 cm^{-1} (Amide III), and 935 cm^{-1} reflect the predominance of an α-helix structure of the proteins, such as keratin.[381,382]

Identification of epidermal lipids

The major lipid classes in SC are non-polar lipids such as ceramides, free fatty acids, and cholesterol whereas in the underlying skin layers, there is a majority of polar lipids such as phospholipids, glycosphingolipids, and free sterols.[383]

Ceramides (*highlighted in orange on the spectrum*) are the most predominant epidermal lipids with four peaks at 1062, 1086, 1102, and 1127 cm^{-1}. The presence of higher intensity peaks at 1062 and 1127 cm^{-1} associated with a trans conformation of lipids suggest a lipid organization. This reflects the ordered lipid bilayers typically observed in the SC.[384,385]

Cholesterol is one of the key skin lipids forming the SC barrier.[386] Its presence is indicated by the vibrations at 699 and 882 cm^{-1}.

Phospholipids (*highlighted in green on the spectrum*) are cell membrane components. They play an important role in the synthesis of free fatty acids which are essential for skin permeability homeostasis.[386] They are characterized by Raman vibrational bands at 721, 758, and 1296 cm^{-1}.

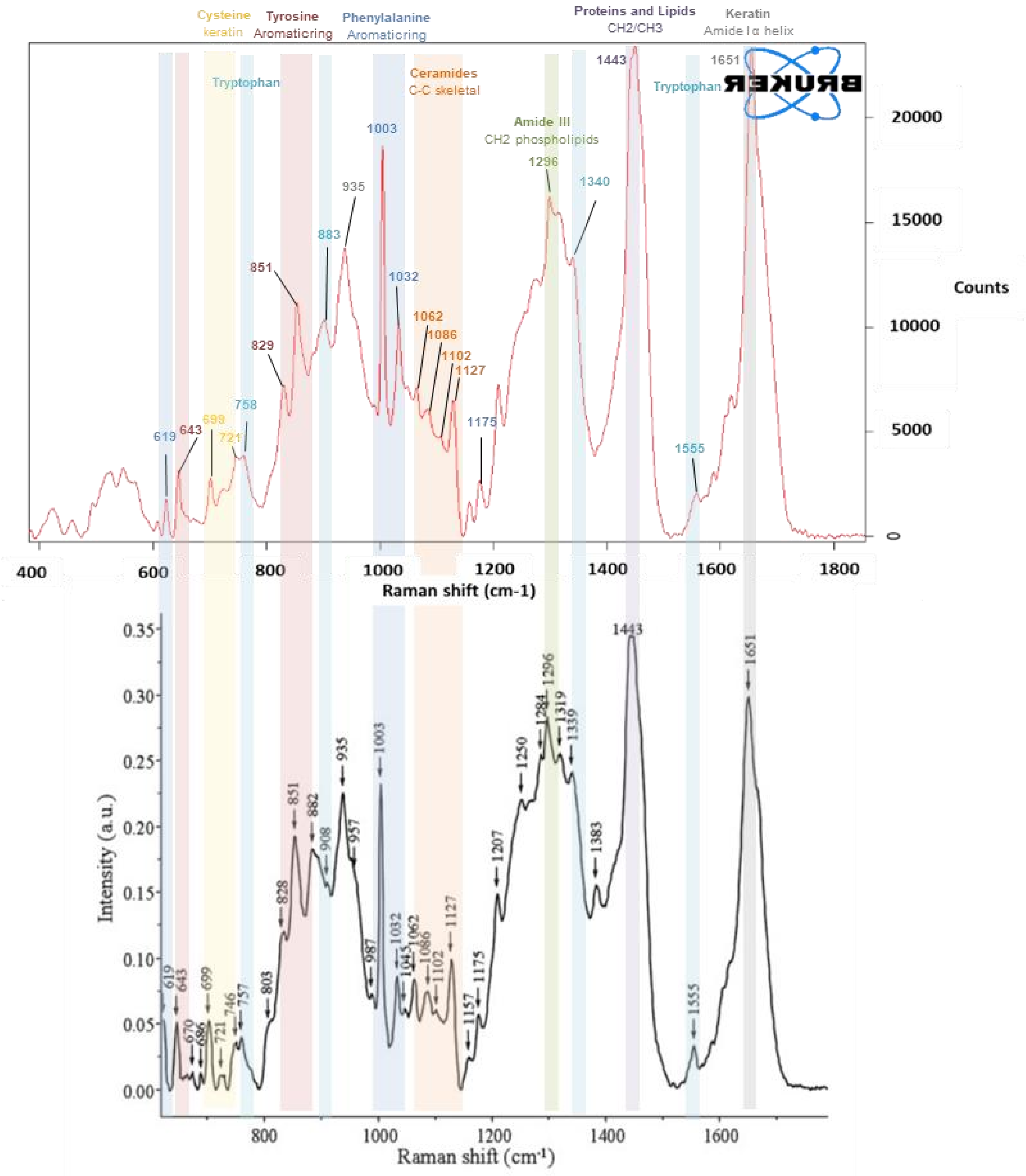

Figure B-I-12. Matching Raman bands between the spectrum of the RHE model (top) and the spectrum of the EpiSkin™ RHE model extracted from literature (bottom).[370]

Table B-I-4. Assignment of the characteristic peaks of the typical Raman spectrum of a RHE model. δ, deformation; τ, twisting; ρ, rocking; ν, stretching.

Raman shift (cm^{-1})	Assignment	Components at the origin of the vibration	Ref
619	C–C twisting	Phenylalanine	387
643	C–C twisting	Tyrosine	388
671	C–S	Cysteine	388
699	C-S gauche; cholesterol ring deformation	Cysteine; cholesterol	388,389
722/721	C-S trans; ν sym $N^+(CH_3)_3$	Cystine; phospholipids	388,389
746	Aromatic ring puckering, ρ (CH_2)		387,388
758	Sym. O-P-O of Lipids; Ethanolamine	Tryptophan; Phospholipids	387,388
788	O-P-O	DNA	390
813	O-P-O	DNA	390
829	Fermi doublet (ring)	Tyrosine	375,388,391
851	Fermi doublet (ring)	Tyrosine	375,388,391
882	δ (CH_2), ν (CC), ν (CN)	Tryptophan cholesterol	388
935	ρ CH_3 terminal, ν CC α helix (secondary structure)	Proteins, phospholipids	387,388,392–394
1003	ν (C-C) aromatic symmetric ring breathing	Phenylalanine	387,388,391,395–399
1032	ν (C-C) skeletal cis conformation	Ceramide	388,391,392
1062	ν (C-C) skeletal trans conformation	Ceramides	388,391,392,395,400,401
1086	ν (C-C) skeletal gauche conformation; O-P-O	Ceramides; DNA	388,390–392,395,400,401
1102	ν (C-C) skeletal gauche conformation	Ceramides	388

1127	ν (C-C) skeletal trans conformation	Ceramides	388,391,392,395,400,401
1175	ν (CH) C-O-C Lipids	Tryptophan, Phenylalanine	388
1254		DNA guanine, cytosine	390
1284	Amide III α-helix	Proteins	388
1296	δ (CH_2); τ(CH_2)	Phospholipid	388,389,392,395,397,401,402
1319	ν (C-C), CH bend Phe, Trp	Tryptophan, Phenylalanine; DNA	388,390
1340	ν (C-C), CH bend Phe, Trp, Adenine guanine	Proteins; DNA	388,403
1443	δ (CH_2) proteins and lipids	Proteins and Lipids	388,391,394–396,401,404
1555	δ (NH), ν (CN) amide II	Tryptophan	388,392
1651	ν (C-O) amide I α-helix	Keratin	388,391–394,405

Empty Modelling analysis

The Empty Modelling™ is a patented chemometric method for extracting chemical information from Raman data. The Empty Modelling™ analysis of the RHE model demonstrates the presence of two major components: component 1 and component 2. The chemical composition of components 1 and 2 is displayed in **Figure B-I-13** with the distribution of bands from phenylalanine (Phe), tyrosine (Tyr), tryptophan (Trp), ceramides, lipids, and proteins. The chemical image indicates that component 2 is present in higher amounts than component 1.

According to **Figure B-I-13**, component 2 is predominantly composed of phospholipids and tryptophan (Trp) while component 1 is richer in ceramides, keratin, tyrosine (Tyr), and phenylalanine (Phe). Regarding the four main bands in the ceramide region (1000-1150 cm^{-1}), component 1 shows a reduced intensity of the 1062 and 1127 cm^{-1} bands simultaneously with a dominating intensity of the 1086 and 1102 cm^{-1} bands, indicating a preponderance of disorganized lipids.[370] The opposite trend is observed in component 2, suggesting domination of organized lipids.

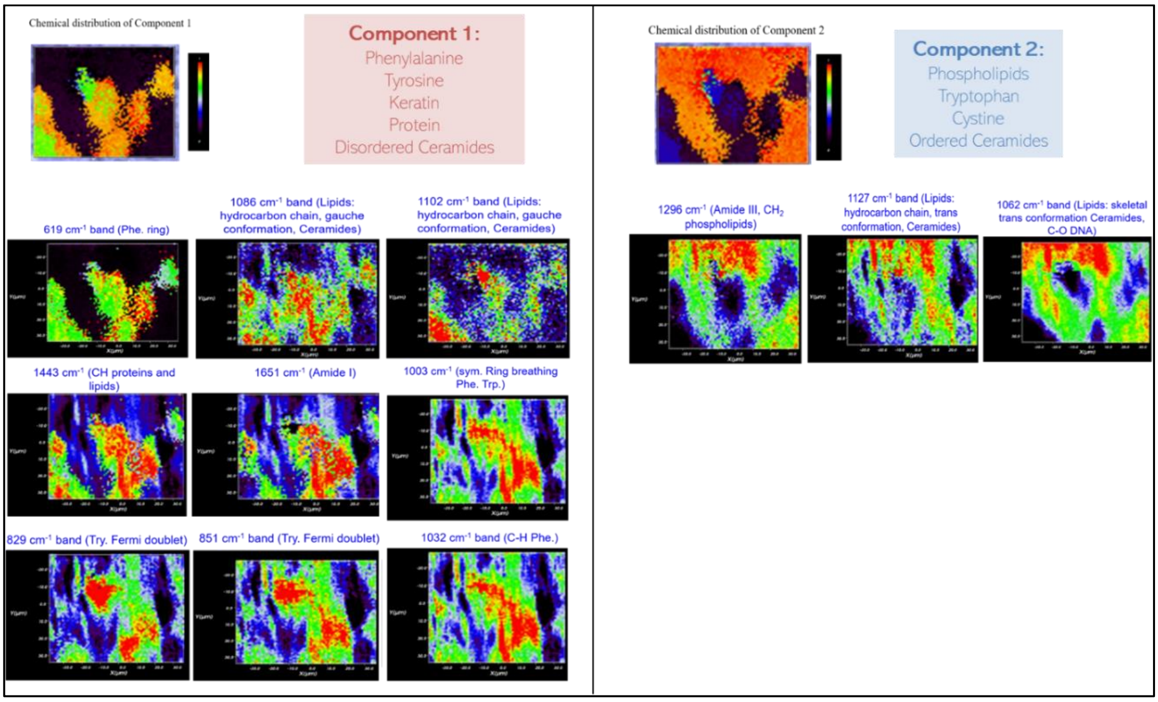

Figure B-I-6. The chemical distribution of components 1 and 2 and associated chemical distributions for the prevalent bands. In the intensity scale, the red color corresponds to high intensity and black color to the low-intensity regions.

The Raman spectrum of component 2, shown in red in **Figure B-I-14**, contains more bands of the DNA such as 722 cm^{-1} (cystine, phospholipids), 746 cm^{-1} (aromatic ring), 757 cm^{-1} (tryptophan; phospholipids), 1175 cm^{-1} (tryptophan, Phenylalanine), 1254 cm^{-1} (DNA guanine cytosine), 1284 cm^{-1} (Amide III band α-helix of proteins), 1296 cm^{-1} (phospholipids), 1319 cm^{-1} (tryptophan, phenylalanine; DNA) and 1340 cm^{-1} (proteins, DNA). The rest of the vibrational bands were significantly higher in component 1, for example in the ceramide region (1000-1140 cm^{-1}), for the vibrations associated to tyrosine (643 cm^{-1}; 829/851 cm^{-1}), at 1443 and 1651 cm^{-1} (keratin).

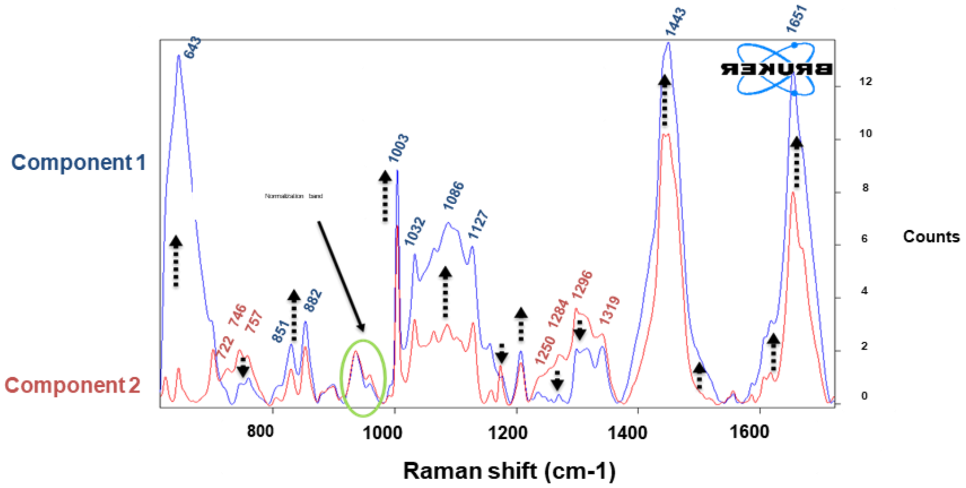

Figure B-I-7. Baseline corrected and normalized spectra of components 1 and 2 highlights the difference between the two components. The normalization was performed w.r.t the band at 937 cm^{-1} (CH_3 rocking of phospholipids). Lower intensity indicates lower amounts.

To conclude, component 2 is a typical epidermal skin layer containing living cells features such as phospholipids from the cell membrane and DNA bands as well as an increased lipid chain order. Furthermore, the predominance of polar lipids indicates similarities with the stratum basal-spinosum layer composition. However, the organization of lipids should normally be random in the deeper epidermal layers compared to the upper layers. As for component 1, the Raman spectrum shows the domination of keratin, ceramides, and a lipid chain disorder. Therefore, the analysis of components 1 and 2 indicates that the RHE model is a very heterogeneous tissue with a mixture of organized and disorganized lipids, nonetheless, the predominance of organized lipids demonstrates a well-formed SC.

This work demonstrated that Raman spectroscopy is a promising tool to assess skin damage/composition before and after challenging with CS. It has been shown that this technique can provide information regarding molecular changes in human skin models upon interaction with external aggressors such as solar radiation.[390] This non-invasive approach is more sensitive in detecting structural changes and DNA damage concerning toxicology and histology assays. Although *in vitro* skin models have the advantage of not exhibiting autofluorescence due to the absence of melanin, this makes them more vulnerable to external aggressors compared to real human skin.

Conclusion to the RHE characterization study

A reliable procedure has been established to reproduce standardized RHE models in different laboratories. Characterizing *in vitro* models to compare it with the *in vivo* models improves our understanding of the skin, from the cellular components to its mechanisms of differentiation and proliferation. Here, the foregoing data demonstrated similar structural-functional properties as native human skin. This standard protocol appears useful for a broad range of research projects from toxicological data generation, cosmetic application to skin disorders treatment[28,406–410]. Indeed, with the recent ban of animal testing in the cosmetic industry standardized RHE represent necessary tools to test cosmetic ingredients as well as finished products[411]. To some extent, they have proved to be helpful to test the efficacy of protective and/or curative solutions against environmental stressors such as UV and air pollution[231,412,413]. Moreover, this RHE reconstruction protocol enables us to simulate acute as well as chronic exposure conditions.

To go further in complexing the model, this simple procedure can be tuned by varying the type of skin cells used, for example, neonatal NHEKs are optimal candidates to study the effect of external stressors for their lack of environmental exposure. To enhance the physiological relevance of the skin model, some researchers have included other skin types in the epidermal compartment such as melanocytes to run phototoxicity studies or immune cells to create more immune-competent models[414,415]. Another option is the development of models based on cells derived from patients with skin disorders to mimic some disease features[416]. Moreover, the culture medium composition can be modulated to reproduce some skin pathological characteristics, for instance challenging the model with a specific cocktail of cytokines reproduces the abnormal morphology, such as epidermal hyperplasia[417], and altered expressions of genes and proteins typically observed in Atopic Dermatitis and Psoriasis[418–420]. Silencing specific genes before build the RHE is another approach used to reproduce some alterations in skin disorders and investigate new therapeutic solutions[421]. Finally, a dermal compartment made of fibroblasts embedded in collagen matrix can be generated a few days before the RHE reconstruction. Keratinocytes are seeded on top of this dermal compartment to generate a FT-model[422]. Adding fibroblasts in the model is essential for aging-related studies, for instance, to study the mechanism of premature skin aging upon external aggressors and test anti-aging solutions[423].

To conclude, the RHE represents a modulable and valuable tool that provides knowledge in skin homeostasis and its defense mechanism upon exposure to exogenous substances. Furthermore, such a model enables a better understanding of the pathways involved in several skin disorders, thus helps towards therapeutic advances.

2. Optimization of the *in vitro* CS exposure conditions

Objective

This part of the thesis will focus on the implementation and optimization of the exposure conditions of a main environmental aggressor, CS. To reproduce human skin exposure to CS *in vitro* in the most realistic way possible, an in-house CS generating box was designed to mimic the whole smoke. Several parameters such as the number of cigarettes and the exposure duration require optimization to achieve conditions that do not significantly affect tissue viability. To determine optimal exposure conditions on RHEs, TEER and LDH were used as biomarkers of CS-induced toxicity.

Evaluation of CS-induced toxicity

To select the exposure conditions, it is important to evaluate the viability of the tissues after exposure. As previously mentioned, the exposure conditions should be strong enough to induce a response in our biological model but not too strong to avoid inducing a toxic effect. Samples allowing a survival above 90% evaluated with LDH cytotoxicity assay will be considered as acceptable. The following data obtained upon exposure to CS have oriented towards the selection of certain exposure parameters such as the exposure duration and number of cigarettes used. The results displayed on the left graph in **Figure B-I-15** show that a one-hour exposure to two cigarettes induces high cytotoxicity in the RHE model. Based on these data, a lower dose of exposure was generated, i.e. 15 and 30 minutes with one or two cigarettes (right graph in **Figure B-I-15**), which resulted in no cytotoxicity. An exposure time of 30 minutes with two cigarettes was therefore selected for the rest of the experiments.

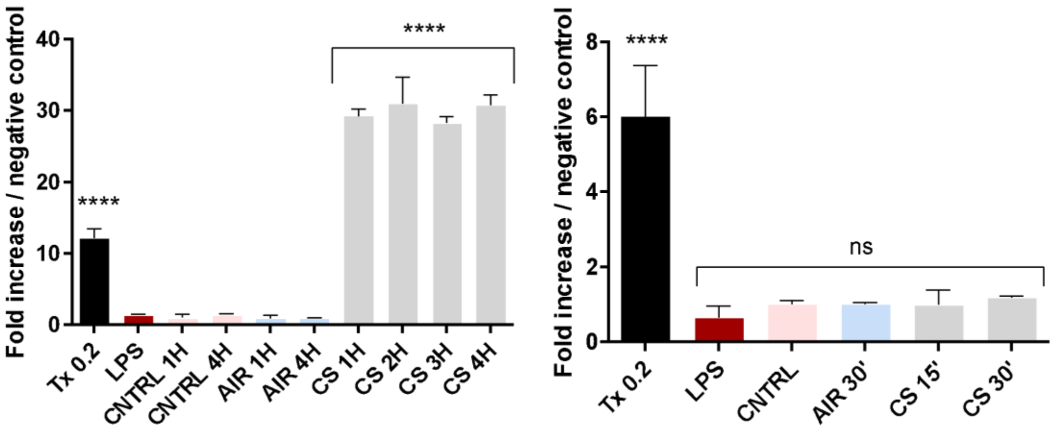

Figure B-I-8. Cytotoxicity was evaluated by lactate dehydrogenase (LDH) release in 1.5 ml of RHE maintenance media after 24h Air/CS post-exposure incubation. A 24h Triton-X treatment (0.2% systemic) was used as a positive control. A kinetic measurement was performed for 30 minutes every 30 seconds at λ=495nm. Data are presented as mean ± SEM respectively to an average mean of negative control; n=3/conditions; One-way ANOVA and Dunnett's multiple comparison test were performed in comparison to the average mean of the negative control (unexposed); ns= non-significant, **** $p<0.0001$.

TEER as a marker to determine optimal in vitro CS exposure condition

The barrier function of the RHE model was evaluated by TEER before and after exposure to CS/Air for different durations: the first set of RHEs was exposed to 1, 2, 3, 4h with two cigarettes and the second set to 15 and 30 minutes with one cigarette. TEER data on **Figure B-I-16** correlate with the release content of LDH in the RHE model. Samples releasing high LDH content exhibit a very weak barrier resistance, i.e. a TEER value around 200 Ohm.cm^2. When using a lower CS exposure dose (15 and 30 minutes with one cigarette), no significant difference between unexposed and exposed RHEs was observed, suggesting that 30 minutes with one cigarette does not compromise the skin barrier.

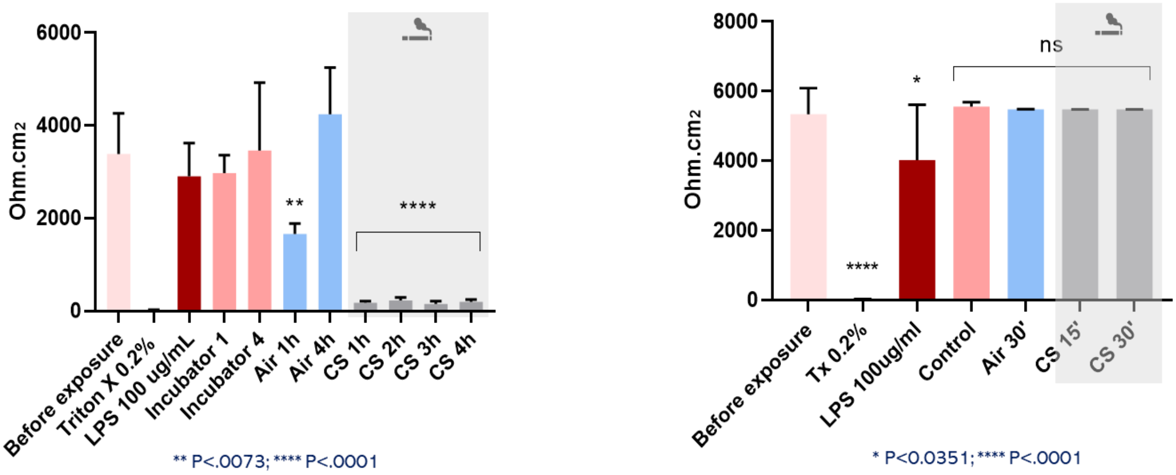

Figure B-I-9. TEER measured in RHE before and after CS/Air exposure. Data are presented as mean ± SEM respectively to an average mean of negative control; n=18 before exposure and n=3 for other conditions; One-way ANOVA and Dunnett's multiple comparison test were performed in comparison to the average mean of the negative control (unexposed); ns = non-significant, ** $p<0.01$, **** $p<0.0001$.

Harsh CS exposure conditions lead to tissue necrosis

Tissues exposed to strong CS exposure, i.e. 4h exposure with 2 cigarettes, were submitted to ultrastructural and morphological analysis. Compared to a healthy skin ultrastructure, characteristics features of necrotic tissues were observed in TEM in **Figure B-I-17**, such as intercellular spaces, cytoplasmic vacuoles, nuclear chromatin condensation, and disruption of the cell membrane.

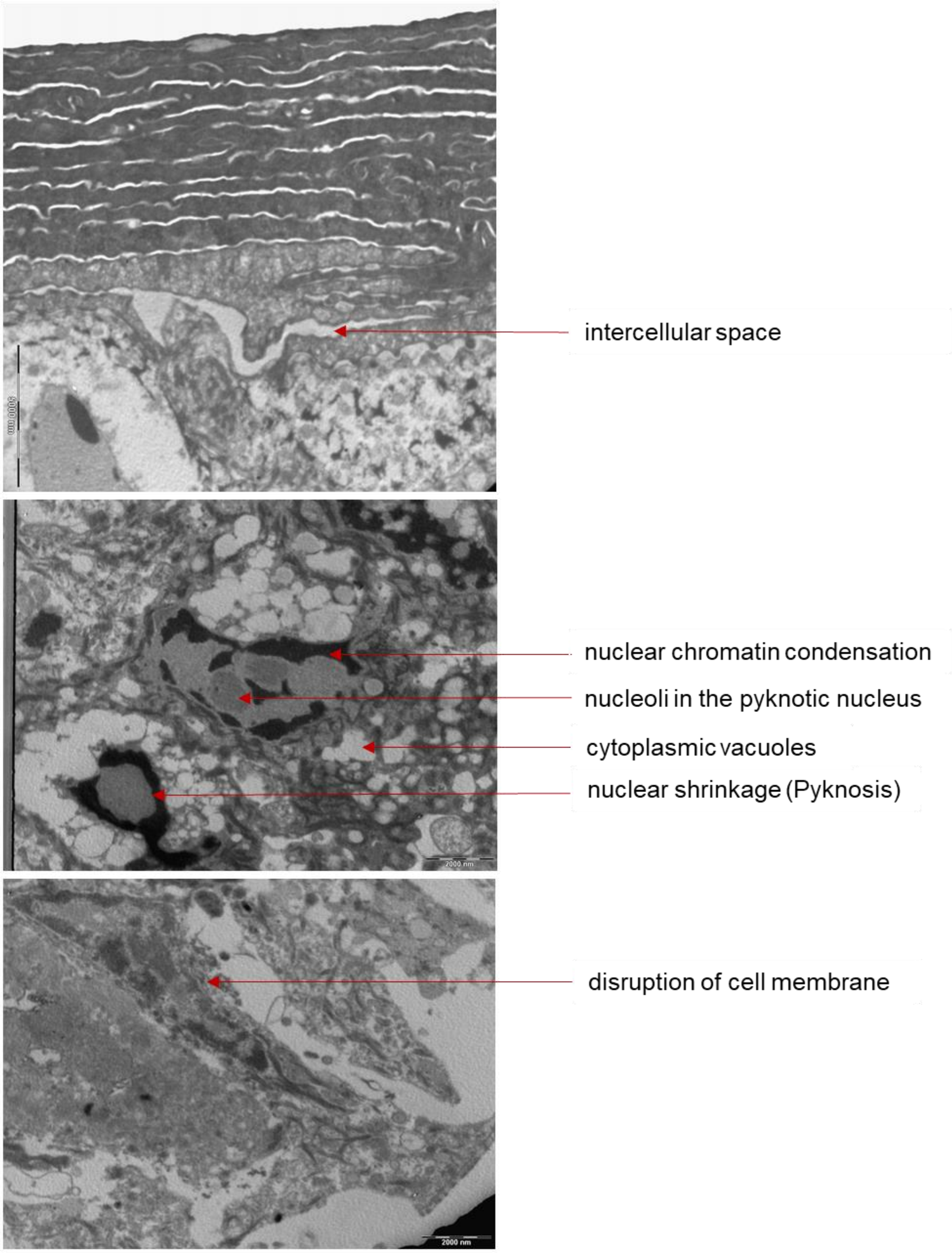

Figure B-I-10. Characteristic features of necrotic tissues were observed with TEM after strong CS exposure (4h exposure with 2 cigarettes). Two samples were examined per condition.

Hitachi H100 transmission electron microscope, magnification 5k X. Scale bar is 5000 nm (top picture) and 2000 nm (middle and bottom pictures).

Regarding the morphology analysis, CS exposed samples appeared more vulnerable and softer during the process of microtome sectioning, resulting in a damaged morphology (**Figure B-I-18**). Despite the presence of a protective Teflon lid on top of the carrier plate during the exposure, we assume that a long duration of CS exposure of a minimum of 1h would result in the direct dissolution of CS components into the medium generating a systemic toxic effect and leading to necrosis.

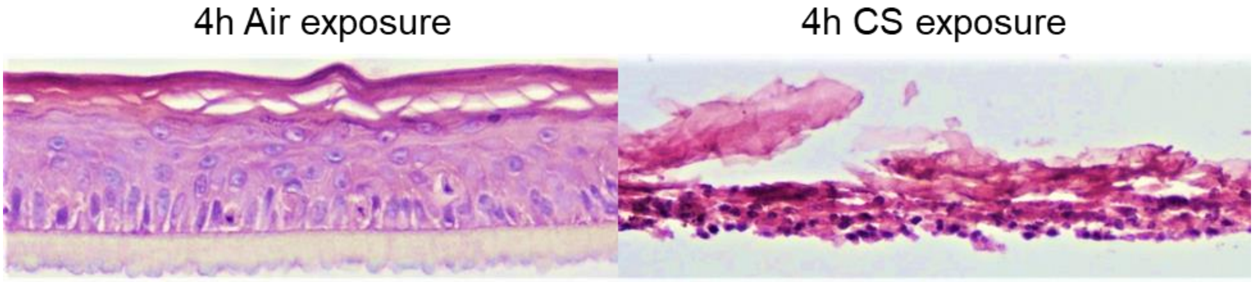

Figure B-I-18. Tissue morphology comparison of the morphology of RHE tissues after 4h exposure to Air/CS (w 2 cigarettes) using H&E staining. Magnification 40x; Nikon Microphot FXA microscope (Nikon Instruments).

Conclusion to the optimization study of CS exposure conditions

To conclude, we have selected the exposure conditions to study the impact of CS on the skin as follows, two successive cycles of CS exposure for the RHE, one cycle is defined as a duration of 15 minutes with one cigarette (**Figure B-I-19**). To simulate a realistic exposure to CS, a CS exposure chamber was designed allowing us to study the effect of the whole smoke on skin. The generation of fresh CS was preferred over the use of CS extract to take into consideration the interactions between all CS components and more importantly not to exclude the exposure to short-lived reactive species coming to the gas phase.

Once set up and optimized, the exposure chamber is a promising device that enables access to numerous investigation studies as well as *in-vitro* toxicological data. It can be easily adapted to evaluate the effect of cigarette alternatives such as IQOS cigarette and e-cigarette vaporizer. To go further, the chamber enables the combination of CS exposure and UV lamps to mimic the photochemical components generated by the interaction of atmospheric pollutants and solar radiation.

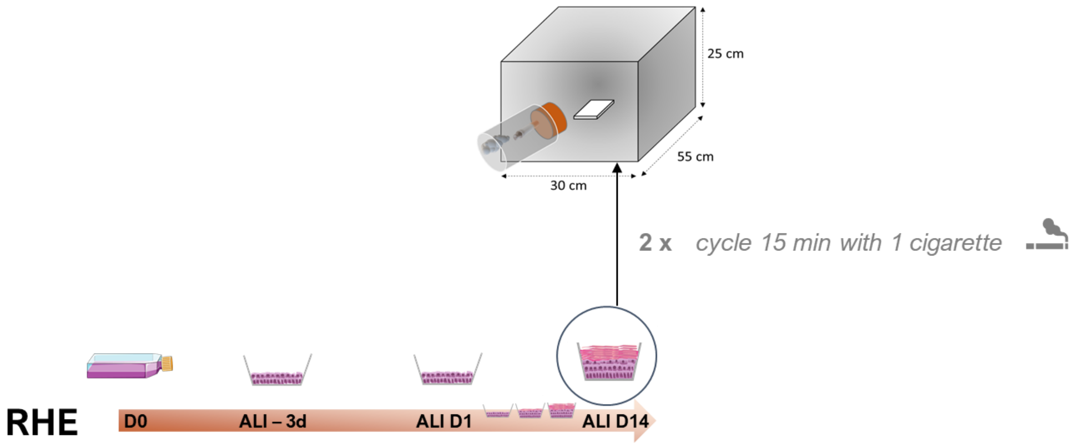

Figure B-I-11. Summary of the *in vitro* culture and exposure conditions selected for the RHE.

II. Evaluation of the impact of CS exposure on cutaneous responses *in vitro*

Objective

The combination of optimized CS exposure conditions combined with a well-characterized 3D reconstructed human epidermis (RHE) model allows us to identify cellular responses and molecular pathways activated by skin keratinocytes in response to CS exposure. Using this reliable and standardized *in vitro* protocol, the impact of CS on the tissue morphology, barrier integrity as well as oxidative stress and pro-inflammatory responses will be investigated in a RHE model.

1. CS-induced pro-inflammatory responses in a RHE

CS exposure causes the pro-inflammatory mediators IL-8 and IL-1α

To confirm the reported CS-induced cytokine release in our 3D *in vitro* skin model with our CS exposure conditions, IL-8 and IL-1α release were measured with the ELISA assay from the culture medium of RHEs that were incubated for 24H post-CS/Air-exposure.[196,240,245] Based on the literature data, we assume the release of IL-8 in response to CS is time-dependent and accumulates for a higher detection 24h after exposure. TNF-α is reported as a potent stimulus of IL-8 production and was used as a positive control for IL-8 release induction in both skin models and resulted in a 6-fold increase (**Figure B-II-1A**).[424] In our experiments, an enhancement of IL-8 release upon CS exposure was detected via ELISA assay in our RHE models. This increase was significant with a 4-fold increase when RHEs remain incubated in the exposed medium (**Figure B-II-1A**) However, when the medium was refreshed after exposure, there was no significant IL-8 secretion. It is supposed that this enhanced release reflects a systemic effect induced by CS components that have been diluted in the supernatant during the 30 minutes of exposure, although the wells were protected by a Teflon cover. As previously described in the literature, aqueous CS components acting as IL-8 stimulus might include small aldehydes like acrolein.[425,426]

IL-1α was detected at a 2-fold increase after three cycles of CS exposure at air-liquid day 9, day 11, and day 14 (**Figure B-II-1B**). Contrary to previous findings from Lecas et al. on

SkinEthic™ RHE models exposed through a VitroCell exposure chamber, IL-1α was not produced using our RHE models harvested 24h after CS exposure, with only one cycle.[196] this discrepancy between our results and the literature could be explained from the lack of standardization and the interlaboratory variability of the CS exposure conditions, making a comparison between our RHE and this commercialized model impractical.

Finally, IL-6 was also measured as often described as a cytokine released from CS-induced inflammation in various cells.[261,427,428] However, no IL-6 release was detected *in vitro* in RHE models, even though other groups were able to observe and IL-6 overexpression and production in mice skin.[245]

To conclude, our data confirm that CS initiates an inflammatory response by inducing the release of IL-8 and IL-1α in our 3D skin models.

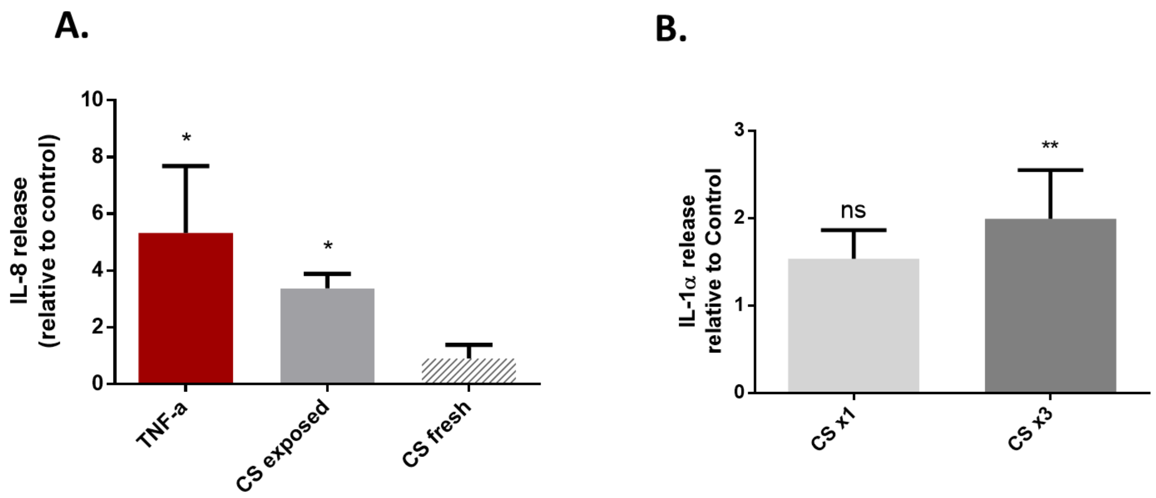

Figure B-II-1. Release of CXCL8/IL-8 measured in the cell culture medium after 24h of RHEs post-exposure to Air/CS and treatment with TNF-α (50 µM) as a positive control. The Grey column represents data for tissues incubated for 24h in the exposed medium while the striped pattern column represents data for CS-exposed RHEs incubated in a fresh post-exposure medium. Data are presented as mean fold increase respective to control ± SEM; n=3 for each condition; One-way ANOVA and Dunnett's multiple comparison test were performed in comparison to the average mean of the negative control (unexposed) using GraphPad software; * $p < 0.05$. B. Release of IL-1α measured in the cell culture medium after 24h of RHEs post-exposure to one cycle or three cycles of CS; CS x1 corresponds to a cycle of CS exposure at ALI D14 (light grey column) and CS x3 corresponds to three cycles of CS exposure at ALI D10, D12, and D14 (dark grey column). Data are presented as mean fold increase respective to control ± SEM; n=5 for each condition; One-way ANOVA and Dunnett's multiple comparison test were performed in comparison to the average mean of the negative control (unexposed) using GraphPad software; $**p < 0.01$.

2. CS impact on the skin barrier and morphology in a RHE

CS exposure directly affects the transepithelial electrical barrier resistance

TEER values in the range of 4000-6000 Ohm.cm^2 reflect a healthy and normal strong barrier function, our control RHEs exposed to Air typically provide TEER between these bounds, as shown in **Figure B-II-2**. During the air-liquid culture of the RHE, the rising thickness of the stratum corneum and the tight junction formation both contribute to a progressive climb of TEER, as observed in **Figure B-II-2A.** Therefore, at the early stages of ALI, the SC is thinner hence more vulnerable to the deleterious effect of toxic substances. To investigate whether exposure to CS and CS components would have a higher impact on the barrier resistance, the epidermal models were exposed to 1, 2, and 3 cycles of Air or CS respectively at air-liquid days 7, 8, and 9, and TEER was assessed 24h post-exposure. After one cycle of CS exposure, a 2-fold increase in TEER is noticed. Surprisingly, in response to the second cycle of CS exposure, the skin tissues initiate an adaptive response translated by a recovery of TEER value similar to the Air exposed tissues.

The barrier resistance of RHEs treated with CS components (H_2O_2, Acrolein) and Nigericin topically applied at air-liquid day 7 was assessed after a 24h treatment. While Nigericin-treated RHE remained intact, exposure to CS single components H_2O_2 and Acrolein resulted in a 2-fold drop in TEER (**Figure B-II-2B**).

The graph **Figure B-II-2C and D** show the impact of CS exposure at air-liquid day 14, i.e. with a more mature and well-formed protective SC. TEER was analyzed 24h post-exposure to Air/CS with and without medium refresh after exposure, respectively represented in **Figure B-II-2C and D**. Graph C represents the difference in TEER which was evaluated before and after exposure to Air/CS and resulted in a decrease of ΔTEER of 2000 Ohm.cm2 in barrier strength in response to CS exposure. Interestingly, TEER was also significantly reduced by approx. 4-fold decrease after exposure to CS and 24h incubation in the exposed medium. This drop-in barrier resistance suggests an additional systemic effect exerted by the CS components that might dissolve in the cell culture medium during the 30 minutes of exposure.

To conclude, CS exposure negatively impacts the skin barrier integrity of the reconstructed human skin model at the early stage of the ALI culture during which the SC layer appears to be more vulnerable and weaker as well as at later stages when the protective SC layer is more mature and fully developed. The impact is even more pronounced when the medium is not refreshed after exposure. Interestingly, a repetitive CS exposure triggers an adaptive response in the exposed RHEs, this is indicated by a barrier resistance restoration similar to the TEER of unexposed RHEs.

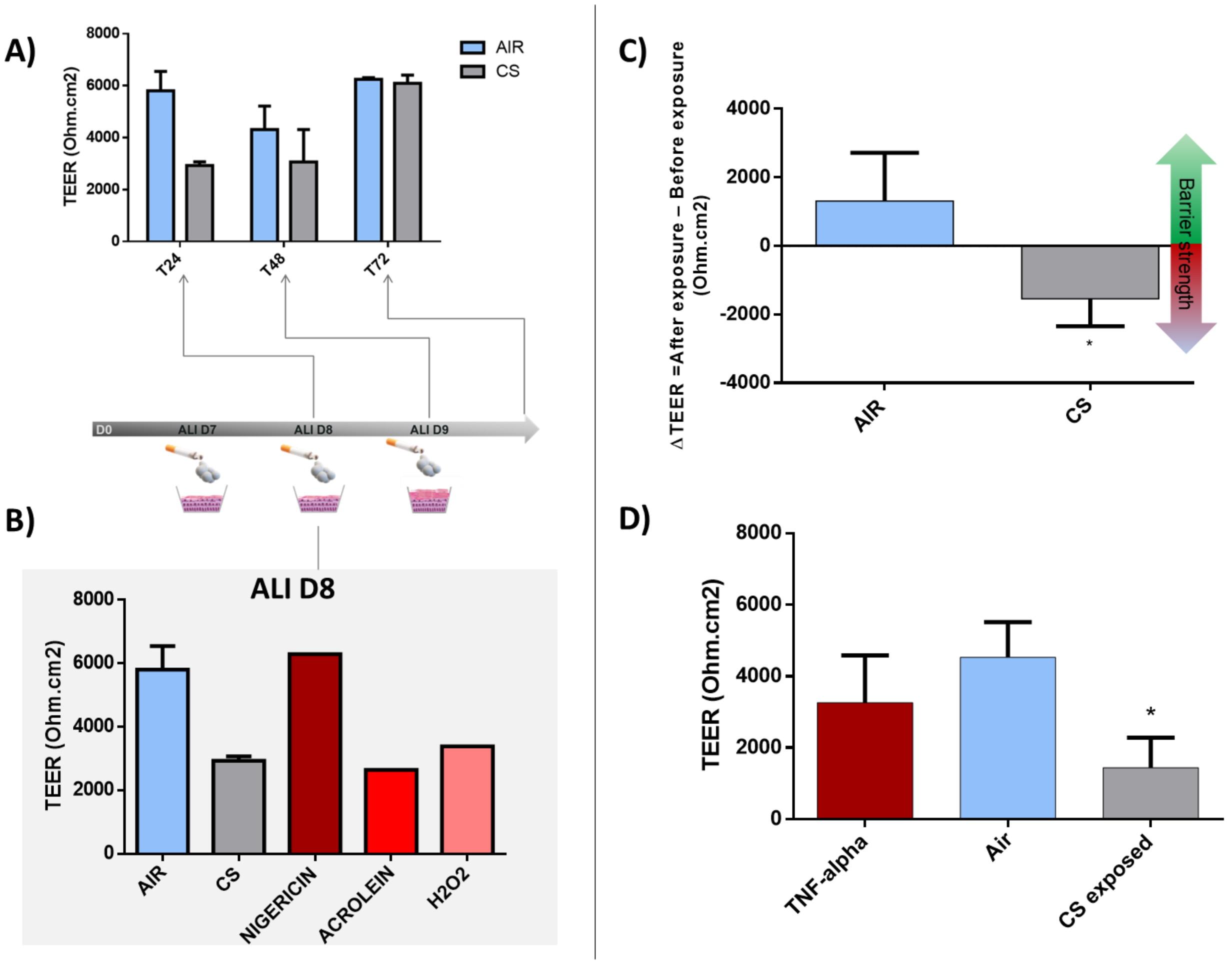

Figure II-2. A). TEER measured after 1, 2, and 3 cycles of Air/CS exposure respectively at air-liquid day 7, 8, and 9 and subsequently harvested 24h after exposure, at respectively ALI D7, D8, and D9. Data are presented as mean TEER ± SEM; n=2 tissues per condition. B). TEER measured 24h after Air/CS exposure or treatment with H_2O_2 (200 µM), Acrolein (30 μM), and Nigericin (5 μM). Data are presented as mean TEER ± SEM; n=2 tissues per condition. C). ΔTEER calculated between TEER values measured before and after exposure to Air/CS at the air-liquid day 14. Data are presented as mean ΔTEER ± SEM and were analyzed by t-test and n=3 tissues per conditions; * $p<0.05$. D). TEER measured 24h after exposure to Air/CS and TNF-α (50 μM) at air-liquid day 14 with no medium refresh after exposure. Data are presented as mean TEER ± SEM and were analyzed by two-way ANOVA with n=3 tissues per conditions; * $p<0.01$.

Effect of whole CS and single CS components on the RHE morphology at early stages of ALI

Tissue morphology was analyzed for the cell shape and observations in all skin layers via Hematoxylin (nuclei stained in purple) and eosin staining (cytoplasm stained in pink-red). It is important to take into account that the RHEs can come out curled and folded following tissue fixation, processing, and dehydration. Non-transversal sectioning may influence the tissue morphology, hence results in a wrong interpretation in terms of thickness or number of viable layers, therefore a qualitative analysis of the morphology was preferred.[429]

H&E staining of RHEs exposed to Air and CS at air-liquid day 14 **Figure B-II-3A** reveals a similar morphology with all epidermal layers from the proliferating basal cells attached to the polycarbonate membrane up to the cornified cells. As no difference in morphology was noted at air-liquid day 14, RHEs were then exposed at earlier stages of the epidermal reconstruction, i.e. at ALI day 7, 8, and 9, in order to evaluate any potential morphological changes. The H&E images on **Figure B-II-3B** show the evolution of the RHE exposed to 1, 2, and 3 cycles of Air/CS and harvested 24h after exposure. No drastic morphological alterations were observed, tissues exposed to Air and CS exhibit a similar and normal skin epidermal morphology with an increase of the SC thickness over time cultured at ALI. Lecas et al. were able to observe morphological impairment after two expositions to a VitroCell cloud chamber mimicking tobacco smoke (TS) such as a damaged stratum spinosum and stratum granulosum compared to tissue exposed to air under the same conditions.[196]

Following these results, the effect of CS components Acrolein and H_2O_2 on the RHE morphology were also evaluated after a topical treatment at air-liquid interface day 7. In addition, the effect of Nigericin was also assessed as a positive control for inflammasome activation. A detailed analysis of the morphology is described in **Table B-II-1** offering a comparison between RHEs exposed to Air, CS and treated with Acrolein, H_2O_2, and Nigericin at air-liquid day 7 and incubated for 24h to be subsequently harvested at ALI D8.

As shown in **Figure B-II-3B and C**, all the tissues present distinct epidermal layers: the stratum basale, stratum spinosum, stratum granulosum, and anuclear stratum corneum. Overall, all SC is relatively thin and the epidermal number of viable cell layers is estimated to 5-6 in all RHEs. The SC layers from the H_2O_2- and Acrolein- treated RHEs appear more packed compared to RHEs exposed to Air, CS, and Nigericin.

Interestingly, a major impact on the morphology was observed upon topical treatment with Nigericin, a potent microbial toxin inducing a drop in intracellular levels of potassium that was used here as an inflammasome inducer[427]. The effect of Nigericin on top of a reconstructed skin model was not described yet in the literature. Its toxic effect is well perceived on the H&E pictures **Figure B-II-3B and C** and is characterized by the detrimental morphologic alterations that mainly affecting the upper viable skin layers. The presence of necrotic cells with pyknotic nuclei and large empty vacuoles due to cytoplasm depletion is revealed in both the stratum granulosum and the stratum spinosum layers. The cells from the stratum basale are abnormally round.

Acrolein-treated RHE also presents a large number of cells with abnormally dilated cytoplasm appearing in white in the SG and SS. The stratum basale of Acrolein, $H_2O_2$and CS-treated RHE contains cells with more intercellular space than in the Air-exposed RHE section.

Table B-II-1. Comparative analysis of the morphology of RHEs harvested at air-liquid day 8 after exposure to AIR/CS or treatment with H_2O_2, Nigericin, and Acrolein.

Treatment	**Stratum Corneum**	**Stratum Basale**	**Stratum Spinosum**	**Stratum Granulosum**
AIR	Presence of a thin SC with few loosed corneocyte layers slightly	Basal cells of the cubical shape	presence of normal round cells	presence of normal elongated cells with visible keratohyalin granules
CS	Presence of a thin SC with few loosed corneocyte layers	Basal cells of cubical shape with intercellular space	presence of normal round cells	presence of normal elongated cells with visible keratohyalin granules
H_2O_2	Presence of a thin SC with few packed corneocyte layers	Basal cells of cubical shape with intercellular space	presence of normal round cells	presence of normal elongated cells with visible keratohyalin granules
NIGERICIN	Presence of a thin SC with few loosed corneocyte layers	Basal cells of round shape	Presence of abnormal necrotic cells, small pyknotic nuclei with dilated cytoplasm (appears white)	Presence of necrotic cells, small pyknotic nuclei with dilated cytoplasm (appears white)
ACROLEIN	Presence of a thin SC with few packed corneocyte layers	Basal cells of cubical shape with intercellular space	Presence of cells with dilated cytoplasm	presence of normal elongated cells with visible keratohyalin granules

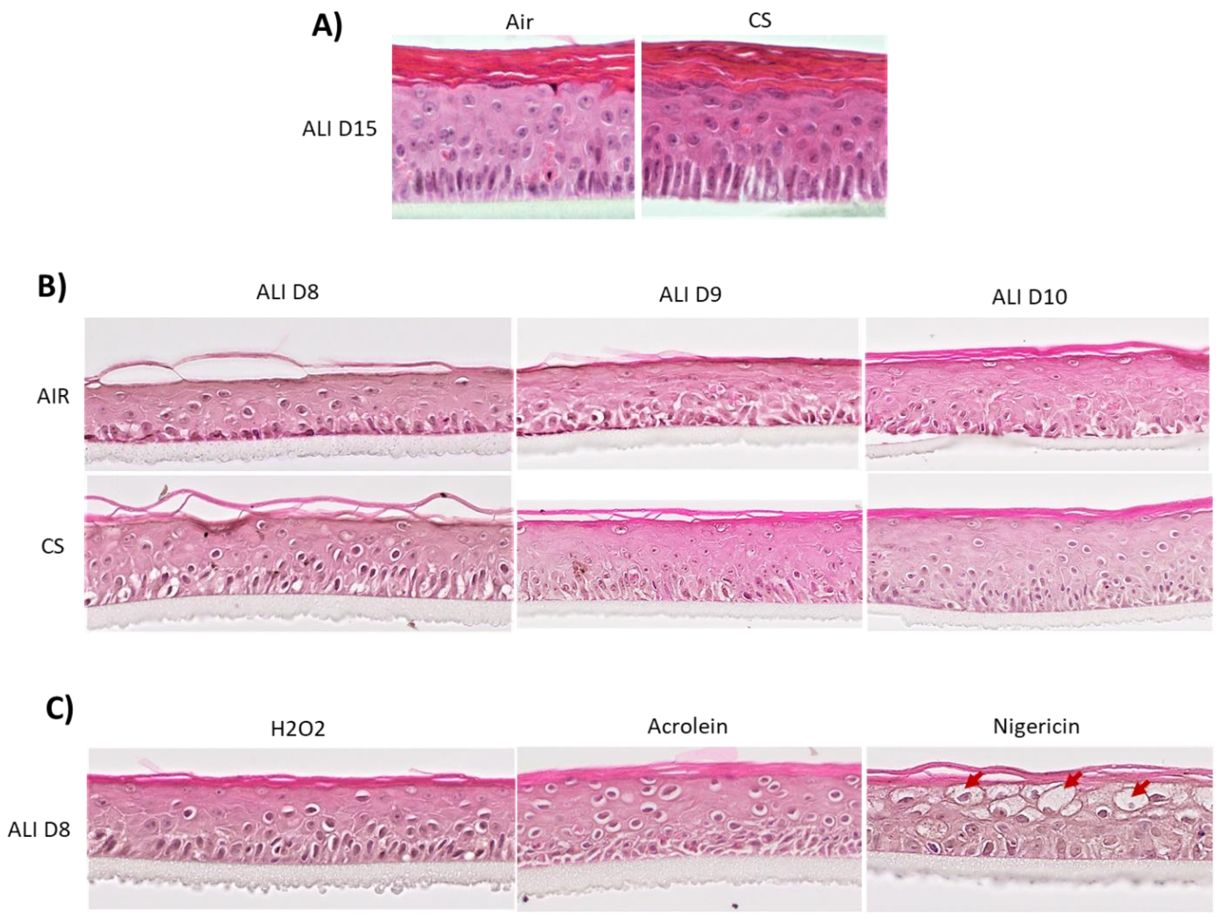

Figure B-II-3. A). Tissue morphology evaluated by H&E staining of RHE exposed to only one cycle of Air/CS and harvested at air-liquid interface day 14. Magnification 40x; Nikon Microphot FXA microscope (Nikon Instruments). B). Tissue morphology evaluated by H&E staining of RHE exposed to respectively 1,2 or 3 cycles of Air/CS and harvested at different stages of air-liquid interface ALI D8, ALI D9, and ALI D10. B). Tissue morphology evaluated by H&E staining of RHE topically treated with H_2O_2 (200 µM), Acrolein (30 µM), and Nigericin (5 µM) and harvested at ALI D8. Red arrows indicate empty vacuoles. Magnification 20x; Nikon Microphot FXA microscope (Nikon Instruments).

Effect of whole CS and single CS components on the RHE ultrastructure at early stages of ALI

A qualitative analysis of the ultrastructure was performed with TEM images of RHE exposed to CS, Air, or treated with Acrolein, H_2O_2, and Nigericin. A detailed description of each skin compartment per treatment condition is summarized in **Table B-II-2**.

Overall, all tissues exposed to CS and Air and tissues treated with Acrolein, H_2O_2, and Nigericin exhibit a normal ultrastructure in the upper skin layers with a normal number of packed corneocyte layers in the SC of approximately 10-15 layers. All tissues present keratohyalin granules in the SG except for Nigericin-treated tissues which display a vast number of empty vacuoles all over the SG due to cytoplasm loss, this reflects a clear sign of necrosis induced by a direct toxic effect of Nigericin topically applied.

At the level of the SB, some differences were observed between all tissues. RHE exposed to Air is inducing cell detachment characterized by visible tight junction proteins stained in darker grey. Moreover, the first signs of apoptosis are noticed with the presence of apoptotic bodies, this might be due to cell turnover.

The SB of CS exposed RHE clearly shows an increased autophagy flux respectively to the other conditions with the vast presence of permeabilized lysosomes that appear as black as electron-dense and digested vacuoles. In addition, perinuclear chromatin condensation that appears stained as darker and cell shrinkage characterize the signs of regulated necrosis. Damaged cells are more vulnerable and start to detach, this can be visualized by the reduction of tight junctions and a consequent increase of intercellular space.

The SB morphology of acrolein-treated tissues was not strongly affected. Nonetheless, SC layers are more loosely packed respectively to other treated tissues.

Similar to CS exposed tissues, the SB of H_2O_2 topically treated RHEs present signs of increased autophagic flux with a vast presence of lysosomes. Cell detachment was also observed with the reduction of tight junctions and large intercellular space. Damaged cells are characterized by cytoplasm loss, loss of cell components, digested bodies, cell shrinkage due to the oxidative effect of H_2O_2 treatment.

The SB cells of nigericin-treated RHE cells present vast vacuoles, damaged cell components such as ER, Golgi apparatus, mitochondria, large intercellular space, and nuclear shape alteration. All of these observations reflect the necrosis induced by the toxic effect of Nigericin from the top layers reaching the bottom layers.

Table B-II-2. Ultrastructure qualitative analysis of RHE exposed to AIR/CS or treated with Acrolein, H_2O_2, and Nigericin. SC: Stratum Corneum, SG: Stratum Granulosum, SP: Stratum Spinosum

	AIR	**CS**	**Acrolein**	**H_2O_2**	**Nigericin**
STRATUM CORNEUM	10-15 of packed SC layers	10-15 of packed SC layers	10-15 of slightly detached SC layers	10-15 of packed SC layers	10-15 of packed SC layers
STRATUM GRANULOSUM	Presence of keratohyalin granules	Presence of keratohyalin granules	Presence of keratohyalin granules	Presence of keratohyalin granules	A vast amount of empty vacuoles present in SG and SP due to cytoplasm loss
STRATUM BASALE	Initiation of cell apoptosis due to the presence of an apoptotic body. Cell detachment signs are characterized by visible tight junctions and large intercellular space.	Autodigestion of cells due to a large number of lysosomes. Signs of necrosis include nuclear chromatin condensation and cell shrinkage.	Presence of cubical cells with degraded cell components dissociated by large intercellular space.	Autodigestion of cells due to a large number of lysosomes. Signs of necrosis include cell shrinkage and the presence of vacuoles. Cell detachment signs are characterized by visible tight junctions and large intercellular space.	Signs of necrosis include cell shrinkage, vacuoles, nuclear chromatin condensation, the presence of damaged cell components (ER, Golgi). Cell detachment signs are characterized by visible tight junctions and large intercellular space.

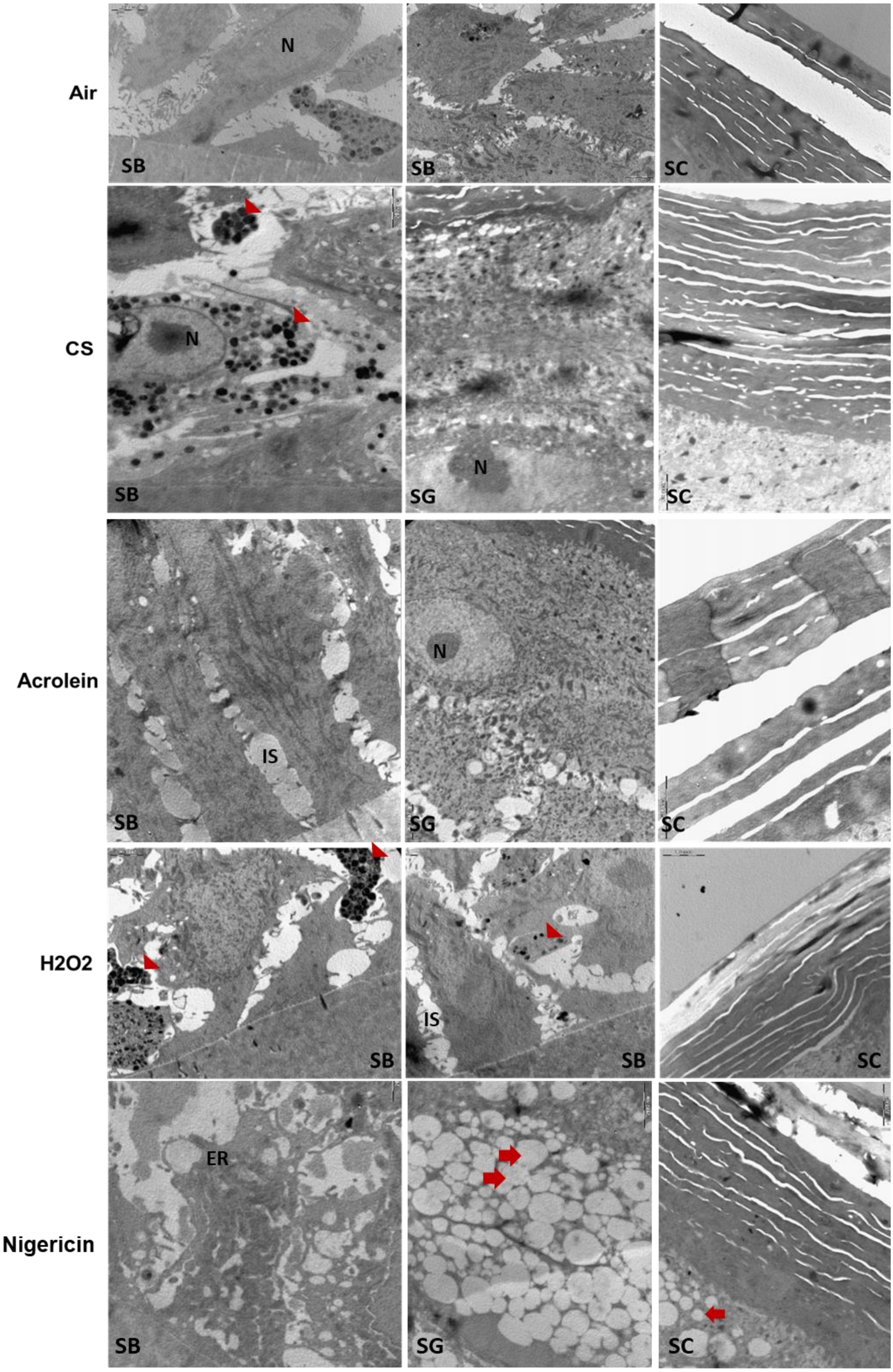
Air
N
SB
SB
SC
CS
N
SB
N
SG
SC
Acrolein
IS
SB
N
SG
SC
H2O2
SB
IS
SB
SC
Nigericin
ER
SB
SG
SC

Figure B-II-4. TEM micrographs of RHE exposed to AIR/CS or treated with Acrolein, H_2O_2, and Nigericin. Red arrows indicate empty vacuoles, red arrowheads indicate lysosomes stained in darker intensity. Hitachi H100 transmission electron microscope, magnification used was 5k X. Scale bar is 2000 nm. ER: Endoplasmic Reticulum; N: nucleus; IS: intercellular space; SC: Stratum Corneum, SG: Stratum Granulosum, SP: Stratum Spinosum, SB: Stratum Basale.

Visualization of CS particles on top of RHE

Small CS particles adhering at the surface of the RHE were visually detected on the transmission electron micrograph (**Figure B-II-5**). Although some studies have demonstrated a transcutaneous penetration of PM into the skin layers of a commercial RHE model (EpiDerm™, MatTek Corporation), highlighting the physiological weakness of the model, this was not perceived with the RHE model.[273] We can conclude that the barrier of the RHE model is a strong permeable barrier resembling the human skin. In addition, a SEM analysis could be useful to identify and visualize potential heavy metals at the surface of the RHE model.

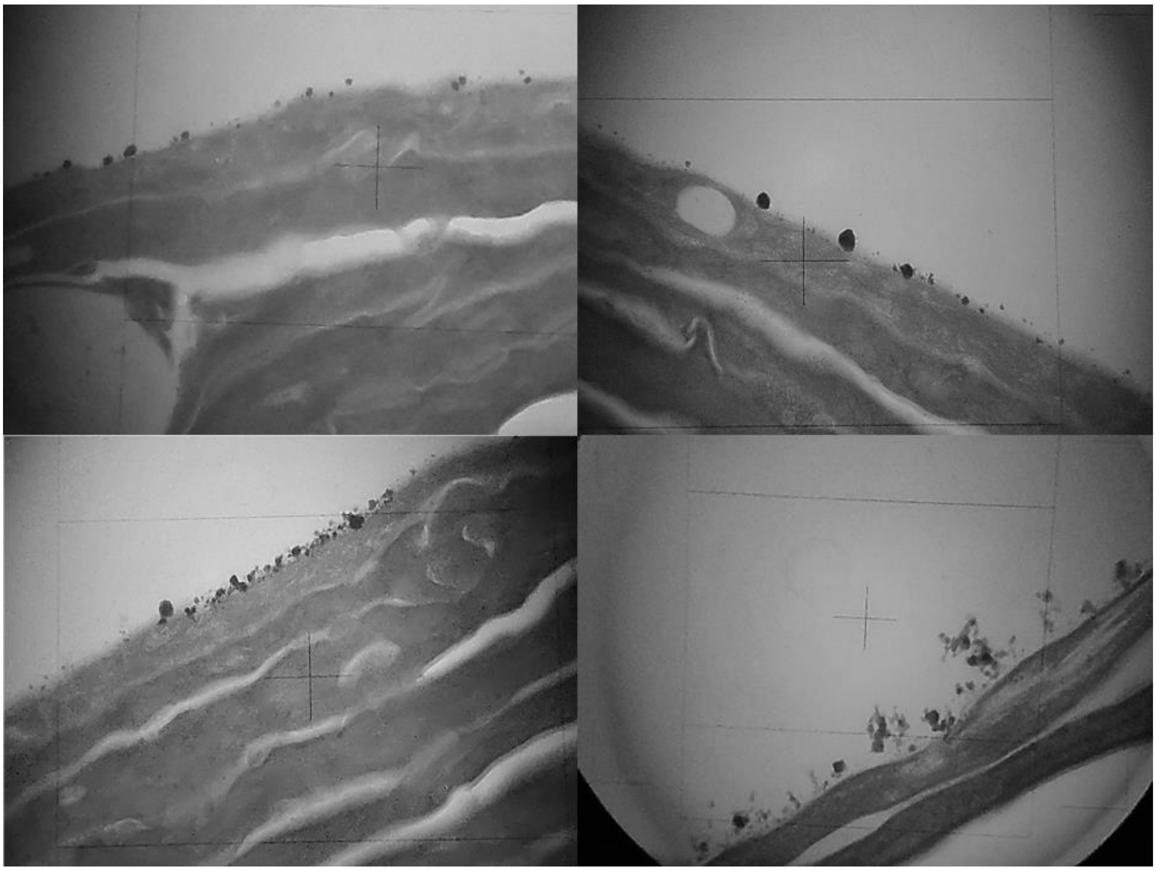

Figure B-II-5. Transmission electron micrograph of the RHE model with detection of CS particles adhering at the surface of the SC after 30 minutes exposure with two cigarettes. Two samples were examined per condition. Hitachi H100 transmission electron microscope, magnification used was 80K.

Effect of whole CS on the RHE surface at early stages of ALI

Based on preliminary SEM analysis results showing no change between the surface of RHE exposed to Air/CS at air-liquid day 14, RHEs were analyzed at an earlier stage of ALI (D8, D9, D10) after 1, 2, and 3 cycles of Air/CS exposure respectively. **Figure B-II-6** displays scanning electron images of RHE sample exposed to Air or CS subjected to a comparative evaluation. The left images show the epidermis cross-section while the right images display the surface topography of the skin. The surface of Air-exposed RHEs appears rougher with a vast number of blisters whereas CS-exposed RHEs surface contains smoother areas. The boundaries between corneocytes are more visible in the air-exposed RHEs. The surface of RHEs exposed to 3 cycles of CS consists of larger spherules and ridges compared to the other samples.

The epidermis cross-section images all present resembling packed scaly corneocytes of the horny layer. Although the thickness of the CS-exposed RHE seems greater, the thickness was preferably not compared since the skin orientation during tissue processing and sectioning strongly influence may lead to a wrong interpretation.

Overall, the surface arrangement of flat corneocytes in the SC was comparable. We were unable to detect CS particles adhered on top of the RHE models.

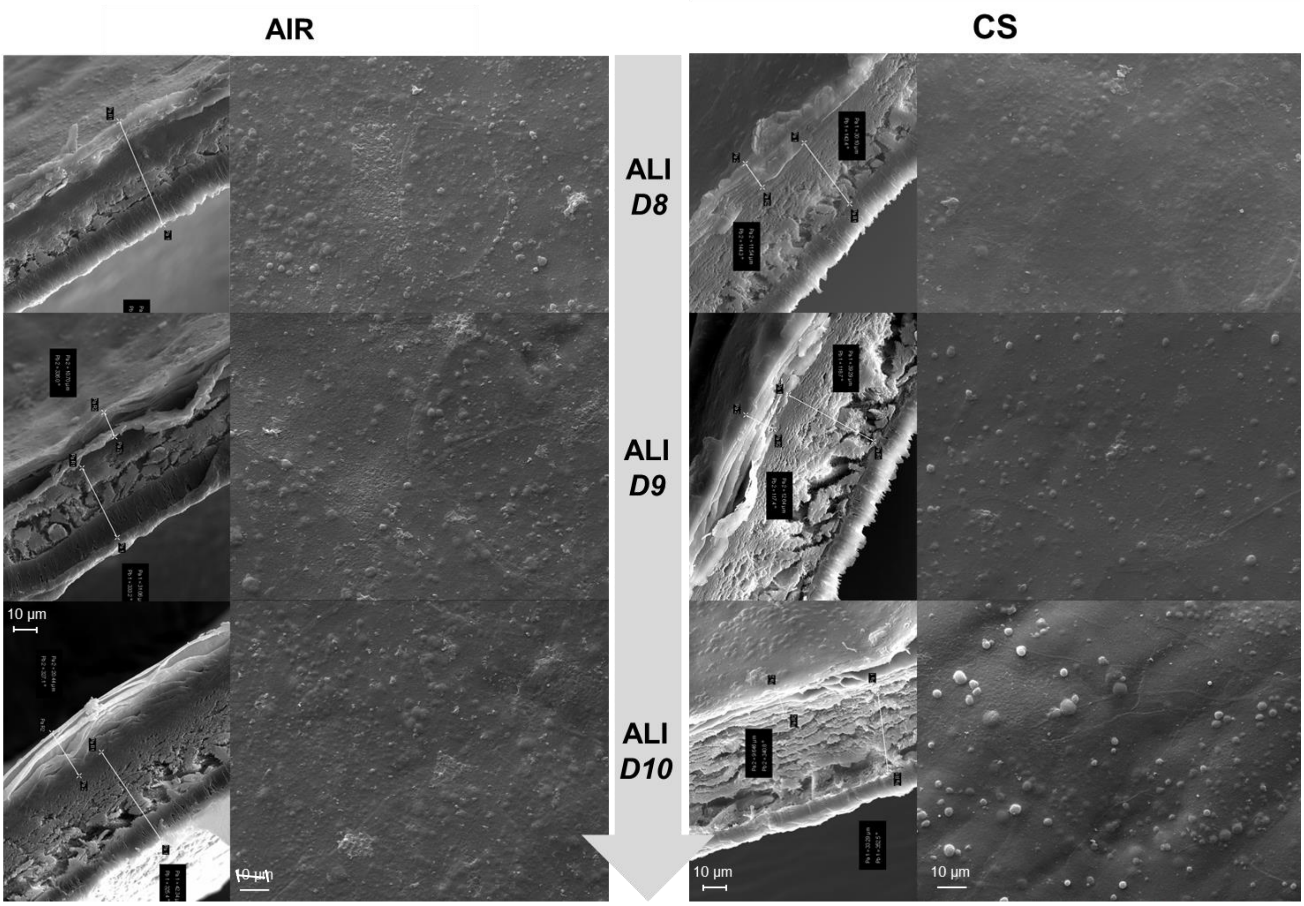

Figure B-II-6. Scanning electron micrograph showing both the cross-section (left images) and surface topography (right images) of RHEs exposed to 1, 2, or 3 cycles AIR/CS and harvested 24h after exposure at a different stage of the air-liquid interface: ALI D8, ALI D9, and ALI D10 respectively. Hitachi H100 transmission electron microscope, magnification used was 2.5k X. Scale bar is 10 µm.

CS exposure does not affect the expression of epidermal proteins cytokeratin 10, involucrin, and loricrin

To further investigate the impact of CS on the skin epidermal barrier, the expression of epidermal proteins cytokeratin 10 (K10), loricrin (LOR), and involucrin (IVL) was evaluated post-CS exposure. These proteins all play an important role in the different stages of epidermal barrier formation. Dysfunction or mutation of these proteins has been associated with several skin diseases.[430]

Cytokeratin 10 (K10) is considered as an early differentiation marker, whereas late differentiation proteins involucrin and loricrin are expressed in the upper layers[431,432].

Figure B-II-7A presents the immunostaining pictures for loricrin and involucrin staining after exposure to Air, CS with or without a medium switch. As confirmed by quantification in **Figure B-II-7B**, no difference was measured between the protein staining intensity between all conditions. Although incubating the RHEs in the exposed medium reduced the barrier resistance, the expression of epidermal proteins was not affected.

We, therefore, measured the effect of CS exposure at an earlier stage of the ALI (**Figure B-II-8**) on the early differentiation marker cytokeratin 10 (K10), and a comparable K10 expression following exposure to Air, CS, and H_2O_2 was detected.

To conclude, CS did not alter the expression of all three markers which are localized in the appropriate epidermal layers. Even though previous studies reported changes in expression, on one hand, loricrin expression was considerably reduced upon tobacco smoke exposure in a commercial RHE model, and on the other hand, an increase in filaggrin expression was noted in RHE treated with CSE for a longer period from an earlier differentiation stage.[196,231] Impacting the proteins involved in the skin barrier formation most likely requires a chronic treatment throughout the ALI culture, such as feeding the skin models with a conditioned medium containing cytokines or chemicals, as it was previously demonstrated to reproduce impaired skin conditions *in vitro*.[418,419]

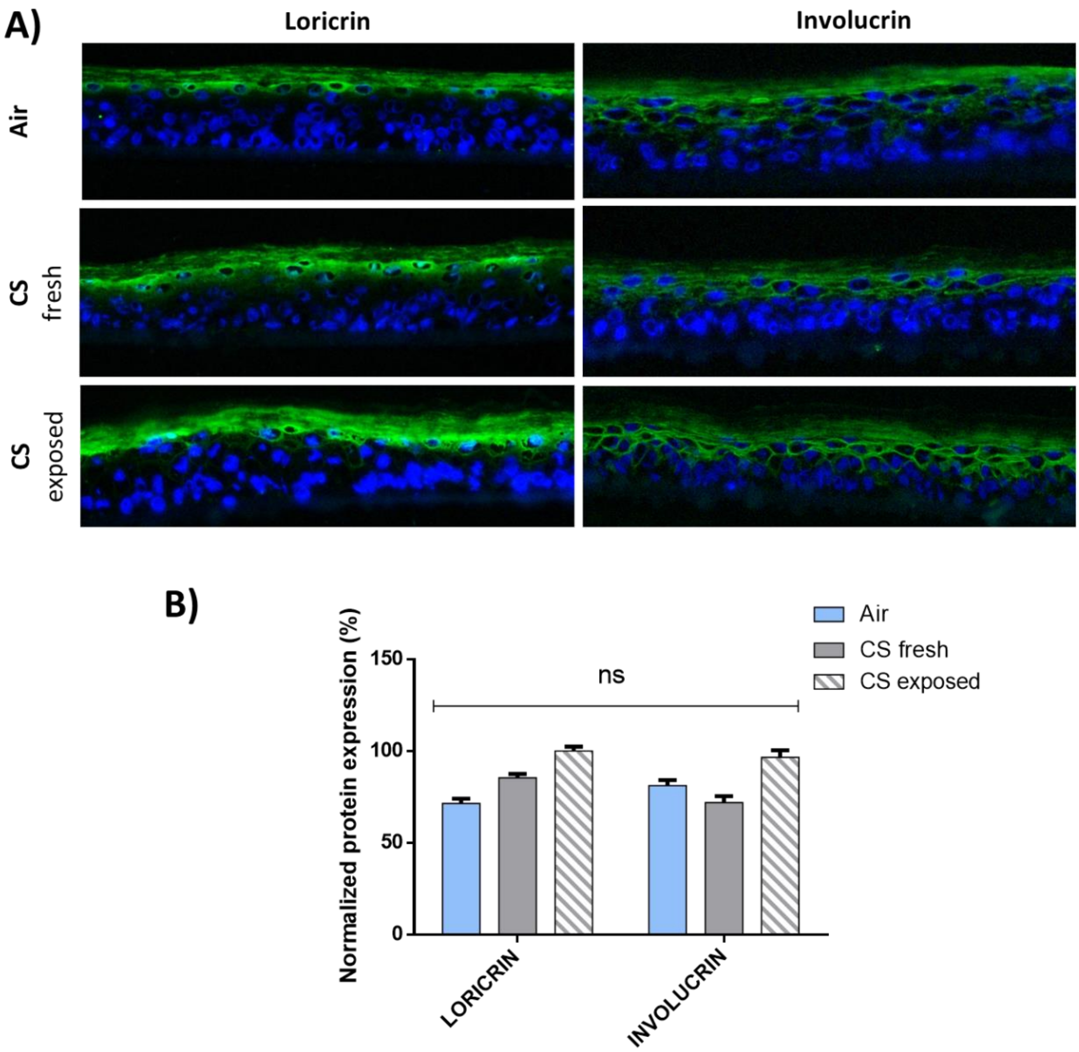

Figure B-II-7 Immunohistochemical staining for A). loricrin (left) and involucrin (right) proteins in RHE after exposure to Air (Control) or CS at air-liquid day 14 with and without post-exposure medium refresh. Nuclei (blue) were stained with DAPI. Magnification 20x; Nikon Microphot FXA microscope (Nikon Instruments). B). Quantification of fluorescence in total RHE of loricrin and involucrin proteins is calculated with ImageJ software and plotted using Graph Pad software. Data were normalized to the highest fluorescence intensity ("CS exposed") and expressed as % protein expression ± SD; n=3 tissues per condition.

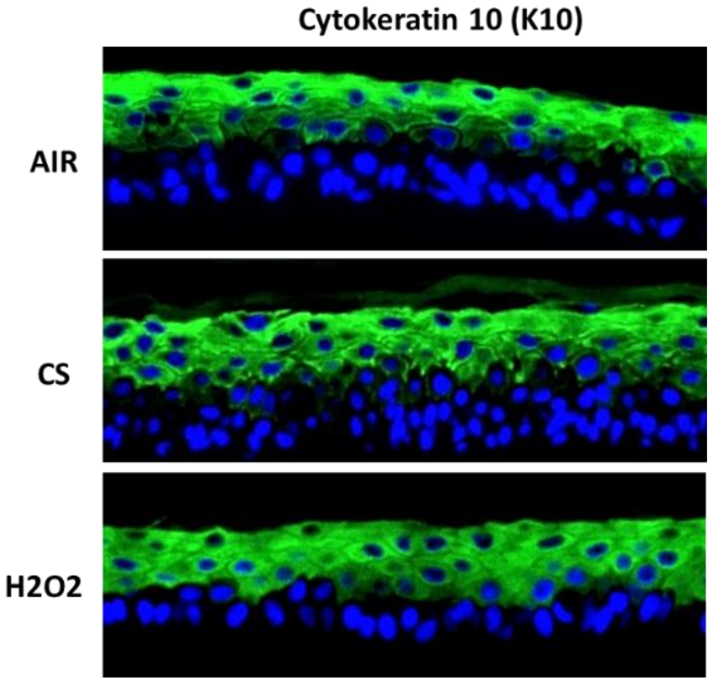

Figure B-II-8. Immunohistochemical staining for cytokeratin 10 (K10) in RHE after exposure to Air (Control), CS, or treatment with H_2O_2 at air-liquid day 7 and harvested 24h after exposure/treatment. Nuclei (blue) were stained with DAPI. Magnification 20x; Nikon Microphot FXA microscope (Nikon Instruments).

3. CS-induced oxidative stress responses in a RHE

CS exposure increases the formation of 4-HNE protein adducts

Our experiments demonstrate an increase in 4-HNE-protein adducts was observed in RHEs exposed to CS for 30 minutes and incubated for 24h with or without medium switch after exposure. A slightly more increased 4-HNE protein adducts level is observed when the skin tissues were incubated in an exposed medium, this might be the consequence of CS diluted components exerting a systemic effect from the basal compartment (**Figure B-II-9A**)

4-HNE half-life has been shown to differ from cell types and tissues which might metabolize it more efficiently or more quickly.[433,434] Therefore, the determination of an appropriate time point to measure 4-HNE is essential since it might be rapidly detoxified by enzymes to avoid its detrimental accumulation within the cells. However, here we were able to detect it 24h after exposure, this reflects a longer half-life than other ROS making it a valuable marker of oxidative stress.

In an additional experiment, 4-HNE expression was evaluated after exposure to Air/CS and treatment with H_2O_2/Acrolein/Nigericin at earlier stages of the air-liquid culture (day 7). **Figure B-II-10B** shows the IF images and quantification revealing a slightly higher 4-HNE stained in the H_2O_2/Acrolein/Nigericin treated sections, however, a similar intensity was measured in both Air- and CS-exposed RHEs.

It was also noticed that the 4-HNE intensity measuring the level of oxidative damage faded over time culturing from ALI D8 to ALI D10 (**Figure B-II-10A**), this could translate to an increase in the strength and resistance against oxidative stress.

To conclude, CS can enhance 4-HNE production in a 3D *in vitro* skin model, this provides insights into the mechanisms involved in the CS-induced cutaneous toxicity.

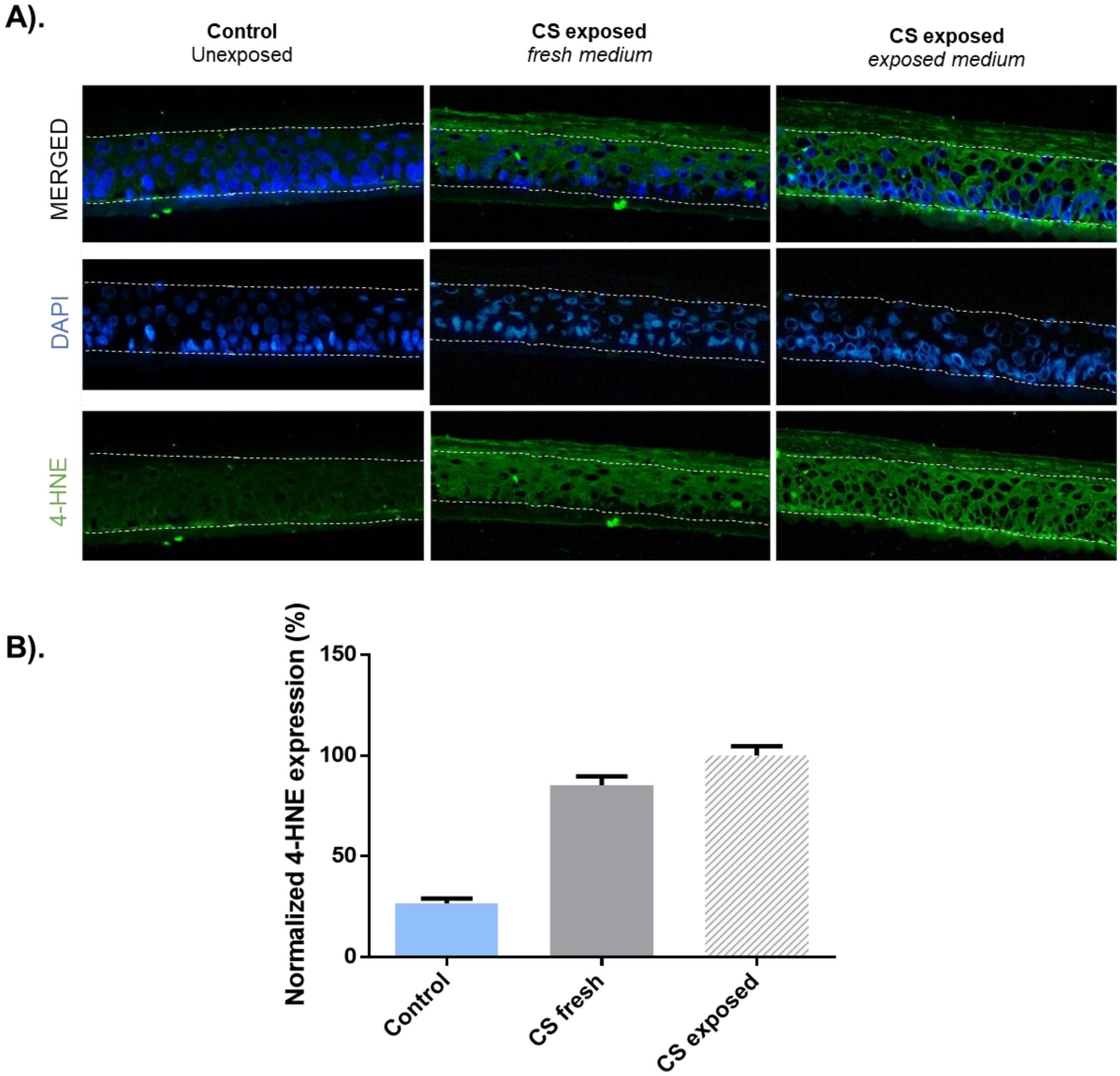

Figure B-II-9. A). Immunohistochemistry of 4-HNE protein adducts of RHEs exposed for 30 minutes to Air/CS with and without medium switch after exposure. Discontinued white lines dissociate the cell viable layers from the membrane (bottom line) and the SC (upper line). Nuclei (blue) were stained with DAPI. Magnification 20x; Nikon Microphot FXA microscope (Nikon Instruments). B). Quantification of fluorescence in total RHE of 4-HNE protein adducts is calculated with ImageJ software and plotted using Graph Pad software. Data were normalized to the highest fluorescence intensity ("CS exposed") and expressed as % protein expression ± SD from n=3 tissues per condition.

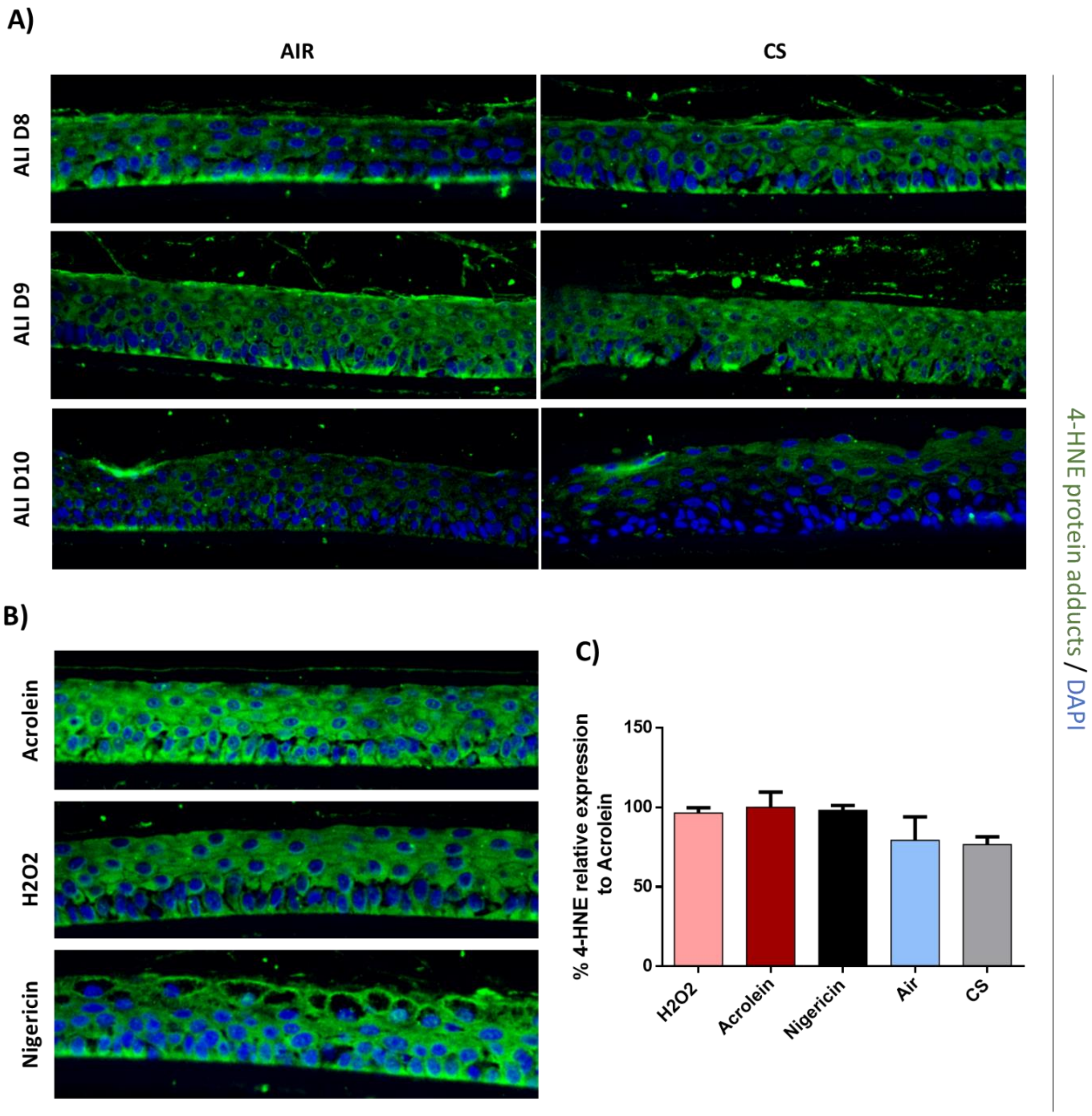

Figure B-II-10. Immunohistochemical analysis of 3D-cultured RHEs. A). RHEs cultured at the air-liquid interface were exposed to Air/CS on ALI day 7, 8, and 9 and post-exposure incubated for 24h before being fixed and immunostained with the anti-4-HNE antibody. B). RHE cultured at the air-liquid interface were topically treated with Acrolein/ H_2O_2/Nigericin at ALI day 7 and incubated for 24h before being fixed and immunostained with the anti-4-HNE antibody. Nuclei (blue) were stained with DAPI. Magnification 20x; Nikon Microphot FXA microscope (Nikon Instruments). C). Quantification of immunofluorescence staining for 4-HNE intensity for tissues treated or exposed at air-liquid interface 7 with Air, CS, H_2O_2, Acrolein, Nigericin and harvested 24h later. Quantification has been performed using ImageJ software and plotted with GraphPad software. Data were normalized to the highest intensity sample (Acrolein) and expressed as % intensity relative to Acrolein ± SD; n=2 tissues/condition.

Nrf2 translocates to the nucleus in response to CS, Acrolein, and H_2O_2 exposure in a RHE

Since Nrf2 is the key transcription factor regulating the antioxidant defense response, twenty-four hours after exposure to Air/CS, we have assessed its expression in reconstructed skin models cultured at the air-liquid interface (ALI) for 14 days, presenting a mature stratum corneum layer. RHEs exposed to CS present a more abundant Nrf2 protein signal especially in the stratum granulosum compared to the Air exposed RHEs. Nuclear translocation of Nrf2 is clearly observed in the bottom cell layers respectively to the Air exposed RHEs where nucleus are not stained and appears empty in **Figure B-II-11a**.

To evaluate the impact of CS on RHEs with a thinner SC, Nrf2 expression was also measured at earlier stages of reconstruction at day 8, 9, 10 of the air-liquid interface (ALI) after one, two, or three cycles of Air/CS exposure respectively (**Figure B-II-11c**). A more abundant Nrf2 expression was observed in the SG and SB layers of the CS-exposed RHEs, in both the cytoplasm and nucleus of cells, highlighting a nuclear translocation. However, the RHE exposed to Air only exhibits cytoplasmic Nrf2 staining while cell nuclei appear black. On day 10 of ALI, the Nrf2 signal was similarly distributed after Air and CS exposure with a higher intensity in the SG layer. It has been assumed that after the second cycle of CS exposure at day 8, the tissues react by triggering an adaptive response and restores unstimulated Nrf2 signaling. This immunocytochemical data are correlated with the transepithelial electrical resistance (TEER) measured at days 8, 9, 10 of the air-liquid interface (ALI), reflecting a barrier resistance recovery already after two cycles of CS exposure.

On day 8, some RHEs were topically treated with two CS components, Acrolein at 30 µM and H_2O_2 at 200 µM and also checked for Nrf2 expression (**Figure B-II-11b**). Upon both treatments, Nrf2 signaling is highly abundant and overall distributed in the skin viable layers. As expected, Nrf2 nuclear translocation was particularly visible in the tissues treated with Acrolein, directly interacting with the Keap1 cysteine moieties which fail Nrf2 inhibition and its subsequent nuclear translocation.

These observations suggest that Nrf2 signaling is increased in case of oxidative stress triggered by CS exposure or treatment with CS components, H_2O_2 and Acrolein. To conclude, CS-induced oxidative injury to the outermost layers of the skin results in Nrf2 nuclear translocation, an important protective response by skin epithelial cells.

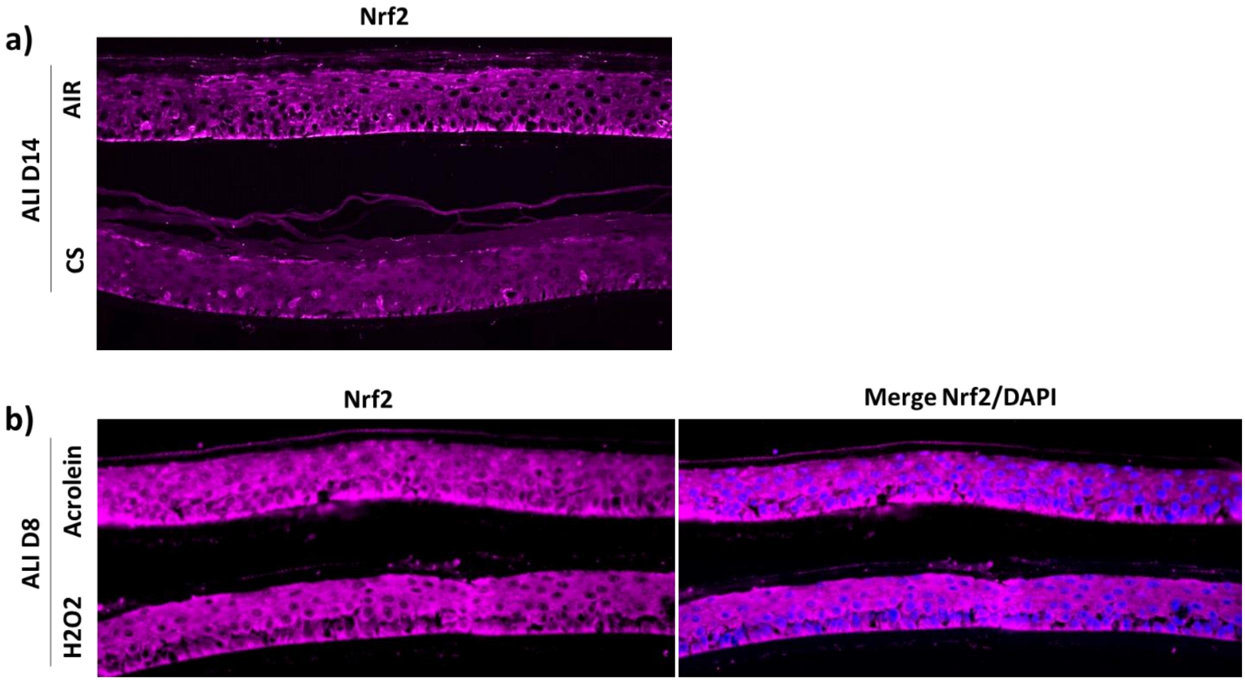

c)

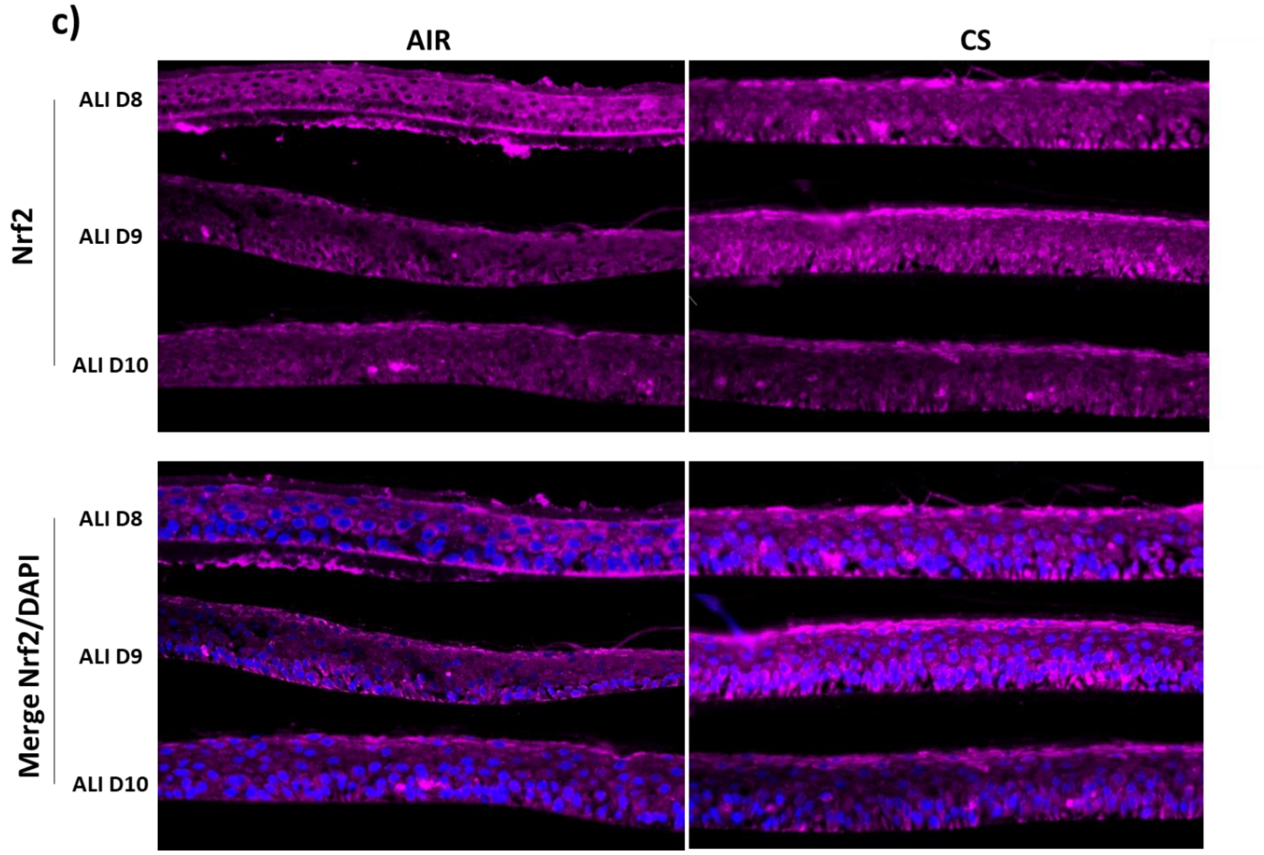

d).

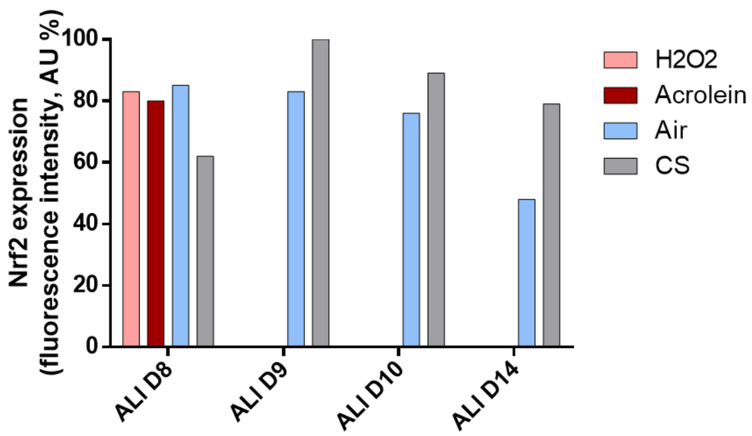

Figure B-II-11. Immunohistochemical analysis of 3D-cultured RHEs. a). RHEs cultured at the air-liquid interface were exposed to Air/CS on ALI day 14 and incubated for 24h before being fixed and immunostained with the anti-Nrf2 antibody. b). RHE cultured at the air-liquid interface were topically treated with Acrolein/H_2O_2 at ALI day 7 and incubated for 24h before being fixed and immunostained with the anti-Nrf2 antibody. c). RHEs cultured at the air-liquid interface were exposed to Air/CS on ALI day 7, 8, and 9 and post-exposure incubated for 24h before being fixed and immunostained with the anti-Nrf2 antibody. Nuclei (blue) were stained with DAPI. Magnification 20x; Nikon Microphot FXA microscope (Nikon Instruments). d). Quantification of immunofluorescence staining for Nrf2 intensity at different days of air-liquid interface for tissues exposed to Air/CS or treated with H_2O_2/Acrolein and harvested 24h later. Quantification has been performed using ImageJ software and plotted with GraphPad software. Data were normalized to the highest intensity sample ("CS ALI D9") and expressed as % intensity relative to "CS ALI D9" ± SD.

4. Using the RHE as a valuable tool to screen protective antioxidant solutions

The stratum corneum is the main skin barrier and represents a major obstacle for the penetration and delivery of active substances. To tackle this issue, ethosome vesicular structures have been developed to specifically enhance active permeation into the lower skin layers by acting mainly on the solubility of the SC lipids and cell permeation enhancement[435,436]. The objective of this investigation was to test some designed and well-characterized ethosome vesicular systems for antioxidant topical delivery into the skin and test their efficiency in our RHE model. Ethosomes vesicles were used as percutaneous delivery systems for coenzyme Q10 active, a known endogenous antioxidant commonly used for skin care applications. The following data have been drawn from Sguizatto et al.[437]

Evaluation of 4-HNE Protein Adducts Levels in RHE Treated with ETHO-CoQ10

Since 4-HNE immunostaining was among the most reliable marker to evaluate the level of oxidative stress on our RHE, it was selected as the endpoint to investigate the efficiency of ethosomes as an active delivery system in our RHE models treated or not with a known oxidative CS component, H_2O_2. Based on previous studies, 90 minutes with H_2O_2 at a concentration of 200 µM was defined as our oxidative stress-inducing treatment. It is essential to test various ethosome pre-treatment duration to identify the optimal efficiency of the active. Indeed, a too-short pre-treatment might be insufficient to observe an anti-oxidant effect while a too-long treatment could lead to metabolic degradation or instability of the active. In this way, 6h and 24h of pretreatment were selected for the study as the shortest and longest time points.

Immunofluorescence analysis highlights an increased level of 4-HNE protein adducts in the H_2O_2 treated RHE compared to the untreated one. This intensity enhancement was reduced by the pretreatment with CoQ10 loaded in ethosomes suggesting a protective effect from oxidative damage (**Figure B-II-12**). The decrease in 4-HNE intensity was noted all over the skin layers including the stratum corneum (SC) with a 24h ETHO-CoQ10 pre-treatment whereas the staining persists in the SC after a 6h pre-treatment diminishing only in the viable layers (**Figure B-II-13)**. It is assumed that a longer pre-treatment influences the mode of action of the coenzyme Q10 resulting in an overall protecting effect.

To conclude, ethosome pre-treatment of 6 and 24h were both able to prevent partly H_2O_2 induced 4-HNE protein adducts formation in a RHE model. Nonetheless, it is important to point out that this *in vitro* skin model lacks physiological relevance about the realistic penetration rate and efficiency of the active which is overestimated compared to the case of native human skin. Therefore, these promising results *in vitro* require further validation *in vivo* to claim the “anti-oxidant” properties in a cosmetic formulation.

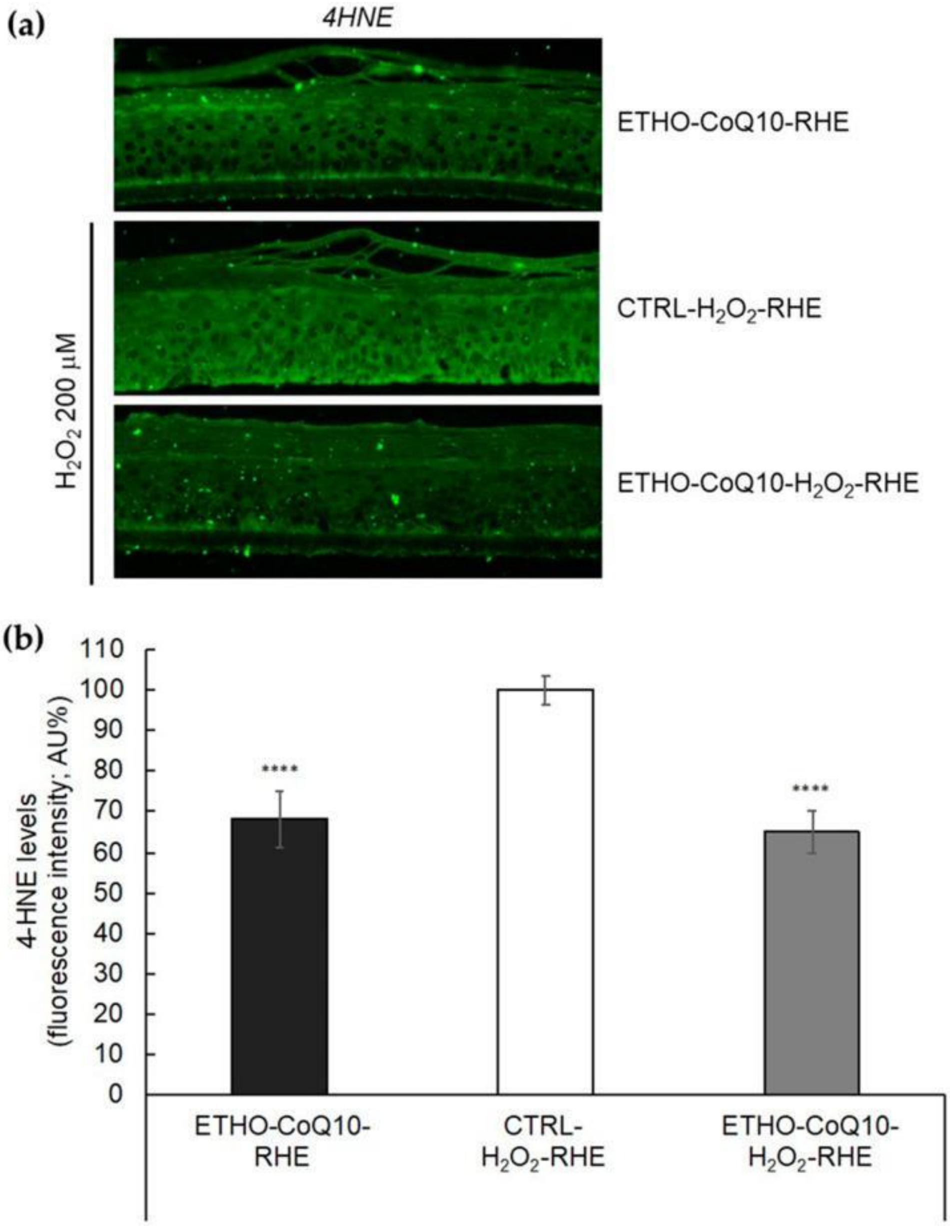

Figure B-II-12. Representative immunocytochemical images for 4-HNE protein adducts in portions of RHE pretreated for 24h with ETHO-CoQ10 (ETHO-CoQ10- H_2O_2-RHE) and compared to control RHE treated with ETHO-CoQ10 not exposed to H_2O_2 (ETHO-CoQ10-RHE), or RHE exposed to H_2O_2 200 μM of H_2O_2 for 90 min (CTRL- H_2O_2-RHE) (published data from Sguizatto et al). Images were taken at 40×. (b) Quantification of immunofluorescence staining for 4-HNE after H_2O_2 exposure. Data were normalized to CTRL- H_2O_2-RHE and expressed as arbitrary units ± SD. **** $p \leq 0.0001$ vs. CTRL.

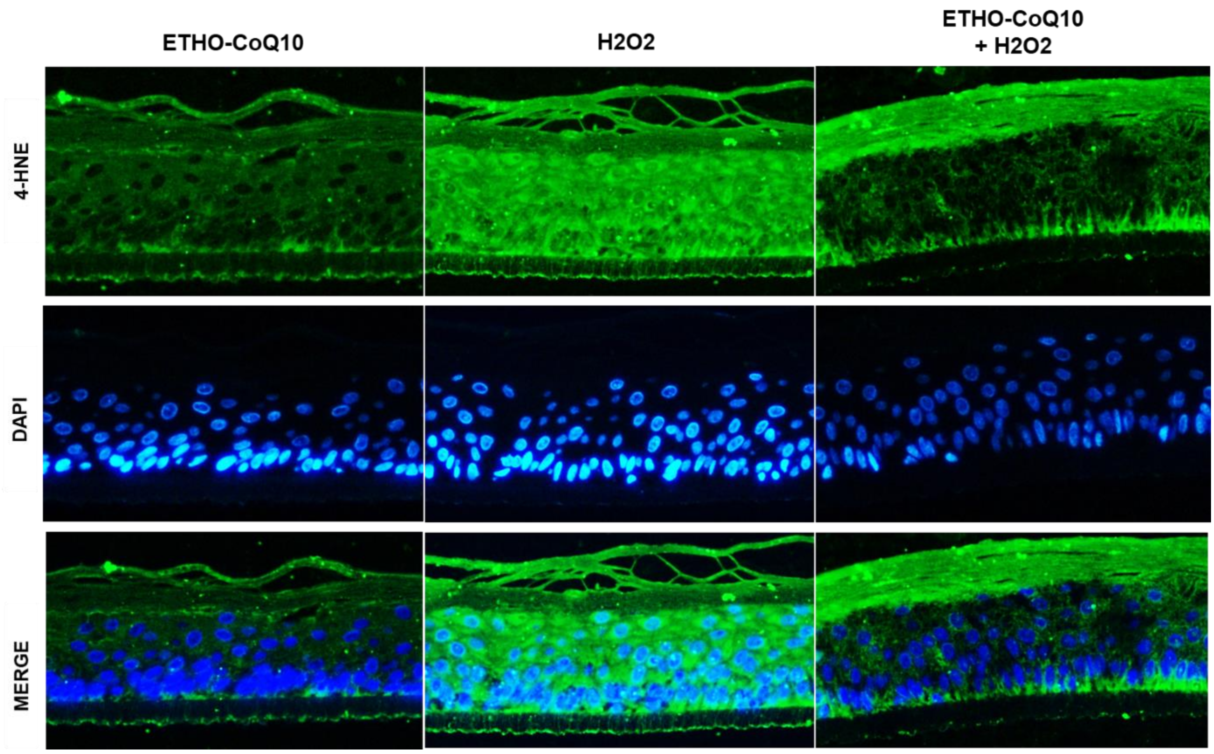

Figure B-II-13. Representative immunocytochemical images for 4-HNE protein adducts in portions of RHE pretreated for 6h with ETHO-CoQ10 (ETHO-CoQ10- H_2O_2-RHE) and compared to control RHE treated with ETHO-CoQ10 not exposed to H_2O_2 (ETHO-CoQ10-RHE), or RHE exposed to H_2O_2 200 µM of H_2O_2 for 90 min (CTRL- H_2O_2-RHE). Nuclei (blue) were stained with DAPI. Magnification 40x; Nikon Microphot FXA microscope (Nikon Instruments).

Conclusion on the assessment of cutaneous responses upon CS exposure

The previous results indicate that our in-house RHE model is responsive to external stressors, hence represents an appropriate model to analyze their impact on a barrier of differentiated keratinocytes. Our *in vitro* study have highlighted altered oxidative stress and pro-inflammatory markers involved in the skin defense mechanism to the detrimental CS exposure. In addition, the morphology and barrier integrity of RHE was also negatively impacted upon CS exposure. Considering the complexity of CS composition, exposure to individual CS components (Acrolein and H_2O_2) helps provide further insight on the exact cellular and molecular mechanisms involved in its toxicity. These components mainly act as oxidative stress inducers through direct oxidative damage of biological molecules but are also able to alter the skin barrier integrity when topically applied. Although we have demonstrated that CS can generate a pro-inflammatory environment in a ROS-formation dependent manner, the exact mechanisms are still under investigation. Complementary data obtained on 2D skin models could help to identify markers of interest involved in CS-induced toxicity quickly and efficiently.

The use of *in vitro* studies to screen molecular pathways implicated in the toxicity of CS simplifies the experiment by limiting the number of variables, hence represent an essential investigative tool. Besides, the reconstructed epidermal model appears as a pragmatic tool to test the efficiency of antioxidant solutions against oxidative stressors. In the first instance, using this RHE could help to find a correlation between external stressors and epidermal barrier disruption observed in the pathogenesis or exacerbation of skin diseases. Subsequently, testing the efficacy of protective and curative solutions to counteract these negative effects becomes possible. Nonetheless, the use of a 3D skin model adds complexity to the data interpretation. For instance, simulating a chronic exposure to CS can lead to an adaptive response over time making it challenging to correlate with an *in vivo* exposure scenario. A RHE model lacks important skin components such as the immune environment, melanocytes, and hair follicles, thus appear more sensitive and vulnerable to environmental stressors than physiological *in vivo* skin. The RHE model mainly focuses on investigating the causes of epidermal barrier disruption challenged upon exposure to environmental aggressors, therefore only takes into consideration the impact on keratinocyte, the first line of skin defense. Consequently, caution should be taken in extrapolating the results of these *in vitro* studies to more complex *in vivo* conditions. Regarding drug development, the use of *in vivo* skin models cannot be entirely replaced by *in vitro* models especially in the context of treating multigenic skin diseases like psoriasis.

C. MATERIALS AND METHODS

Human primary keratinocytes culture

Human primary keratinocytes extracted from the foreskin were purchased from Lonza (Lonza, Walkersville, MD, USA). Neonatal cells have been selected for their lack of environmental exposure, furthermore, cells from donors of Caucasian ethnicity were preferable to limit the production of melanin. The culture of primary keratinocytes was initiated in a complete KGM-Gold medium (Lonza). Before reaching confluency, proliferating keratinocytes were harvested by trypsinization, frozen, and preserved in liquid nitrogen.

Reconstruction of the RHE

The protocol used to build the RHE model was based on the published protocol from Frankart *et al.*[438] Briefly, third passage proliferating keratinocytes were used for the reconstruction of the epidermis. Cell suspensions containing approximately 1 million cells, thawed after preservation in liquid nitrogen, were diluted in complete KGM™ Gold medium in two 75 cm^2 culture flask for 10 hours and then in a complete **EpiLife™ basal medium** (Gibco™, Life Technologies, Carlsbad, CA, USA) which was renewed after 2 days. When keratinocytes were subconfluent (usually on the 5th day after thawing), cells were harvested by trypsinization and centrifuged for 5 minutes. The pellet was resuspended in **EpiLife™ submerged medium** containing 1.5 mM $CaCl_2$. Polycarbonate culture inserts (0.47 cm^2 of diffusion area and 0.4 µm pore size) (Nunc™, ThermoFisher Scientific, Tustin, CA) were placed in a 24-well plate containing 1.5 ml of a pre-warmed submerged medium using a specific carrier system (Nunc™, ThermoFisher Scientific, Tustin, CA). Each inserts received about 500 µl of keratinocyte suspension to reach a cell density of 350.000 cells/cm^2. After three-day incubation at 37°C in a humidified atmosphere containing 5% CO_2, cells were exposed to the air-liquid interface by removal of the medium in the upper compartment of the insert. The 1.5 ml of submerged medium in the lower compartment were replaced by 1.5 ml of complete **EpiLife™ ALI medium** and renewed every 2-3 days. A table of the medium composition for each step of the process is shown in the supplementary information section.

RHE medium recipes

The basal medium for the culture of primary keratinocytes, KGM™ Gold (Lonza, Walkersville, MD, USA), was supplemented with SingleQuot KGM™ Gold (Lonza, Walkersville, MD, USA) according to the manufacturer's instructions to contain as final concentrations 50 µg/ml bovine pituitary extract, 10 ng/ml EGF, 5 µg/ml insulin, 5.10^{-7} M hydrocortisone, 5 µg/ml transferrin and 0.15 mM Ca^{2+}. EpiLife medium (Gibco™, Life Technologies, Carlsbad, CA, USA) supplemented with HKGS (Gibco™, Life Technologies, Carlsbad, CA, USA) was used according to the manufacturer's instructions for the proliferation of keratinocytes and contains 0.2% bovine pituitary extract, 0.2 ng/ml EGF, 5 µg/ml insulin, 5.10^{-7} M hydrocortisone, 5 µg/ml transferrin and 0.06 mM of Ca^{2+}. The medium used on the first day of tissue reconstruction is composed of the complete EpiLife™ medium supplemented by $CaCl_2$ to reach 1.5 mM Ca^{2+}. After exposure to the air-liquid interface, the complete EpiLife™ culture medium supplemented with 1.5 mM Ca^{2+}, 50 µg/ml ascorbic acid (Sigma-Aldrich, Saint Louis, MO, USA), and 10 ng/ml keratinocyte growth factor (KGF; R&D Systems, Minneapolis, MN, USA) was used to culture the growing tissues.

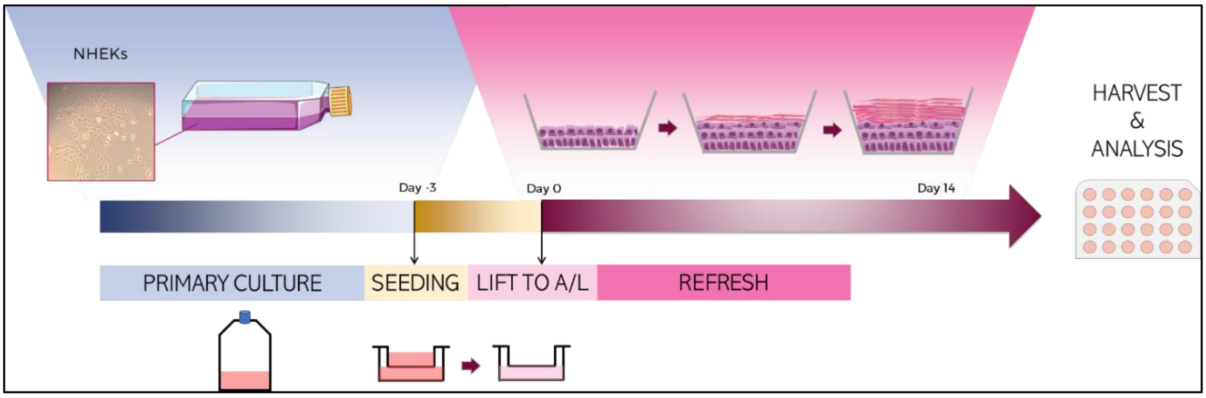

Figure C-1. Illustration of the experimental process to build the RHE model

Reconstruction of the FT skin model

Third passage proliferating keratinocytes and third passage fibroblasts were thawed on the same day respectively in KGM-Gold and FGM-Gold medium. For the dermal matrix formation, primary human fibroblasts suspension in FBS at a concentration of 10^6 cells/ml was mixed carefully with the collagen mix to form a dermal matrix solution containing 80%

collagen G 4mg/mL (cat., PureCol), 10% HBSS 10X with phenol red (cat., Gibco), 10% of fibroblasts suspension in FBS and NaOH dropwise until the color turns from yellow to red as an indicator of the pH above 8. A volume of 2,5 ml of Collagen mix was transferred in the center of each insert, corresponding to 250 000 cells per FT skin model. The inserts were incubated for 2 hours at 37°C with no CO2 supply and after 2h, 2 ml of KGM-2 media was added on top of the insert containing collagen matrix and 14 ml KGM-Gold medium in the wells below the inserts and plates were incubated at 37°C, 5% CO2.

To form the epidermal compartment, a volume of 2 mL of keratinocyte suspension at $1x10^6$ of cells/mL was seeded on top of each FT skin model and incubated overnight to allow the cells to settle down and attach to the collagen matrix. After 24h, the matrix was detached carefully from the insert sides and bottom using a p200 sterile tip. On the next day, the medium was discarded from the wells and the inserts and 10 mL of ALI medium were added in the basal compartment under the inserts and refreshed every two days for 7 days. The medium composition was detailed in the supplementary information section.

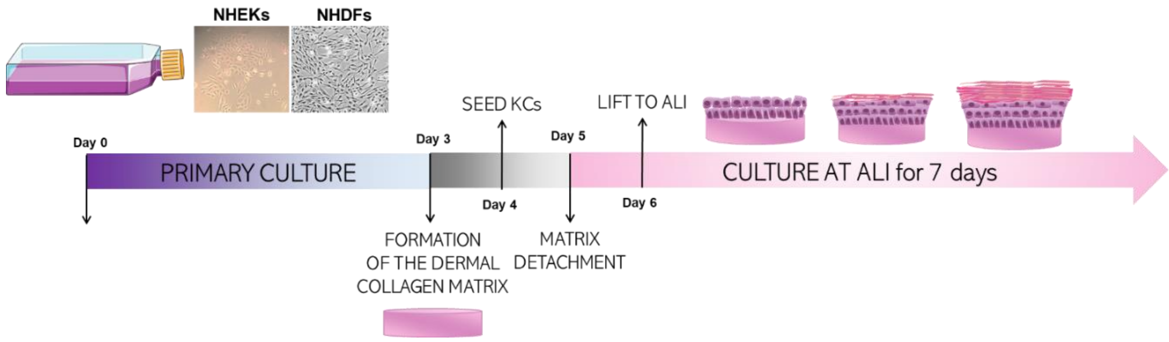

Figure C-2. Illustration of the experimental process to build the FT model

CS exposure system

Biological samples are placed in the exposure chamber that is sealed tightly to avoid any leakage of the smoke during the exposure. The chamber is built with two electrical fans to allow the extraction of the smoke into the chamber and to provide an appropriate distribution of the smoke inside the chamber. The cigarette (without the filter) is inserted into a cigarette holder at the outside of the exposure chamber and lighted up allowing full consumption to occur. During the whole exposure, the cigarette is kept in a closed environment to allow both the primary and the secondary smoke to be extracted into the chamber thanks to an electrical fan. Once the cigarette is entirely consumed (after approximately 8 minutes), the aspiration and ventilation inside the chamber are interrupted.

Several parameters (number of cigarettes used, time of exposure, medium switch, and post-exposure incubation time) need to be optimized before and during the exposure to achieve conditions that do not affect significantly tissue viability. The design and dimension of the CS exposure chamber are presented in **Figure C-3.**

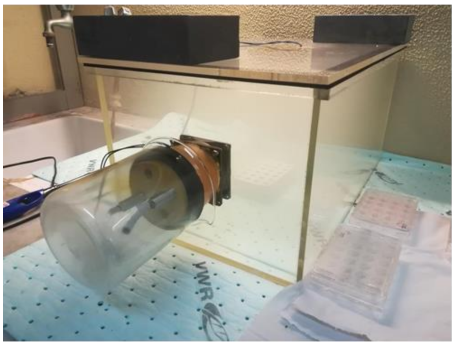

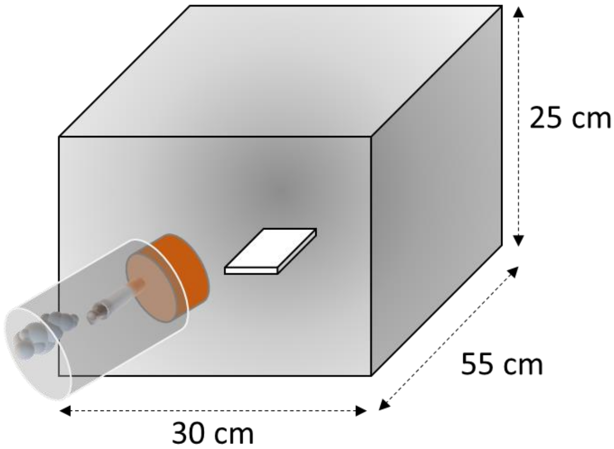

Figure C-3. Picture and schematic illustration of the CS chamber (volume: 41.25 dm^3) placed under a chemical hood.

CS exposure on Reconstructed Human Epidermis (RHE)

Before exposure, tissues were transferred into the submerged EpiLife™ medium, without ascorbic acid and KGF supplements to stop the differentiation process in keratinocytes. A Teflon cover was applied on top of the carrier plate to avoid any potential CS substances dissolution in the medium during the exposure. Tissues were exposed to two 3R4F research cigarettes or ambient air for different duration of exposure ranging from 15 minutes to 4 hours, in the conditions previously described. After the exposure (air or CS), tissues were fed with fresh EpiLife™ submerged medium and incubated for 24h at 37°C, 98% humidity, and 5% CO_2. Negative controls consisting of non-exposed tissues were left incubated at 37°C, 98% humidity, 5% CO_2 during the exposure time. Any difference observed between the non-exposed and air-exposed samples will indicate the potential toxicity induced by the change of environment (temperature, humidity, and sterility). Based on the cytotoxicity results, duration of exposure of 30 minutes with two cigarettes replaced every 15 minutes were the selected conditions for the endpoint measurements.

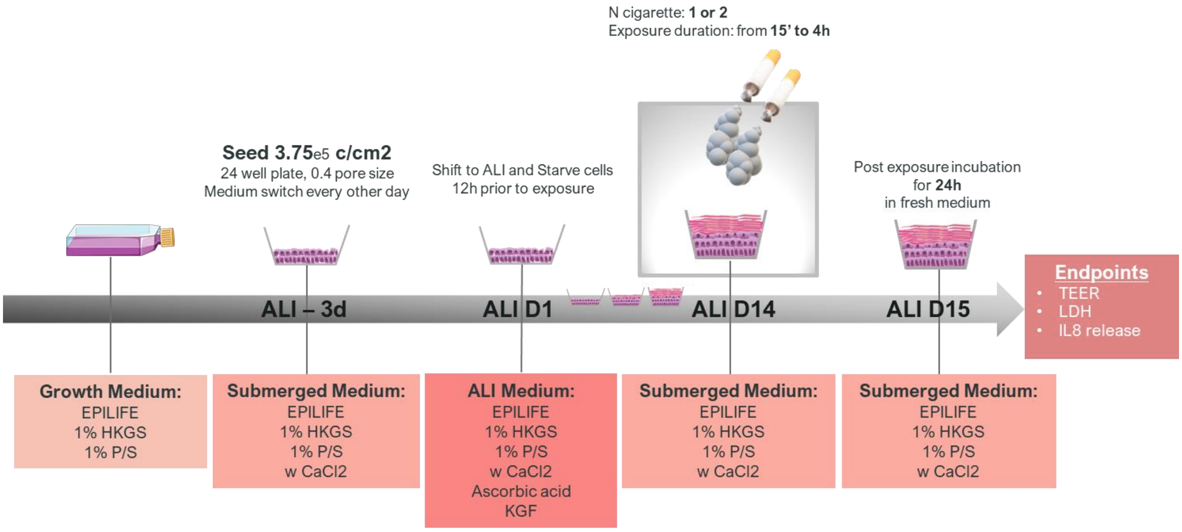

Figure C-4. Illustration of the experimental protocol of exposure on a RHE model

Lactate dehydrogenase (LDH) Assay

After 14 days at the air-liquid interface, the reconstructed epidermis tissues were switched to a submerged medium for 24h. Positive control RHEs were treated with Triton X-100, a nonionic surfactant, either topically (0.1%) or systemically (0.2%). Cytotoxicity was evaluated by the release of lactate dehydrogenase (LDH) in 1.5 ml of the reconstructed human epidermis (RHE) maintenance media 24h after CS exposure. LDH measurement was taken after 30 minutes of incubation in the dark at room temperature.

Treatment of positive controls

A volume of 30 µL of the following chemicals was applied on top of the RHEs or dissolved in the cell culture medium of 2D cells. For the RHEs, the selected doses were dissolved in PBS: 200 µM of Hydrogen peroxide (cat. H1009, Sigma Aldrich), 5 µM Nigericin (cat. N7143-5MG, Sigma Aldrich) and 30 µM of Acrolein (cat. 89116, Sigma Aldrich).

Transepithelial Electrical Resistance (TEER)

TEER was determined using the Millicell® ERS-2 Voltohmmeter (Merck KGaA, Darmstadt, Germany). RHE tissues were placed in a 24-well plate and 0.5 ml of PBS was dispensed in both the basal and apical compartments of the tissue inserts for the time required to measure electrical resistance.

Lucifer yellow permeability assay

The barrier function of 3D skin models can be characterized by determining their permeability to the Lucifer yellow fluorescent dye. In this test, 30 µl of a 1mM Lucifer yellow solution diluted in PBS was topically applied on the tissues for 6h at 37°C. After the incubation period with the dye, tissues were fixed in a 10% formalin solution and subsequently embedded in paraffin. 4 µm thick slices were cut from the paraffin blocks using a manual microtome (Leica RM 2245, Leica Microsystems GmbH Wetzlar) and then analyzed using a fluorescence microscope equipped with a fluorescein isothiocyanate (FITC) filter.

Hematoxylin & Eosin staining

The morphology of the RHE model was analyzed by H&E staining. Tissues were fixed in a 10% formalin solution, progressively dehydrated, and vertically embedded in paraffin. 6 µm thick slices were cut from the paraffin blocks and laid over microscopic slides before staining with H&E.

Immunohistochemistry

Formalin-fixed paraffin-embedded (FFPE) sections were used to quantify involucrin expression in the RHE model while optimum cutting temperature (OCT) embedded cryosections with a thickness of 4 µm were used for assessing the expression of filaggrin and loricrin. FFPE sections were deparaffinized, rehydrated, and rinsed with water. An antigen retrieval step was performed by incubating the FFPE sections in a 10 mM citrate buffer pH 6 at 90°C for 20 min. OCT cryosections were fixed in methanol for 15 minutes. All FFPE and OCT sections were then washed twice in PBS, blocked for 1h in PBS containing 0.2% bovine serum albumin and 0.02% Triton X-100 and incubated overnight at 4°C with the appropriate antibodies. Primary antibodies were used to label **involucrin** (dilution 1:250; Novus Biologicals, Milan, Italy), **filaggrin** (dilution 1:100; Novus Biologicals, Milan, Italy), **loricrin** (dilution 1:100; Novus Biologicals, Milan, Italy), **Nrf2** (cat. ab31163, Abcam, USA) 1:100, **Cytokeratin 10** (NBP2-32962, Novus Biologicals, USA) 1:100 and **4-HNE** (AB5605, Merck, USA) 1:200.

For immunofluorescence staining, tissue sections were washed twice for 10 minutes in PBS containing 0.2% bovine serum albumin and 0.02% Triton X-100 before incubation with Goat Anti-Rabbit IgG (Catalog # NL006; Biotechne) 1:200 and Goat Anti-Mouse (Catalog # NL020, Biotechne) 1:200 for 2h. After several washes, sections were finally stained with a 300mM DAPI (Tocris Biosciences, Bristol, UK) solution for 5 minutes then washed three times in PBS-T. Coverslips were subsequently mounted in an aqueous mounting medium (R&D Systems, Minneapolis, USA) and tissue sections were observed under a fluorescence microscope (Nikon Microphot FXA microscope; Nikon Instruments) equipped with DAPI, FITC, and ROD filters. DAPI, FITC, and ROD pictures were finally overlapped with ImageJ software.

Transmission electron microscopy (TEM)

For ultrastructural analysis, RHE tissues were fixed at different stages of the differentiation process (Day 7, 10, and 13) in 2.5% glutaraldehyde in cacodylate buffer for 3h at 4°C. Tissues were then post-fixed in 1% osmium tetroxide for 2h at 4°C, dehydrated in a graded series of alcohol, embedded in Araldite resins, and polymerized in an oven for 48h at 60°C. Ultrathin sections of 60 nm were cut with an ultramicrotome (Ultratome Reichert SuperNova Leica, Wien, Austria), stained with uranyl acetate and lead citrate, and examined in a Hitachi H100 transmission electron microscope.

Surface electron microscopy (SEM)

At high resolution and magnification, scanning electron microscopy (SEM) gives information on the arrangement of the corneocytes in the SC.[439] Tissues were fixed with 2.5% glutaraldehyde in cacodylate buffer (pH 7.0) and dehydrated with increasing gradients of ethyl alcohol up to 100% concentration. The cell surface was metalized with a 100% thick layer of gold-platinum, using a sputter coater Reichard 100. Samples were observed with a scanning electron microscope (Zeiss EVO 140) source LaB6, at 20 KV accelerating voltage, equipped with a computerized microanalysis system (ISIS Link), with the possibility to operate both conventionally in high vacuum and variable pressure (SEM XVP), maximum pressure 6 torr. Images were captured at 3190 X in variable pressure.

Raman spectroscopy

As a preliminary analysis, RHE tissues (surface area of 0.47 cm^2) were washed in PBS, detached from the polycarbonate membrane, and transferred to aluminum capsules for Raman measurements. A small region on the samples was selected. Raman spectra and images were acquired using a Renishaw inVia Qontor confocal Raman microscope. The sample was put under the microscope and the measurements were performed at ambient conditions.

The excitation source was a variable power diode laser (300 mW) emitting at 785 nm. The power of the laser source was kept at 30 mW (which is non-destructive for biological samples). Typical point measurements took 1-2 minutes. The spectrum was collected using 10s exposure time and 2 accumulations over the 100 to 3200 cm^{-1} spectral range. The objective used was ×50 LD (Leica N Plan, NA 0.5, WD 8.2 mm). All measurements were performed in a standard confocal mode using 1200 lines/mm grating, giving a resolution of 4 cm^{-1}.

For 2D imaging measurements, 9075 spectra were accumulated with an exposure time of 0.5s and a step size of 1 x 1 µm over the 614 to 1722 cm^{-1} spectral range. The typical measurement time was 90 min for an area of 100 x 100 µm. An automatic focus tracking feature in the software was selected throughout the measurement to maintain optimum focus during data collection.

To create Raman images, cosmic ray removal, noise filtering, and baseline subtraction were performed on the spectra using the Renishaw Wire software. Empty modeling component analysis was used to analyze the Raman image dataset of the tissue sample. It is an ideal method when the chemistry of the different components present in a sample is unknown. The generated image revealed information regarding the chemical composition and distribution of various components within the sample.

Detection of IL-1α, IL-1β, IL-18, and IL-8 using ELISA assay

The levels of interleukins were measured in the medium of RHEs, using the IL-1β ELISA kit (cat. AB100562, Abcam), IL-18 ELISA kit (cat. AB215539, Abcam), IL-8 Human uncoated ELISA kit (cat. 88-8086-88, Invitrogen) and IL-1α Human coated ELISA kit (cat. BMS243-2, Invitrogen), according to the manufacturer's instructions. Supernatants were harvested at specific time points after CS/Air exposure. Absorbance was measured at 450 nm using a plate reader (Tecan-infinite M200) and a four-parameter logistic (4PL) curve was the regression model used to analyze the results. Data were analyzed with GraphPad Prism software (GraphPad Software Inc, La Jolla, CA, USA).

OVERALL CONCLUSION

CS exposure has been associated with cutaneous toxicity by its ability to induce oxidative damage and inflammatory responses disrupting the skin barrier function which can lead to the development or exacerbation of inflammatory skin diseases, premature skin aging, and possibly skin cancer. Considering the large and complex composition of CS, it is highly challenging to establish a correlation between CS and smoke-related skin diseases. Another challenge is to dissociate clinically the effect of smoking from the impact of environmental CS exposure. Cigarette smoking surely contributes to premature skin aging. The route of exposure by CS inhalation directly engages the delivery of toxic chemicals by the biological fluids to the dermal capillaries, this does not only affect the skin biophysical parameters, thickness, and elasticity but also depletes the levels of essential vitamins in the plasma and delays wound healing.

While a long-term systemic effect of smoking is more likely to be predominant in unbalancing the skin homeostasis, CS environmental exposure has been shown to alter the skin barrier function. Long-term CS exposure dysregulates the oxidants-antioxidants balance as reflected by increased products of lipid peroxidation and depleted levels of skin antioxidants. Assessing the impact of CS *in vitro* could help provide further knowledge in the mechanisms and endpoints that come into play.

As there is no perfect *in vitro* skin model to mimic human real exposure to CS, the first challenge is to select the appropriate biological target according to the research application. Although animal models remain essential for risk analysis and genetic manipulation, alternatives should be used whenever non-animal-based experimental set up with similar relevance are available. Being comparable and consistent, *in vitro* skin models, especially the 3D reconstituted model is considered a valuable and powerful tool for a wide range of applications such as cosmetic product evaluation and irritation testing. Indeed, the RHE model enables the researcher to explain and predict the behavior of skin after exposure to environmental aggressors. Future data generated from this simple and reliable RHE model could help lead to an overall understanding of a toxicological response. Moreover, the RHE might be modulated to reproduce some skin disease features, i.e. hyperkeratosis or a disrupted barrier.

Another important challenge remains to mimic the CS exposure *in vitro* as realistically as possible. For this purpose, it is necessary to establish standardized exposure conditions to allow cross-comparison studies between laboratories, however, most of them cannot afford the high costs of commercial exposure chamber systems.

Thus far, *in vitro* studies have proved themselves useful and will continue to help to identify and screen the cellular responses and molecular pathways involved in CS toxicity. Along with the generation of toxicological data, they provide guidance towards a preventive or a curative treatment such as topical anti-inflammatory technologies, receptor antagonists, and barrier enhancers. However, special caution must be taken in extrapolating *in vitro* results to real-life conditions. In any case, congruence between *in vitro* studies and *in vivo* studies is critical before clinical trials.

As a concluding remark, quit smoking remains the most efficient means to restore the oxidant/antioxidant balance within the skin.

ABBREVIATIONS AND UNITS

Abbreviation	In full
± SEM	± Standard Error of Mean
4-HNE	4-Hydroxy-2-Nonenal
8-OHdG	8-hydroxy-2' -deoxyguanosine
Ach	Acetylcholine
AD	Atopic Dermatitis
AGA	Androgenetic alopecia
AhR	Aryl hydrocarbon receptor
AIM2	inflammasome sensor Absent In Melanoma 2
ALI	Air Liquid Interface
ALR	Aim2-like receptor
AMPs	Antimicrobial Peptides
AP-1	Activator Protein-1
ARNT	AhR nuclear translocator
ATP	Adenosine Triphosphate
BPE	Bovine Pituitary Extract
BSA	Bovine Serum Albumin
CAT	Catalase
CCL20	Chemokine (C-C motif) ligand 20
CDSN	Corneodesmosin
CS	Cigarette Smoke
CSC	Cigarette Smoke Chamber
CSE	Cigarette Smoke Extract
CXCL10	IFN-γ-inducible protein 10
CXCL8	interleukin-8
CYP1A1	Cytochrome P450, family 1, subfamily A, polypeptide 1
DMSO	Dimethyl sulfoxide
EDTA	ethylene diamine tetraacetic acid
EGF	Epidermal Growth Factor
EGR-1	Early growth response protein 1
EPA	Environmental Protection Agency
ETS	Environmental Tobacco Smoke
FBS	Fetal bovine serum
FDA	Food and Drug Administration
FFPE	Formalin Fixed Paraffin Embedded

FITC	Fluorescein Isothiocyanate filter
FLG	Filaggrin
FT	Full-thickness
GPX	Glutathione peroxidase
GSH	Glutathione
GPX	Glutathione peroxidase
H&E	Hematoxylin & Eosin
H_2O_2	Hydrogen Peroxide
HKGS	Human keratinocyte growth supplement
HO-1	Heme oxygenase-1
HSP	Heat Shock Protein
IF	Immunofluorescence
IgE	Immunoglobulin E
IL-18	interleukin-8
IL-1β	interleukin-1β
INV	Involucrin
IFN-γ	Interferon-γ
IR	InfraRed
IκBα	inhibitor of nuclear factor kappa B
Keap1	Kelch-like ECH-associated protein 1
KGF	Keratinocyte growth factor
LCO	Lipo-chitooligosaccharides
LDH	Lactate dehydrogenase
LL-37	Antimicrobial peptide
LNA	Local lymph node assay
LOR	Loricrin
LPS	Lipopolysaccharide
MAPKs	Mitogen-activated protein kinases
MDA	Malondialdehyde
MITF	Microphtalmia-associated Transcription Factor
MMPs	Matrix metalloproteinases
MPO	Myeloperoxidase
MTT	3-(4,5-Dimethylthiazol-2-yl)-2,5-Diphenyltetrazolium Bromide
nAChRs	Nicotinic acetylcholine receptors
NADPH	Nicotinamide adenine dinucleotide phosphate
NALP1	NACHT leucine-rich-repeat protein 1
NF-κB	Nuclear factor-kappa B
NHDF	Neo natal Human Dermal Fibroblasts
NHEKs	Normal human epidermal keratinocytes

NLR	NOD-like Receptors
NLRC4	NOD-like Receptor Family amino-terminal CARD domain 4
NLRP1	NOD-like Receptor Family Pyrin Domain Containing 1
NLRP3	NOD-like Receptor Family Pyrin Domain Containing 3
NMF	Natural moisturizing factor
NO_2	Nitrogen dioxide
NOX	NADPH oxydase
NOX2	NADPH oxidase 2
Nrf2	Nuclear factor (erythroid-derived 2)-like 2
O_2	Dioxygen
$O2^-$	Superoxide ion
O_3	Ozone
OCT	Optimal cutting temperature compound
$OH^\cdot$	Hydroxyl radical
PAHs	Polycyclic Aromatic Hydrocarbons
AMP	AMP-activated protein kinase
PBS	Phosphate Buffered Saline
PM	Particulate Matter
PM_{10}	Particles with diameters that are generally 10 micrometers and smaller.
$PM_{2.5}$	Particles with diameters that are generally 2.5 micrometers and smaller.
RH	Relative Humidity
RHE	Reconstructed Human Epidermis
RNS	Reactive Nitrogen species
ROS	Reactive Oxygen Species
SB	Stratum Basale
SC	Stratum Corneum
SEM	Scanning Electron Microscopy
SG	Stratum Granulosum
SO_2	Sulfur dioxide
SOD	Superoxide Dismutase
SRB1	Scavenger receptor class B type 1
SS	Stratum Spinosum
STAT3	Signal transducer and activator of transcription 3
TBS	Tris-Buffered Saline
TBS-T	Tris-Buffered Saline (TBS) solution with 0.1% v/v of Tween 20
TEER	Trans Epithelial Electrical Resistance
TEM	Transmission Electron Microscopy

Th17	T helper 17 cells
TNF-α	Tumour necrosis factor-alpha receptor
TS	Tobacco Smoke
TSLP	Thymic stromal lymphopoietin
TSNA	Tobacco-specific nitrosamine
TβR-II	Transforming growth factor β-II
UFPs	Ultra Fine Particles
UV	UltraViolet
VOCs	Volatile Organic Compounds
XRE	Xenobiotic response element

4-HNE as an essential marker of oxidative stress

4-hydroxy-2-nonenal (4-HNE) is one of the main indicators of oxidative stress, it is a product of lipid peroxidation, i.e. derived from the oxidation of Polyunsaturated fatty acids (PUFAs). This highly reactive small aldehyde can form adducts with proteins (histidine, cysteine, and lysine moieties) through Michael or Schiff base additions as well as with DNA by forming a covalent bond with deoxyguanosine nucleoside. Its high reactivity is due to the presence of three functional groups: one double bond, one carbonyl group, and a hydroxyl group. This chemical structure makes it amphiphilic and electrophilic and enables an efficient binding with a vast number of biomolecules like membrane phospholipids, transporter, and receptor molecules as well as molecules localized inside the cells.

4-HNE increase plays a role in the modulation of enzyme activity, signal transduction, and gene expression.[433,434] Indeed, its interactions with nucleophilic biomolecules likely alter response mechanisms to stress such as mitochondrial metabolism, detoxification mechanisms, inflammatory and redox-sensitive transcription factors including nuclear factor-kappa B (NFκB), activator protein-1 (AP1), and nuclear factor (erythroid-derived 2)-like 2 (Nrf2).[440] These protein alterations may consequently lead to loss of normal cell functions and eventually to cell death. As a long-term consequence, 4-HNE may influence cell growth, differentiation, and apoptosis thus may be involved in the pathogenesis of oxidative stress-related diseases.[441] The skin organ is particularly rich in lipid compounds which makes it an attractive target for 4-HNE binding. An increase in 4-HNE production subsequently has been associated with the generation and/or exacerbation of many cutaneous conditions such as psoriasis, premature aging, skin yellowing, and AD.[442–445]

Nrf2 as an essential marker of the antioxidant response

Nuclear factor-erythroid 2-related factor 2 (Nrf2) is a transcription factor that regulates the expression of antioxidant and cytoprotective enzymes via the antioxidant response element (ARE)[295,446]. Nrf2 plays an essential role in modulating the cellular redox status and detoxification mechanism. At a basic state, Nrf2 is localized in the cytoplasm and guarded by its inhibitor the Kelch-like ECH-associated protein 1 (Keap1). Exposure to electrophilic molecules such as 4-HNE causes conformational changes of Keap1 protein thus results in Nrf2 accumulation into the cytoplasm that quickly induces its translocation to the nucleus where it binds the ARE sequences of antioxidant genes. As a consequence, Nrf2 nuclear translocation induces the transcription of cytoprotective and antioxidant genes. Nrf2 also influences the inflammation response by cross-talking with NF-κB and Inflammasomes.[447] Therefore, Nrf2 plays a crucial role in the skin defense mechanism in response to environmental stressors such as CS providing antioxidant protection.

Epidermal proteins as essential markers of keratinocyte differentiation

Filaggrin (FLG), loricrin (LOR), involucrin (IVL), and cytokeratin 10 (K10) are proteins that have an important role in the formation of the epidermal barrier. Filaggrin is responsible for keratin filament aggregation promoting the cytoskeleton formation of the cornified envelope.[448] Loricrin accounts for the majority of the cornified layer protein mass and is expressed in the granular layer.[431] Involucrin is the first cross-linked protein forming the scaffold for the cornified envelope. Its expression is normally localized early in the stratum spinosum and persists in the stratum granulosum.[432] Cytokeratin 10 (K10**)** is induced in early differentiated cells at the stratum spinosum and maintained through all differentiated layers. Considered as an early differentiation marker, its expression by post-mitotic suprabasal keratinocytes arises ahead of cornified envelope proteins and late differentiation marker proteins such as involucrin and loricrin.[430,449]

A short introduction to Raman Spectroscopy

Raman effect was discovered in 1930 by Nobel prized Indian scientist Chandrasekhara Venkata Raman, his work has shown that "*In every case in which light is scattered by the molecules in dust-free liquids or gases, the diffuse radiation of the ordinary kind, having the same wave-length as the incident beam, is accompanied by a modified scattered radiation of degraded frequency*".[450] Raman scattering involves inelastic collisions causing energy changes. If the scattered photons lose energy compared to the incident photons, Stokes scattering occurs (detected at higher λ) and the contrary process is called anti-Stokes scattering (detected at lower λ)**.** Raman spectroscopy is based on the interaction between radiation and material. The incident light transfers its energy to molecular vibrations, therefore high polarizability molecules and bonds are more specifically detected. The resulting Raman spectrum is like a "fingerprint" of a material allowing the qualitative characterization at the molecular, spatial, and temporal levels.

Confocal Raman Spectroscopy (CFR) appears as a non-invasive and promising tool in skin research by providing data such as (i) the skin distribution of lipids, proteins, keratins, ceramides, nucleic acids, carotenoids, and natural moisturizing factors (NMF), (ii) the detection of structural changes associated to protein degradation or lipid organization, (iii) the depth profile of compounds such as drug or water indicating the state of skin hydration, and (iv) the spatial differentiation of skin layers and their thickness.[401,451–457] The CFR technique can be used for a wide range of applications from the identification and characterization of skin tissues and cells for early diagnosis of pathological states to the kinetic study of drug/penetration enhancers penetration within skin layers. **Figure 5** displays similar spectral features for an *in vivo* and an *in vitro* skin model.[458]

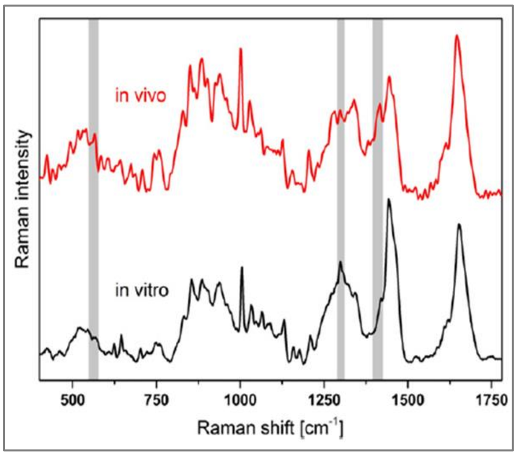

Figure C-5. Characteristic Raman spectrum of skin *in vivo* and *vitro*[458]

Monitoring the CS chamber humidity and temperature

To be as reproducible as possible, it is important to control the humidity and the temperature inside and outside the chamber. By monitoring the evolution of the temperature (°C) and relative humidity (%) every 30 minutes for 4 hours, following the generation of fresh CS inside the chamber by burning one cigarette, it was observed that CS increases the temperature by approximately +3°C and the humidity of +20% (**Figure C-6**). As a result, a negative control incubated at 37°C, 98% humidity, 5% CO_2 is required to minimize the effect of temperature and humidity on our results.

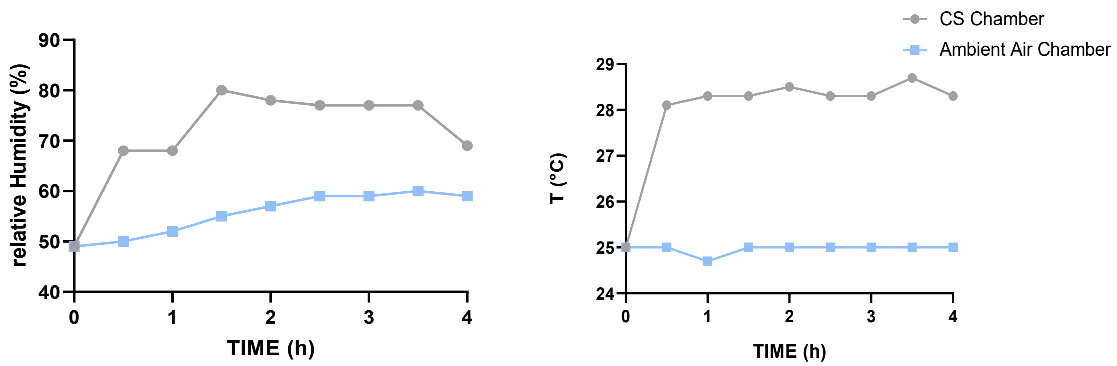

Figure C-6. Evolution of the temperature (right) and relative humidity (left) in the exposure chamber and in the surrounding environment following the generation of fresh CS inside the chamber by burning one cigarette.

Reconstruction of RHE and FT skin model

Table C-1. Composition of the different culture media used to produce the RHE model

RHE building phase	Medium	Supplements
GROWTH MEDIUM Keratinocytes 2D culture passage < 3	KGM™ Gold medium	+ SingleQuots: ● 50 µg/ml bovine pituitary extract ● 10 ng/ml EGF ● 5 µg/ml insulin ● 5.10^{-7} M hydrocortisone ● 5 lg/ml transferrin ● 0.15 mM Ca^{2+}
BASAL MEDIUM Keratinocytes 2D culture passage > 3	EpiLife™ medium	+ 1% HKGS + 1% Pen/Strip
SUBMERGED MEDIUM Seeding (from D-3 to D0)	EpiLife™ medium	+ 1% HKGS + 1% Pen/Strip + 1.5 mM $CaCl_2$
ALI MEDIUM Air-Liquid Interface (from D0 to D14)	EpiLife™ medium	+ 1% HKGS + 1% Pen/Strip + 1.5 mM $CaCl_2$ + 50 µg/ml vitamin C + 10 ng/ml keratinocyte growth factor

Table C-2. Composition of the different culture media used to produce the FT skin model

Components	Preparation of stock solution
Fibroblast culture medium	FGM-Gold Fibroblast Growth Medium-2 Bullet Kit (Lonza, Catalog #: CC-4126): 1 x Lilac Cap Vial with Insulin 0.50 mL 1 x Gray Cap Vial with hFGF-B 0.50 mL *1 x Red Cap Vial with GA-1000 0.50 mL* - substituted by 100 U/100 µg P/S 1 x Bottle FBS 10.00 mL
Keratinocyte culture medium	KGM-Gold bullet kit (Lonza, Catalog #: 00192060) 1 x Natural Cap Vial with Transferrin, 0.50 mL 1 x Amber Vial with Epinephrine, 0.25 mL 1 x Red Cap Vial with GA-1000, 0.50 mL 1 x Orange Cap Vial with BPE, 2.00 mL 1 x Green Cap Vial with hEGF, 0.50 mL 1 x Lilac Cap Vial with Insulin, 0.50 m
Epidermal submerged medium	KGM-Gold bullet kit (Lonza, Catalog #: 00192060) 1 x Natural Cap Vial with Transferrin, 0.50 mL 1 x Amber Vial with Epinephrine, 0.25 mL 1 x Red Cap Vial with GA-1000, 0.50 mL 1 x Orange Cap Vial with BPE, 2.00 mL 1 x Green Cap Vial with hEGF, 0.50 mL 1 x Lilac Cap Vial with Insulin, 0.50 m
ALI- medium	KGM-Gold bullet kit (Lonza, Catalog #: 00192060) 1 x Natural Cap Vial with Transferrin, 0.50 mL 1 x Red Cap Vial with GA-1000, 0.50 mL 1 x Green Cap Vial with hEGF, 0.50 mL 1 x Lilac Cap Vial with Insulin, 0.50 m *No Epinephrine and BPE* • 0.1% BSA: 0,5 g in 500 ml [0.1%] • 50 µg/mL ascorbic acid: 25 mg in 500 ml [0.005%] • 1.15 mM calcium chloride: 575 µl in 500 ml [1.15 mM] if necessary, filtrate the medium using Stericup filters

Western Blot (WB) buffer recipes for a volume of 1L

RUNNING BUFFER (1X)
TRIS 3g
GLYCINE 14.4g
SDS 1g
H_2O 1L
TRANSFER BUFFER (1X)
TRIS 3g
GLYCINE 14.4g
Dissolve in 800 mL H_2O
Add 200 mL of MeOH
TBS-T (1X)
NaCl 8g
TRIS 2.4g
Dissolve in 500 mL H_2O
Add HCl 2N to pH 7,4
Add H_2O to 1L
Add 1 ml of Tween 20

Select the percentage of SDS-Polyacrylamide gel according to protein molecular size

Acrylamide concentration (%)	Linear range of separation (KD)
15	12-43
10	16-68
7.5	36-94
5	57-212

WB gel recipe (15 mL for 2 gels)					STACKING GEL (3mL for 2 gels)
Gel components	**8%**	**10%**	**12%**	**15%**	
H2O	4.6	4	3.3	2.3	2.1
30% Acrylamide	2.7	3.3	4	5	0.5
1.5M Tris pH 6.8	2.5	2.5	2.5	2.5	
10% SDS	0.1	0.1	0.1	0.1	0.03
10% APS	0.1	0.1	0.1	0.1	0.03
TEEMED	0.006	0.004	0.004	0.004	0.003
1 M Tris pH 8.8					0.38

LIST OF PUBLICATIONS

- **Prieux, R**., Eeman, M., Rothen-Rutishauser, B. & Valacchi, G. Mimicking CS exposure to assess cutaneous toxicity. Toxicology *in vitro* 62, 104664 (2020)
- Sguizzato, M.; Mariani, P.; Spinozzi, F.; Benedusi, M.; Cervellati, F.; Cortesi, R.; Drechsler, M.; **Prieux, R**.; Valacchi, G.; Esposito, E. Ethosomes for Coenzyme Q10 Cutaneous Administration: From Design to 3D Skin Tissue Evaluation. Antioxidants 2020, 9, 485.
- Pecorelli A, Woodby B, **Prieux R**, Valacchi G. Involvement of 4-hydroxy-2-nonenal in pollution-induced skin damage. BioFactors. 2019;1–12. https://doi.org/10.1002/biof.1513
- Ferrara F/**Prieux R**, Woodby B, Valacchi G. "Inflammasome activation in pollution-induced skin conditions" Plastic and Reconstructive Surgery, Science of Aging
- Dijkhoff I, Petracca B, **Prieux R**, Eeman M, Rothen B, Valacchi G., "A Reliable Procedure to Cultivate Three-dimensional Human Epidermal Equivalents at Large Scale" – JOVE - *Manuscript accepted*
- **Prieux R**, Benedusi M, Guiotto A, Ferrara F, Cervellati F, Valacchi G, "Effect of CS on the inflammasome in skin" - *Manuscript in preparation*
- **Prieux R**/Petracca B, Dijkhoff I, Eeman M, Valacchi G., "Impact of pollutants on a reconstructed skin epidermis analyzed by Raman Spectroscopy" - *Manuscript in preparation*

REFERENCES

1. Monteiro-Riviere, N. A. *Toxicology of the Skin.* (CRC Press, 2010).
2. Epidermis and Its Renewal by Stem Cells - Molecular Biology of the Cell - NCBI Bookshelf. Available at: https://www.ncbi.nlm.nih.gov/books/NBK26865/. (Accessed: 9th April 2020)
3. Tobin, D. J. Biochemistry of human skin—our brain on the outside. *Chem. Soc. Rev.* **35**, 52–67 (2006).
4. Bouwstra, J. A. & Ponec, M. The skin barrier in healthy and diseased state. *Biochim. Biophys. Acta - Biomembr.* **1758**, 2080–2095 (2006).
5. Kolarsick, P. A., Ann Kolarsick, M. & Goodwin, C. *Anatomy and Physiology of the Skin*. (2006).
6. Idrees, A. *et al.* Validation of *in vitro* assays in three-dimensional human dermal constructs. *Int. J. Artif. Organs* 039139881877551 (2018). doi:10.1177/0391398818775519
7. Boukamp, P. *et al.* Normal keratinization in a spontaneously immortalized aneuploid human keratinocyte cell line. *J. Cell Biol.* **106**, 761–771 (1988).
8. Teimouri, A., Yeung, P. & Agu, R. 2D vs. 3D Cell Culture Models for *In vitro* Topical (Dermatological) Medication Testing. in *Cell Culture* (IntechOpen, 2019). doi:10.5772/intechopen.79868
9. Pastore, S. *et al.* Differential modulation of stress-inflammation responses by plant polyphenols in cultured normal human keratinocytes and immortalized HaCaT cells. *J. Dermatol. Sci.* **63**, 104–114 (2011).
10. Ridd, K., Dhir, S., Smith, A. G. & Gant, T. W. Defective TPA signalling compromises HaCat cells as a human *in vitro* skin carcinogenesis model. *Toxicol. Vitr.* **24**, 910–915 (2010).
11. Barnes, D. W. *Epidermal Growth Factor Inhibits Growth of A431 Human Epidermoid Carcinoma in Serum-free Cell Culture*. *THE JOURNAL OF CELL BIOLOGY* **93**, (1982).
12. Kashyap, C. P. *et al.* Human cancer cell lines-A brief communication. *J. Chem. Pharm. Res* **3**, 514–520 (2011).
13. Cmarik, J. L. & Colburn, N. H. Use of Mouse JB6 Cells to Identify Molecular Targets and Novel Agents for Prevention of Carcinogenesis. in *Food Factors for Cancer Prevention* 67–76 (Springer Japan, 1997). doi:10.1007/978-4-431-67017-9_13
14. Soumelis, V. *et al.* Human epithelial cells trigger dendritic cell–mediated allergic inflammation by producing TSLP. *Nat. Immunol.* **3**, 673–680 (2002).
15. Wojtowicz, A. M. *et al.* The importance of both fibroblasts and keratinocytes in a bilayered living cellular construct used in wound healing. *Wound Repair Regen.* **22**, 246–55 (2014).

16. Wells, W. A. A cell line that is under control. *J. Cell Biol.* **168**, 988–989 (2005).

17. Wever, B. D. E., Petersohn, D. & Mewes, K. R. TO ANIMAL TESTING Overview of human. **8**, 18–23 (2013).

18. Rodrigues Neves, C. & Gibbs, S. Progress on Reconstructed Human Skin Models for Allergy Research and Identifying Contact Sensitizers. in *Current topics in microbiology and immunology* (2018). doi:10.1007/82_2018_88

19. Gordon, S. *et al.* t 4 Workshop Report * Non-Animal Models of Epithelial Barriers (Skin , Intestine and Lung) in Research , Industrial Applications and Regulatory Toxicology. *ALTEX* **32**, 327–378 (2015).

20. Mori, N., Morimoto, Y. & Takeuchi, S. Skin integrated with perfusable vascular channels on a chip. *Biomaterials* **116**, 48–56 (2017).

21. Alexander, F., Eggert, S. & Wiest, J. Skin-on-a-Chip: Transepithelial Electrical Resistance and Extracellular Acidification Measurements through an Automated Air-Liquid Interface. *Genes (Basel).* **9**, 114 (2018).

22. Herron, A. *Pigs as Dermatologic Models of Human Skin Disease. In: Proceedings of ACVP and ASVCP Meeting, Monterey, California, USA - 2009*.

23. Summerfield, A. & Ricklin, M. E. The immunology of the porcine skin and its value as a model for human skin. *Mol. Immunol.* **66**, 14–21 (2015).

24. Chang Jung, E., Maibach, H. I., Jung, E. C. & Maibach, H. I. Animal Models for Percutaneous Absorption. doi:10.1007/978-1-4939-1289-6_2

25. Hoffmann, S. LLNA variability: An essential ingredient for a comprehensive assessment of non-animal skin sensitization test methods and strategies. *ALTEX* (2015). doi:10.14573/altex.1505051

26. Bielfeldt, S., Springmann, G., Seise, M., Wilhelm, K.-P. & Callaghan, T. An updated review of clinical methods in the assessment of ageing skin - New perspectives and evaluation for claims support. *Int. J. Cosmet. Sci.* **40**, 348–355 (2018).

27. Lebonvallet, N. *et al.* The evolution and use of skin explants: potential and limitations for dermatological research. *Eur. J. Dermatol.* **20**, 671–84

28. Abd, E. *et al.* Skin models for the testing of transdermal drugs. *Clin. Pharmacol.* **8**, 163–176 (2016).

29. Andrade, T. A. *et al. Ex vivo* Model of Human Skin (hOSEC) as Alternative to Animal use for Cosmetic Tests. *Procedia Eng.* **110**, 67–73 (2015).

30. Farahmand, S. & Maibach, H. I. Estimating skin permeability from physicochemical characteristics of drugs: A comparison between conventional models and an *in vivo*-based approach. *Int. J. Pharm.* **375**, 41–47 (2009).

31. Wild, C. P. Complementing the genome with an 'exposome': The outstanding challenge of environmental exposure measurement in molecular epidemiology. *Cancer Epidemiology Biomarkers and Prevention* **14**, 1847–1850 (2005).

32. Aly, R. *Microbial Infections of Skin and Nails*. *Medical Microbiology* (University of Texas Medical Branch at Galveston, 1996).

33. Erin Chen, Y., Fischbach, M. A. & Belkaid, Y. Skin microbiota-host interactions. *Nature* **553**, 427–436 (2018).

34. Radiation: Ionizing radiation. Available at: https://www.who.int/news-room/q-a-detail/radiation-ionizing-radiation. (Accessed: 27th November 2020)

35. Engebretsen, K. A., Johansen, J. D., Kezic, S., Linneberg, A. & Thyssen, J. P. The effect of environmental humidity and temperature on skin barrier function and dermatitis. *J. Eur. Acad. Dermatology Venereol.* **30**, 223–249 (2016).

36. *Significance of humidity and temperature on skin and upper airway symptoms*.

37. D'Orazio, J., Jarrett, S., Amaro-Ortiz, A. & Scott, T. UV Radiation and the Skin. *Int. J. Mol. Sci.* **14**, 12222 (2013).

38. Gies, P., Roy, C. & Udelhofen, P. Solar and ultraviolet radiation. in 21–54 (Springer, Dordrecht, 2004). doi:10.1007/978-94-017-0511-0_3

39. Krutmann, J., Morita, A. & Chung, J. H. Sun exposure: What molecular photodermatology tells us about its good and bad sides. *J. Invest. Dermatol.* **132**, 976–984 (2012).

40. Krutmann, J., Bouloc, A., Sore, G., Bernard, B. A. & Passeron, T. The skin aging exposome. *J. Dermatol. Sci.* **85**, 152–161 (2017).

41. Burke, K. E. Mechanisms of aging and development-A new understanding of environmental damage to the skin and prevention with topical antioxidants. *Mech. Ageing Dev.* 1–8 (2018). doi:10.1016/j.mad.2017.12.003

42. Battie, C. *et al.* New insights in photoaging, UVA induced damage and skin types. *Exp. Dermatol.* **23**, 7–12 (2014).

43. Darvin, M. E. *et al.* Formation of free radicals in human skin during irradiation with infrared light. *J. Invest. Dermatol.* **130**, 629–631 (2010).

44. Mutchell, D. Revisiting the photochemistry of solar UVA in human skin. *PNAS* **103**, 13567–13568 (2006).

45. Herrling, T., Jung, K. & Fuchs, J. Measurements of UV-generated free radicals/reactive oxygen species (ROS) in skin. *Spectrochim. Acta - Part A Mol. Biomol. Spectrosc.* **63**, 840–845 (2006).

46. Kammeyer, A. & Luiten, R. M. Oxidation events and skin aging. *Ageing Res. Rev.* **21**, 16–29 (2015).

47. Armstrong, B. K. & Kricker, A. The epidemiology of UV induced skin cancer. *J. Photochem. Photobiol. B Biol.* **63**, 8–18 (2001).

48. Young, A. R., Claveau, J. & Rossi, A. B. Ultraviolet radiation and the skin: Photobiology and sunscreen photoprotection. *J. Am. Acad. Dermatol.* **76**, S100–S109 (2017).

49. Kim, K. E., Cho, D. & Park, H. J. Air pollution and skin diseases: Adverse effects of airborne particulate matter on various skin diseases. *Life Sciences* **152**, 126–134 (2016).

50. Lorente, J. *et al.* Influence of Urban Aerosol on Spectral Solar Irradiance. *J. Appl. Meteorol.* **33**, 406–415 (1994).

51. Liu, S. C., McKeen, S. A. & Madronich, S. Effect of anthropogenic aerosols on biologically active ultraviolet radiation. *Geophys. Res. Lett.* **18**, 2265–2268 (1991).

52. Barnard, W. F. & Wenny, B. N. Ultraviolet Radiation and Its Interaction with Air Pollution. in *UV Radiation in Global Climate Change* 291–330 (Springer Berlin Heidelberg, 2010). doi:10.1007/978-3-642-03313-1_11

53. Seckmeyer, G. & McKenzie, R. L. Increased ultraviolet radiation in New Zealand (45° S) relative to Germany (48° N). *Nature* **359**, 135–137 (1992).

54. Burke, K. & Wei, H. Synergistic damage by UVA radiation and pollutants. *Toxicol. Ind. Health* **25**, 219–224 (2009).

55. Marrot, L. Pollution and Sun Exposure: a Deleterious Synergy. Mechanisms and Opportunities for Skin Protection. *Curr. Med. Chem.* 1–18 (2017). doi:10.2174/0929867324666170918123907

56. Soeur, J. *et al.* Photo-pollution stress in skin: Traces of pollutants (PAH and particulate matter) impair redox homeostasis in keratinocytes exposed to UVA1. *J. Dermatol. Sci.* **86**, 162–169 (2017).

57. Trommer, H. & Neubert, R. H. H. Overcoming the stratum corneum: The modulation of skin penetration. A review. in *Skin Pharmacology and Physiology* **19**, 106–121 (Skin Pharmacol Physiol, 2006).

58. Percutaneous Absorption | Drugs, Cosmetics, Mechanisms, Methods | Taylor & Francis Group. Available at: https://www.taylorfrancis.com/books/e/9780429186493. (Accessed: 21st May 2020)

59. Lademann, J. *et al.* Penetration von mikropartikeln in die menschliche haut. *Hautarzt* **55**, 1117–1119 (2004).

60. Kammer, R., Tinnerberg, H. & Eriksson, K. Evaluation of a tape-stripping technique for measuring dermal exposure to pyrene and benzo(a)pyrene. *J. Environ. Monit.* **13**, 2165–2171 (2011).

61. 9 out of 10 people worldwide breathe polluted air, but more countries are taking action. (2018). Available at: https://www.who.int/news-room/detail/02-05-2018-9-out-of-10-people-worldwide-breathe-polluted-air-but-more-countries-are-taking-action. (Accessed: 8th September 2019)

62. Backes, C., Nelin, T., Gorr, M. & Wold, L. Early life exposure to air pollution: how bad is it? *Toxicol. Lett.* **216**, 47–53 (2013).

63. Brunekreef, B. & Holgate, S. T. Air pollution and health. *Lancet* **360**, 1233–1242 (2002).

64. Drakaki, E., Dessinioti, C. & Antoniou, C. V. Air pollution and the skin. *Front. Environ. Sci.* **2**, (2014).

65. *WHO's Ambient Air Pollution database-Update 2014*.

66. Schneider, P. & van der A, R. J. A global single-sensor analysis of 2002-2011

tropospheric nitrogen dioxide trends observed from space. *J. Geophys. Res. Atmos.* **117**, n/a-n/a (2012).

67. US EPA, O. Criteria Air Pollutants.

68. WHO air quality guidelines for Europe, 2nd edition, 2000 (CD ROM version). (2017).

69. Air pollution, facts and information. Available at: https://www.nationalgeographic.com/environment/global-warming/pollution/. (Accessed: 19th May 2020)

70. Kim, K. E., Cho, D. & Park, H. J. Air pollution and skin diseases: Adverse effects of airborne particulate matter on various skin diseases. *Life Sci.* **152**, 126–134 (2016).

71. Pöschl, U. Atmospheric aerosols: Composition, transformation, climate and health effects. *Angew. Chemie - Int. Ed.* **44**, 7520–7540 (2005).

72. Stedman, R. L. The chemical composition of tobacco and tobacco smoke. *Chem. Rev.* **68**, 153–207 (1968).

73. Valacchi, G. *et al.* Cutaneous responses to environmental stressors. *Ann. N. Y. Acad. Sci.* **1271**, 75–81 (2012).

74. Ferrara, F. *et al.* Additive effect of combined pollutants to UV induced skin OxInflammation damage. Evaluating the protective topical application of a cosmeceutical mixture formulation. *Redox Biol.* 101481 (2020). doi:10.1016/j.redox.2020.101481

75. Marrot, L. Pollution and Sun Exposure: A Deleterious Synergy. Mechanisms and Opportunities for Skin Protection. *Curr. Med. Chem.* **25**, 5469–5486 (2018).

76. Loidl-Stahlhofen, A., Hannemann, K. & Spiteller, G. Generation of α-hydroxyaldehydic compounds in the course of lipid peroxidation. *Biochim. Biophys. Acta (BBA)/Lipids Lipid Metab.* **1213**, 140–148 (1994).

77. Ayala, A., Muñoz, M. F. & Argüelles, S. Lipid peroxidation: Production, metabolism, and signaling mechanisms of malondialdehyde and 4-hydroxy-2-nonenal. *Oxidative Medicine and Cellular Longevity* **2014**, (2014).

78. Breitzig, M., Bhimineni, C., Lockey, R. & Kolliputi, N. 4-Hydroxy-2-nonenal: A critical target in oxidative stress? *Am. J. Physiol. - Cell Physiol.* **311**, C537–C543 (2016).

79. Uchida, K. 4-Hydroxy-2-nonenal: A product and mediator of oxidative stress. *Prog. Lipid Res.* **42**, 318–343 (2003).

80. Niki, E. Lipid oxidation in the skin. *Free Radic Res* **49(7):827**-, 827–834 (2015).

81. Magnani, N. D. *et al.* Skin damage mechanisms related to airborne particulate matter exposure. *Toxicol. Sci.* **149**, 227–236 (2016).

82. Li, N. *et al.* Ultrafine particulate pollutants induce oxidative stress and mitochondrial damage. *Environ. Health Perspect.* **111**, 455–460 (2003).

83. Piao, M. J. *et al.* Particulate matter 2.5 damages skin cells by inducing oxidative stress, subcellular organelle dysfunction, and apoptosis. *Arch. Toxicol.* **92**, 2077–2091 (2018).

84. Ferrara, F. *et al.* Additive effect of combined pollutants to UV induced skin OxInflammation damage. Evaluating the protective topical application of a cosmeceutical mixture formulation. *Redox Biol.* 101481 (2020). doi:10.1016/j.redox.2020.101481

85. Cervellati, F. *et al.* Proinflammatory properties and oxidative effects of atmospheric particle components in human keratinocytes. *Chemosphere* **240**, (2020).

86. Sticozzi, C. *et al.* CS affects keratinocytes SRB1 expression and localization via H_2O_2 production and HNE protein adducts formation. *PLoS One* **7**, 1–14 (2012).

87. Sticozzi, C. *et al.* Resveratrol protects SR-B1 levels in keratinocytes exposed to CS. *Free Radic. Biol. Med.* **69**, 50–57 (2014).

88. Cadenas, E. & Davies, K. J. A. Mitochondrial free radical generation, oxidative stress, and aging. *Free Radic. Biol. Med.* **29**, 222–230 (2000).

89. Ray, P. D., Huang, B. W. & Tsuji, Y. Reactive oxygen species (ROS) homeostasis and redox regulation in cellular signaling. *Cellular Signalling* **24**, 981–990 (2012).

90. Pecorelli, A., Woodby, B., Prieux, R. & Valacchi, G. Involvement of 4-hydroxy-2-nonenal in pollution-induced skin damage. *BioFactors* **45**, 536–547 (2019).

91. GIUSEPPE VALACCHI, ELISA PAGNIN, ANA M. CORBACHO, ESTIBALIZ OLANO, PAUL A. DAVIS, P. L. & E., C. C. *IN VIVO* OZONE EXPOSURE INDUCES ANTIOXIDANT/STRESS-RELATED RESPONSES IN MURINE LUNG AND SKIN. **36**, 673–681 (2004).

92. Valacchi, G. *et al.* Ozone exposure activates oxidative stress responses in murine skin. *Toxicology* **179**, 163–170 (2002).

93. Woodby, B., Penta, K., Pecorelli, A., Lila, M. A. & Valacchi, G. Skin Health from the Inside Out. (2020). doi:10.1146/annurev-food-032519

94. Codreanu, S. G., Zhang, B., Sobecki, S. M., Billheimer, D. D. & Liebler, D. C. Global analysis of protein damage by the lipid electrophile 4-hydroxy-2-nonenal. *Mol. Cell. Proteomics* **8**, 670–680 (2009).

95. Davies, K. J. & Delsignore, M. E. Protein damage and degradation by oxygen radicals. III. Modification of secondary and tertiary structure. *J. Biol. Chem.* **262**, 9908–9913 (1987).

96. Poli, G. *et al.* Enzymatic impairment induced by biological aldehydes in intact rat liver cells. *Research Communications in Chemical Pathology and Pharmacology* **38**, 71–76 (1982).

97. Sottero, B. *et al.* Lipid Oxidation Derived Aldehydes and Oxysterols Between Health and Disease. doi:10.1002/ejlt.201700047

98. Grune, T. *et al.* Increased levels of 4-hydroxynonenal modified proteins in plasma of children with autoimmune diseases. *Free Radic. Biol. Med.* **23**, 357–360 (1997).

99. Pecorelli, A. *et al.* Increased levels of 4-HNE-protein plasma adducts in Rett syndrome. *Clin. Biochem.* **44**, 368–371 (2011).

100. Morita, A., Torii, K., Maeda, A. & Yamaguchi, Y. Molecular basis of tobacco smoke-

induced premature skin aging. *J. Investig. Dermatology Symp. Proc.* **14**, 53–55 (2009).

101. Vogel, C. F. A., Van Winkle, L. S., Esser, C. & Haarmann-Stemmann, T. The aryl hydrocarbon receptor as a target of environmental stressors – Implications for pollution mediated stress and inflammatory responses. *Redox Biol.* 101530 (2020). doi:10.1016/j.redox.2020.101530

102. Neavin, D. R., Liu, D., Ray, B. & Weinshilboum, R. M. The role of the aryl hydrocarbon receptor (AHR) in immune and inflammatory diseases. *Int. J. Mol. Sci.* **19**, (2018).

103. Afaq, F. *et al.* Aryl hydrocarbon receptor is an ozone sensor in human skin. *J. Invest. Dermatol.* **129**, 2396–2403 (2009).

104. Watson, A. J. & Hankinson, O. Dioxin- and Ah receptor-dependent protein binding to xenobiotic responsive elements and G-rich DNA studied by *in vivo* footprinting. *J. Biol. Chem.* **267**, 6874–6878 (1992).

105. Qiao, Y. *et al.* Airborne polycyclic aromatic hydrocarbons trigger human skin cells aging through aryl hydrocarbon receptor. *Biochem. Biophys. Res. Commun.* **488**, 445–452 (2017).

106. Ono, Y. *et al.* Role of the aryl hydrocarbon receptor in tobacco smoke extract-induced matrix metalloproteinase-1 expression. *Exp. Dermatol.* **22**, 349–353 (2013).

107. Kim, M. J. *et al.* Particulate matter induces pro-inflammatory cytokines via phosphorylation of p38 MAPK possibly leading to dermal inflammaging. *Exp. Dermatol.* **28**, 809–815 (2019).

108. Okayama, Y. Oxidative stress in allergic and inflammatory skin diseases. *Curr. Drug Targets Inflamm. Allergy* **4**, 517–519 (2005).

109. Baek, J. & Lee, M. G. Oxidative stress and antioxidant strategies in dermatology. *Redox Rep.* **21**, 164–169 (2016).

110. Xu, F., Xu, J., Xiong, X. & Deng, Y. Salidroside inhibits MAPK, NF-κB, and STAT3 pathways in psoriasis-associated oxidative stress via SIRT1 activation. *Redox Rep.* **24**, 70–74 (2019).

111. Wagner, K. H., Cameron-Smith, D., Wessner, B. & Franzke, B. Biomarkers of aging: From function to molecular biology. *Nutrients* **8**, 8–10 (2016).

112. Kudryavtseva, A. V. *et al.* Mitochondrial dysfunction and oxidative stress in aging and cancer. *Oncotarget* **7**, 44879–44905 (2016).

113. Franceschi, C., Garagnani, P., Parini, P., Giuliani, C. & Santoro, A. Inflammaging: a new immune–metabolic viewpoint for age-related diseases. *Nature Reviews Endocrinology* **14**, 576–590 (2018).

114. Man, M. Q. & Elias, P. M. Could inflammaging and its sequelae be prevented or mitigated? *Clin. Interv. Aging* **14**, 2301–2304 (2019).

115. Zhuang, Y. & Lyga, J. Inflammaging in skin and other tissues - the roles of complement system and macrophage. *Inflamm. Allergy - Drug Targets* **13**, 153–161 (2014).

116. Martinon, F., Burns, K., Boveresses, C. & Epalinges, C.-. The Inflammasome : A Molecular Platform Triggering Activation of Inflammatory Caspases and Processing of proIL- ⊠. **10**, 417–426 (2002).

117. Rathinam, V. A. K. & Chan, F. K. M. Inflammasome, Inflammation, and Tissue Homeostasis. *Trends Mol. Med.* **24**, 304–318 (2018).

118. Harder, J. & Nũez, G. Functional expression of the intracellular pattern recognition receptor NOD1 in human keratinocytes. *J. Invest. Dermatol.* **129**, 1299–1302 (2009).

119. Sand, J. *et al.* Expression of inflammasome proteins and inflammasome activation occurs in human, but not in murine keratinocytes article. *Cell Death Dis.* **9**, (2018).

120. Burian, M. & Yazdi, A. S. NLRP1 Is the Key Inflammasome in Primary Human Keratinocytes. *J. Invest. Dermatol.* **138**, 2507–2510 (2018).

121. Khare, S., Luc, N., Dorfleutner, A. & Stehlik, C. *Inflammasomes and Their Activation*. *Critical reviews in immunology* **30**, (2010).

122. Burian, M. & Yazdi, A. S. NLRP1 Is the Key Inflammasome in Primary Human Keratinocytes. *Journal of Investigative Dermatology* **138**, 2507–2510 (2018).

123. Kummer, J. A. *et al.* Inflammasome components NALP 1 and 3 show distinct but separate expression profiles in human tissues suggesting a site-specific role in the inflammatory response. *J. Histochem. Cytochem.* **55**, 443–452 (2007).

124. Zhong, F. L. *et al.* Germline NLRP1 Mutations Cause Skin Inflammatory and Cancer Susceptibility Syndromes via Inflammasome Activation. *Cell* **167**, 187-202.e17 (2016).

125. Marie, J. *et al.* Inflammasome activation and vitiligo/nonsegmental vitiligo progression. *Br. J. Dermatol.* **170**, 816–823 (2014).

126. Levandowski, C. B. *et al.* NLRP1 haplotypes associated with vitiligo and autoimmunity increase interleukin-1β processing via the NLRP1 inflammasome. *Proc. Natl. Acad. Sci. U. S. A.* **110**, 2952–2956 (2013).

127. Gurung, P. & Kanneganti, T. D. Autoinflammatory Skin Disorders: The Inflammasomme in Focus. *Trends in Molecular Medicine* **22**, 545–564 (2016).

128. Mogensen, T. H. Pathogen recognition and inflammatory signaling in innate immune defenses. *Clin. Microbiol. Rev.* **22**, 240–273 (2009).

129. Latz, E., Xiao, T. S. & Stutz, A. Activation and regulation of the inflammasomes. **13**, (2013).

130. Fink, S. L. & Cookson, B. T. Caspase-1-dependent pore formation during pyroptosis leads to osmotic lysis of infected host macrophages. *J. Immunol.* **202**, 1913–1926 (2006).

131. Toldo, S., Mauro, A. G., Cutter, Z. & Abbate, A. Inflammasome, pyroptosis, and cytokines in myocardial ischemia-reperfusion injury. *Am. J. Physiol. - Hear. Circ. Physiol.* **315**, H1553–H1568 (2018).

132. He, W. T. *et al.* Gasdermin D is an executor of pyroptosis and required for interleukin-1β secretion. *Cell Res.* **25**, 1285–1298 (2015).

133. Garlanda, C., Dinarello, C. A. & Mantovani, A. The Interleukin-1 Family: Back to the Future. *Immunity* **39**, 1003–1018 (2013).

134. Sedimbi, S. K., Hägglöf, T. & Karlsson, M. C. I. IL-18 in inflammatory and autoimmune disease. *Cell. Mol. Life Sci.* **70**, 4795–4808 (2013).

135. Bonnekoh, H. *et al.* Spectrum of Genetic Autoinflammatory Diseases Presenting with Cutaneous Symptoms. *Acta Derm. Venereol.* 0 (2020). doi:10.2340/00015555-3427

136. Azam, S. *et al.* Regulation of Toll-Like Receptor (TLR) Signaling Pathway by Polyphenols in the Treatment of Age-Linked Neurodegenerative Diseases: Focus on TLR4 Signaling. *Front. Immunol.* **10**, 1000 (2019).

137. Saresella, M. *et al.* The NLRP3 and NLRP1 inflammasomes are activated in Alzheimer's disease. *Mol. Neurodegener.* **11**, 1–15 (2016).

138. Guo, H., Callaway, J. B. & Ting, J. P. Y. Inflammasomes: Mechanism of action, role in disease, and therapeutics. *Nat. Med.* **21**, 677–687 (2015).

139. Wang, D., Duncan, B., Li, X. & Shi, J. The role of NLRP3 inflammasome in infection-related, immune-mediated and autoimmune skin diseases. *J. Dermatol. Sci.* 1–6 (2020). doi:10.1016/j.jdermsci.2020.03.001

140. Iversen, L. & Johansen, C. Inflammasomes and inflammatory caspases in skin inflammation. *Expert Review of Molecular Diagnostics* **8**, 697–705 (2008).

141. Duan, S. *et al.* NLRP3 inflammasome activation is associated with PM2.5-induced cardiac functional and pathological injury in mice. *Environ. Toxicol.* **34**, 1246–1254 (2019).

142. Du, X. *et al.* Fine particulate matter-induced cardiovascular injury is associated with NLRP3 inflammasome activation in Apo E -/- mice. *Ecotoxicol. Environ. Saf.* **174**, 92–99 (2019).

143. Sayan, M. & Mossman, B. T. The NLRP3 inflammasome in pathogenic particle and fibre-associated lung inflammation and diseases. *Part. Fibre Toxicol.* **13**, 1–15 (2016).

144. Zheng, R. *et al.* NLRP3 inflammasome activation and lung fibrosis caused by airborne fine particulate matter. *Ecotoxicol. Environ. Saf.* **163**, 612–619 (2018).

145. Wang, Y. *et al.* Activation of NLRP3 inflammasome enhances the proliferation and migration of A549 lung cancer cells. *Oncol. Rep.* **35**, 2053–2064 (2016).

146. Zhou, L. *et al.* Carbon black nanoparticles induce pulmonary fibrosis through NLRP3 inflammasome pathway modulated by miR-96 targeted FOXO3a. *Chemosphere* **241**, 125075 (2020).

147. Eltom, S. *et al.* Role of the inflammasome-caspase1/11-IL-1/18 axis in CS driven airway inflammation: An insight into the pathogenesis of COPD. *PLoS One* **9**, (2014).

148. Buscetta, M. *et al.* CS inhibits the NLRP3 inflammasome and leads to caspase-1 activation via the TLR4-TRIF-caspase-8 axis in human macrophages. *FASEB J.* **34**, 1819–1832 (2020).

149. Che, L. *et al.* Ozone-induced IL-17A and neutrophilic airway inflammation is orchestrated by the caspase-1-IL-1 cascade. *Sci. Rep.* **6**, 1–11 (2016).

150. Li, F. *et al.* Roles of mitochondrial ROS and NLRP3 inflammasome in multiple ozone-induced lung inflammation and emphysema. *Respir. Res.* **19**, 1–12 (2018).

151. Michaudel, C., Couturier-maillard, A., Chenuet, P., Maillet, I. & Mura, C. Inflammasome , IL-1 and inflammation in ozone-induced lung injury. **5**, 33–40 (2016).

152. Gruber, J. V. & Holtz, R. *In vitro* expression of NLRP inflammasome-induced active Caspase-1 expression in normal human epidermal keratinocytes (NHEK) by various exogenous threats and subsequent inhibition by naturally derived ingredient blends. *J. Inflamm. Res.* **12**, 219–230 (2019).

153. Fenini, G. *et al.* Genome Editing of Human Primary Keratinocytes by CRISPR/Cas9 Reveals an Essential Role of the NLRP1 Inflammasome in UVB Sensing. *J. Invest. Dermatol.* **138**, 2644–2652 (2018).

154. Hasegawa, T., Nakashima, M. & Suzuki, Y. Nuclear DNA damage-triggered NLRP3 inflammasome activation promotes UVB-induced inflammatory responses in human keratinocytes. *Biochem. Biophys. Res. Commun.* **477**, 329–335 (2016).

155. Feldmeyer, L. *et al.* The Inflammasome Mediates UVB-Induced Activation and Secretion of Interleukin-1β by Keratinocytes. *Curr. Biol.* **17**, 1140–1145 (2007).

156. Hung, S. J. *et al.* Photoprotective Potential of Glycolic Acid by Reducing NLRC4 and AIM2 Inflammasome Complex Proteins in UVB Radiation-Induced Normal Human Epidermal Keratinocytes and Mice. *DNA Cell Biol.* **36**, 177–187 (2017).

157. Ferrara, F. *et al.* Redox regulation of cutaneous inflammasome by ozone exposure. *Free Radic. Biol. Med.* 0–1 (2019). doi:10.1016/j.freeradbiomed.2019.11.031

158. Ghofranian, A. & Maibach, H. I. *Effects of Air Pollution on Skin: Dermatologic options*. *Cosmetic Science and Technology: Theoretical Principles and Applications* (Elsevier Inc., 2017). doi:10.1016/B978-0-12-802005-0.00047-1

159. Kantor, R. & Silverberg, J. I. Environmental risk factors and their role in the management of atopic dermatitis. *Expert Rev. Clin. Immunol.* **13**, 15–26 (2017).

160. Ahn, K. The role of air pollutants in atopic dermatitis. *J. Allergy Clin. Immunol.* **134**, 993–999 (2014).

161. Song, S. *et al.* Acute health effects of urban fine and ultrafine particles on children with atopic dermatitis. *Environ. Res.* **111**, 394–399 (2011).

162. Eberlein-König, B. *et al.* Influence of airborne nitrogen dioxide or formaldehyde on parameters of skin function and cellular activation in patients with atopic eczema and control subjects. *J. Allergy Clin. Immunol.* **101**, 141–143 (1998).

163. Kim, J. *et al.* Symptoms of atopic dermatitis are influenced by outdoor air pollution. *J. Allergy Clin. Immunol.* **132**, (2013).

164. Peden, D. & Reed, C. E. Environmental and occupational allergies. *J. Allergy Clin. Immunol.* **125**, (2010).

165. Lee, Y. L., Su, H. J., Sheu, H. M., Yu, H. S. & Guo, Y. L. Traffic-related air pollution,

climate, and prevalence of eczema in Taiwanese school children. *J. Invest. Dermatol.* **128**, 2412–2420 (2008).

166. Boutin-Forzano, S., Gouitaa, M. & Charpin, D. [Pollution and atopy]. *Eur Ann Allergy Clin Immunol* **36**, 192–196 (2004).

167. Morgenstern, V. *et al.* Atopic diseases, allergic sensitization, and exposure to traffic-related air pollution in children. *Am. J. Respir. Crit. Care Med.* **177**, 1331–1337 (2008).

168. Gehring, U. *et al.* Traffic-related air pollution and the development of asthma and allergies during the first 8 years of life. *Am. J. Respir. Crit. Care Med.* **181**, 596–603 (2010).

169. Yi, O. *et al.* Effect of environmental tobacco smoke on atopic dermatitis among children in Korea. *Environ. Res.* **113**, 40–45 (2012).

170. Xu, F. *et al.* Ambient ozone pollution as a risk factor for skin disorders. *British Journal of Dermatology* **165**, 224–225 (2011).

171. Özden, M. G. *et al.* Environmental Risk Factors in Pediatric Psoriasis: A Multicenter Case-Control Study. *Pediatr. Dermatol.* **28**, 306–312 (2011).

172. Armstrong, A. W., Harskamp, C. T., Dhillon, J. S. & Armstrong, E. J. Psoriasis and smoking: A systematic review and meta-analysis. *British Journal of Dermatology* **170**, 304–314 (2014).

173. Vierkötter, A. *et al.* Airborne particle exposure and extrinsic skin aging. *J. Invest. Dermatol.* **130**, 2719–2726 (2010).
174. Vierkötter, A. *et al.* Airborne particle exposure and extrinsic skin aging. *J. Invest. Dermatol.* **130**, 2719–2726 (2010).
175. O'Hare, P. M. *et al.* Tobacco smoking contributes little to facial wrinkling. *J. Eur. Acad. Dermatology Venereol.* **12**, 133–139 (1999).

176. Bernhard, D., Moser, C., Backovic, A. & Wick, G. CS - an aging accelerator? *Exp. Gerontol.* **42**, 160–165 (2007).

177. Burke, K. & Wei, H. Synergistic damage by UVA radiation and pollutants. *Toxicol. Ind. Health* **25**, 219–224 (2009).

178. Puntoni, R. *et al.* Occupational exposure to carbon black and risk of cancer. *Cancer Causes Control* **15**, 511–516 (2004).

179. Boffetta, P., Jourenkova, N. & Gustavsson, P. Cancer risk from occupational and environmental exposure to polycyclic aromatic hydrocarbons. *Cancer Causes Control* **8**, 444–472 (1997).

180. Liu, W. *et al.* A Time-Series Study of the Effect of Air Pollution on Outpatient Visits for Acne Vulgaris in Beijing. *Skin Pharmacol. Physiol.* **31**, 107–113 (2018).

181. Krutmann, J. *et al.* Pollution and acne: Is there a link? *Clinical, Cosmetic and Investigational Dermatology* **10**, 199–204 (2017).

182. Sorg, O. Tobacco Smoke and Chloracne: An Old Story Comes to Light. *Dermatology*

231, 297–297 (2015).

183. Schäfer, T., Nienhaus, A., Vieluf, D., Berger, J. & Ring, J. Epidemiology of acne in the general population: the risk of smoking. *Br. J. Dermatol.* **145**, 100–4 (2001).

184. Yang, Y. S. *et al.* CS-induced interleukin-1 alpha may be involved in the pathogenesis of adult acne. *Ann. Dermatol.* **26**, 11–16 (2014).

185. Su, L. H. & Chen, T. H. H. Association of androgenetic alopecia with smoking and its prevalence among Asian men: A community-based survey. *Arch. Dermatol.* **143**, 1401–1406 (2007).

186. Skin, A. *Aging and Intrinsic Aging; Cellular Energy Metabolism and Oxidative Stress. Textbook of Aging Skin* (2010). doi:0133-ch0124-9780723435716.indd2072

187. Peng, W. & Novak, N. Pathogenesis of atopic dermatitis. *Clin. Exp. Allergy* **45**, 566–74 (2015).

188. Orion, E., Ruocco, E. & Ruocco, V. Abnormal epidermal barrier in the pathogenesis of psoriasis. *Clin. Dermatol.* **30**, 323–328 (2012).

189. Segre, J. A. Epidermal barrier formation and recovery in skin disorders. *Journal of Clinical Investigation* **116**, 1150–1158 (2006).

190. Farage, M. A., Miller, K. W., Elsner, P. & Maibach, H. I. Intrinsic and extrinsic factors in skin ageing: a review. *Int. J. Cosmet. Sci.* **30**, 87–95 (2008).

191. Valacchi, G. *et al.* Cutaneous responses to environmental stressors. *Ann. N. Y. Acad. Sci.* **1271**, 75–81 (2012).

192. Farage, M. A. & Maibach, H. I. Sensitive skin: Closing in on a physiological cause. *Contact Dermatitis* **62**, 137–149 (2010).

193. Jeffrey Atkinson. COPD: Pathogenesis, Epidemiology, and the Role of CS. Available at: http://www.pulmonologyadvisor.com/pulmonary-medicine/copd-pathogenesis-epidemiology-and-the-role-of-cigarette-smoke/article/661027/. (Accessed: 4th October 2018)

194. Furrukh, M. Tobacco Smoking and Lung Cancer: Perception-changing facts. *Sultan Qaboos Univ. Med. J.* **13**, 345 (2013).

195. Bakhru, A. & Erlinger, T. P. Smoking Cessation and Cardiovascular Disease Risk Factors: Results from the Third National Health and Nutrition Examination Survey. *PLoS Med.* **2**, e160 (2005).

196. Ambrose, J. A. & Barua, R. S. The pathophysiology of cigarette smoking and cardiovascular disease. *J. Am. Coll. Cardiol.* **43**, 1731–1737 (2004).

197. EPIDEMIC, W. R. O. T. G. T. *The global tobacco crisis Tobacco-global agent of death*. (2018).

198. Cooke, M. The Chemical Components of Tobacco and Tobacco Smoke. *Chromatographia* **71**, 977–977 (2010).

199. Hahn, J. *et al.* Electronic cigarettes: overview of chemical composition and exposure estimation. *Tob. Induc. Dis.* **12**, 23 (2014).

200. Cervellati, F. *et al.* Comparative effects between electronic and CS in human keratinocytes and epithelial lung cells. *Toxicol. Vitr.* **28**, 999–1005 (2014).

201. Clapp, P. W. & Jaspers, I. Electronic Cigarettes: Their Constituents and Potential Links to Asthma. *Curr. Allergy Asthma Rep.* **17**, 79 (2017).

202. Clunes, L. A., Bridges, A., Alexis, N. & Tarran, R. *In vivo* versus *in vitro* airway surface liquid nicotine levels following CS exposure. *J. Anal. Toxicol.* **32**, 201–7 (2008).

203. Metelitsa, A. I. & Lauzon, G. J. Tobacco and the skin. *Clin. Dermatol.* **28**, 384–390 (2010).

204. Egawa, M., Kohno, Y. & Kumano, Y. Oxidative effects of CS on the human skin. *Int. J. Cosmet. Sci.* **21**, 83–98 (1999).

205. Schick, S. & Glantz, S. Philip Morris toxicological experiments with fresh sidestream smoke: More toxic than mainstream smoke. *Tob. Control* **14**, 396–404 (2005).

206. Freiman, A., Bird, G., Metelitsa, A. I., Barankin, B. & Lauzon, G. J. Cutaneous effects of smoking. *J. Cutan. Med. Surg.* **8**, 415–423 (2004).

207. Ernster, V. L. *et al.* Facial wrinkling in men and women, by smoking status. *Am. J. Public Health* **85**, 78–82 (1995).

208. Doshi, D. N., Hanneman, K. K. & Cooper, K. D. Smoking and skin aging in identical twins. *Arch. Dermatol.* **143**, 1543–1546 (2007).

209. Wagner, H. L. & Triggle, D. J. *Nicotine*. (Chelsea House Publishers, 2003).

210. Guttman-Yassky, E. & Krueger, J. G. Atopic dermatitis and psoriasis: two different immune diseases or one spectrum? *Curr. Opin. Immunol.* **48**, 68–73 (2017).

211. Lecas, S. *et al. In vitro* model adapted to the study of skin ageing induced by air pollution. *Toxicol. Lett.* **259**, 60–68 (2016).

212. Avezov, K., Reznick, A. Z. & Aizenbud, D. Oxidative damage in keratinocytes exposed to CS and aldehydes. *Toxicol. Vitr.* **28**, 485–491 (2014).

213. Roemer, E. *et al.* Mainstream smoke chemistry and *in vitro* and *in vivo* toxicity of the reference cigarettes 3R4F and 2R4F. *Beitrage zur Tab. Int. Contrib. to Tob. Res.* **25**, 316–335 (2012).

214. Kim, J. N., Kim, H. J., Jeong, S. H., Kye, Y. C. & Son, S. W. CS-induced early growth response-1 regulates the expression of the cysteine-rich 61 in human skin dermal fibroblasts. *Exp. Dermatol.* **20**, 992–997 (2011).

215. Crivellari, I. *et al.* SRB1 as a new redox target of CS in human sebocytes. *Free Radic. Biol. Med.* **102**, 47–56 (2017).

216. Jeong, S. H. *et al.* Up-regulation of TNF-alpha secretion by CS is mediated by Egr-1 in HaCaT human keratinocytes. *Exp. Dermatol.* **19**, 206–212 (2010).

217. Yang, G. Y., Zhang, C. L., Liu, X. C., Qian, G. & Deng, D. Q. Effects of CS extracts on the growth and senescence of skin fibroblasts *In vitro*. *Int. J. Biol. Sci.* **9**, 613–623 (2013).

218. Yin, L., Morita, A. & Tsuji, T. Skin aging induced by ultraviolet exposure and tobacco smoking: evidence from epidemiological and molecular studies. *Photodermatol. Photoimmunol. Photomed.* **17**, 178–83 (2001).

219. Ono, Y. *et al.* Role of the aryl hydrocarbon receptor in tobacco smoke extract-induced matrix metalloproteinase-1 expression. *Exp. Dermatol.* **22**, 349–353 (2013).

220. Romero, A. *et al.* CS condensate inhibits collagen gel contraction and prostaglandin E2 production in human gingival fibroblasts. *J. Periodontal Res.* **50**, 371–379 (2015).

221. Church, D. F. & Pryor, W. A. Free-radical chemistry of CS and its toxicological implications. *Environ. Health Perspect.* **VOL. 64**, 111–126 (1985).

222. Pryor, W. A., Dooley, M. M. & Church, D. F. Mechanisms of CS toxicity: the inactivation of human α-1-proteinase inhibitor by nitric oxide/isoprene mixtures in air. *Chem. Biol. Interact.* **54**, 171–183 (1985).

223. Chatterjee, I. B. & Dey, N. Regarding detection of hydrogen peroxide in CS. *{FASEB} J. Off. Publ. Fed. Am. Soc. Exp. Biol.* **22**, 3755; author reply 3755--3756 (2008).

224. Rajagopalan, P. *et al.* How Does Chronic CS Exposure Affect Human Skin? A Global Proteomics Study in Primary Human Keratinocytes. *Omi. A J. Integr. Biol.* **20**, 615–626 (2016).

225. Bishop, E. *et al.* An approach to testing undiluted e-cigarette aerosol *in vitro* using 3D reconstituted human airway epithelium. *Toxicol. Vitr.* 0–1 (2018). doi:10.1016/j.tiv.2018.01.010

226. Thorne, D., Larard, S., Baxter, A., Meredith, C. & Gaça, M. The comparative *in vitro* assessment of e-cigarette and CS aerosols using the γH2AX assay and applied dose measurements. *Toxicol. Lett.* **265**, 170–178 (2017).

227. Li, X. *In vitro* toxicity testing of CS based on the air-liquid interface exposure: A review. *Toxicol. Vitr.* **36**, 105–113 (2016).

228. Adamson, J., E, L., Phillips, G. & D, M. *In vitro* Models of Chronic Obstructive Pulmonary Disease (COPD). in *Bronchitis* (InTech, 2011). doi:10.5772/18247

229. Vardavas, C. I. *et al.* Short-term Pulmonary Effects of Using an Electronic Cigarette: Impact on Respiratory Flow Resistance, Impedance, and Exhaled Nitric Oxide. *Chest* **141**, 1400–1406 (2012).

230. Layden, J. E. *et al.* Pulmonary Illness Related to E-Cigarette Use in Illinois and Wisconsin — Preliminary Report. *N. Engl. J. Med.* NEJMoa1911614 (2019). doi:10.1056/NEJMoa1911614

231. Misery, L. Nicotine effects on skin: Are they positive or negative? *Exp. Dermatol.* **13**, 665–670 (2004).

232. Hess, C. A. *et al.* E-cigarettes as a source of toxic and potentially carcinogenic metals. *Environ. Res.* **152**, 221–225 (2017).

233. Khlystov, A. & Samburova, V. Flavoring Compounds Dominate Toxic Aldehyde Production during E-Cigarette Vaping. *Environ. Sci. Technol.* **50**, 13080–13085 (2016).

234. Bahl, V. *et al.* Comparison of electronic cigarette refill fluid cytotoxicity using embryonic and adult models. *Reprod. Toxicol.* **34**, 529–537 (2012).

235. Cervellati, F. *et al.* Comparative effects between electronic and CS in human keratinocytes and epithelial lung cells. *Toxicol. Vitr.* **28**, 999–1005 (2014).

236. Laporta, R. & Mercer, N. Quid causit perioral wrinkles? (2013). doi:10.1016/j.bjps.2012.09.037

237. Neilson, L. *et al.* Development of an *in vitro* cytotoxicity model for aerosol exposure using 3D reconstructed human airway tissue; application for assessment of e-cigarette aerosol. *Toxicol. Vitr.* **29**, 1952–1962 (2015).

238. Callahan-Lyon, P. Electronic cigarettes: human health effects. *Tob. Control* **23**, ii36–ii40 (2014).

239. Robinson, M. K. *et al.* Non-animal testing strategies for assessment of the skin corrosion and skin irritation potential of ingredients and finished products. *Food Chem. Toxicol.* **40**, 573–92 (2002).

240. Ono, Y. *et al.* Role of the aryl hydrocarbon receptor in tobacco smoke extract-induced matrix metalloproteinase-1 expression. *Exp. Dermatol.* **22**, 349–353 (2013).

241. Jeong, S. H. *et al.* Up-regulation of TNF-alpha secretion by CS is mediated by Egr-1 in HaCaT human keratinocytes. *Exp. Dermatol.* **19**, e206–e212 (2009).

242. Dong, J., Segawa, R., Mizuno, N., Hiratsuka, M. & Hirasawa, N. Inhibitory effects of nicotine derived from CS on thymic stromal lymphopoietin production in epidermal keratinocytes. *Cell. Immunol.* **302**, 19–25 (2016).

243. Yin, L., Morita, a & Tsuji, T. Alterations of extracellular matrix induced by tobacco smoke extract. *Arch. Dermatol. Res.* **292**, 188–194 (2000).

244. Kim, J. N. *et al.* CS-induced Egr-1 represses TβR-II expression in human skin dermal fibroblasts. *Toxicology* **275**, 29–35 (2010).

245. Nakamura, M. *et al.* Tobacco smoke-induced skin pigmentation is mediated by the aryl hydrocarbon receptor. *Exp. Dermatol.* **22**, 556–558 (2013).

246. Hubaux, R., Weisgerber, F. & Salmon, M. *In vitro* assays to study the effects of air pollutants on skin: exposure to urban dust and CS extract.

247. Tsuji, H. *et al.* Comparison of dermal tumor promotion activity of CS condensate from prototype (heated) cigarette and reference (combusted) cigarette in SENCAR mice. *Food Chem. Toxicol.* **72**, 187–194 (2014).

248. Ejaz, S. & Lim, C. W. Impaired wound healing by exposure of different mainstream whole smoke solutions of commercial cigarettes. *Environ. Toxicol. Pharmacol.* **21**, 290–300 (2006).

249. Naserzadeh, P., Hosseini, M. J., Arbabi, S. & Pourahmad, J. A comparison of toxicity mechanisms of CS on isolated mitochondria obtained from rat liver and skin. *Iran. J. Pharm. Res.* **14**, 271–277 (2015).

250. Sticozzi, C. *et al.* CS affects keratinocytes SRB1 expression and localization via H 2O 2 production and HNE protein adducts formation. *PLoS One* **7**, 1–14 (2012).

251. Sticozzi, C., Pecorelli, A., Belmonte, G. & Valacchi, G. CS affects ABCAl expression via liver X receptor nuclear translocation in human keratinocytes. *Int. J. Mol. Sci.* **11**, 3375–3386 (2010).

252. Sticozzi, C. *et al.* Resveratrol protects SR-B1 levels in keratinocytes exposed to CS. *Free Radic. Biol. Med.* **69**, 50–57 (2014).

253. Avezov, K., Reznick, A. Z. & Aizenbud, D. Oxidative damage in keratinocytes exposed to CS and aldehydes. *Toxicol. Vitr.* **28**, 485–491 (2014).

254. Hammer, T. R., Fischer, K., Mueller, M. & Hoefer, D. Effects of CS residues from textiles on fibroblasts, neurocytes and zebrafish embryos and nicotine permeation through human skin. *Int. J. Hyg. Environ. Health* **214**, 384–391 (2011).

255. Costa, A. *et al.* Honokiol protects skin cells against inflammation, collagenolysis, apoptosis, and senescence caused by CS damage. *Int. J. Dermatol.* **56**, 754–761 (2017).

256. Muresan, X. M. *et al.* Modulation of cutaneous scavenger receptor B1 levels by exogenous stressors impairs "*in vitro*" wound closure. *Mech. Ageing Dev.* 0–1 (2017). doi:10.1016/j.mad.2017.11.006

257. Rasmussen, C. *et al.* The StrataTest®human skin model, a consistent *in vitro* alternative for toxicological testing. *Toxicol. Vitr.* **24**, 2021–2029 (2010).

258. Chen, H. *et al.* EGR-1 regulates Ho-1 expression induced by CS. *Biochem. Biophys. Res. Commun.* **396**, 388–393 (2010).

259. Martins-Green, M. *et al.* CS Toxins Deposited on Surfaces: Implications for Human Health. *PLoS One* **9**, e86391 (2014).

260. Sticozzi, C. *et al.* Modulation of skin oxidative stress and inflammatory markers by environmental stressors. Differences between young and old. *J. Dermatol. Sci.* **65**, 226–228 (2012).

261. Chaichalotornkul, S. *et al.* Secondhand smoke exposure-induced nucleocytoplasmic shuttling of HMGB1 in a rat premature skin aging model. *Biochem. Biophys. Res. Commun.* **456**, 92–97 (2015).

262. Valacchi, G., Virgili, F., Cervellati, C. & Pecorelli, A. OxInflammation: From Subclinical Condition to Pathological Biomarker. *Front. Physiol.* **9**, 858 (2018).

263. Yang, Y. S. *et al.* CS-Induced Interleukin-1 Alpha May Be Involved in the Pathogenesis of Adult Acne. *Ann. Dermatol.* **26**, 11 (2014).

264. Magcwebeba, T. *et al.* Interleukin-1 α Induction in Human Keratinocytes (HaCaT): An *In vitro* Model for Chemoprevention in Skin . *J. Skin Cancer* **2012**, 1–10 (2012).

265. Feghali, C. A. & Wright, T. M. Cytokines in acute and chronic inflammation. *Frontiers in bioscience : a journal and virtual library* **2**, (1997).

266. Bou-Dargham, M. J., Khamis, Z. I., Cognetta, A. B. & Sang, Q.-X. A. The Role of Interleukin-1 in Inflammatory and Malignant Human Skin Diseases and the Rationale for Targeting Interleukin-1 Alpha. *Med. Res. Rev.* **37**, 180–216 (2017).

267. Kupper, T. S., Lee, F., Birchall, N., Clark, S. & Dower, S. Interleukin 1 binds to

specific receptors on human keratinocytes and induces granulocyte macrophage colony-stimulating factor mRNA and protein. A potential autocrine role of interleukin 1 in epidermis. *J. Clin. Invest.* **82**, 1787–1792 (1988).

268. Kupper, T. S., Chua, A. O., Flood, P., McGuire, J. & Gubler, U. Interleukin 1 gene expression in cultured human keratinocytes is augmented by ultraviolet irradiation. *J. Clin. Invest.* **80**, 430–436 (1987).

269. Coquette, A. *et al.* Analysis of interleukin-1α (IL-1α) and interleukin-8 (IL-8) expression and release in *in vitro* reconstructed human epidermis for the prediction of *in vivo* skin irritation and/or sensitization. *Toxicol. Vitr.* **17**, 311–321 (2003).

270. Wilmer, J. L., Burleson, F. G., Kayama, F., Kanno, J. & Luster, M. I. Cytokine induction in human epidermal keratinocytes exposed to contact irritants and its relation to chemical-induced inflammation in mouse skin. *J. Invest. Dermatol.* **102**, 915–922 (1994).

271. Dae, H. S., Jai, I. Y. & Hee, C. E. Effects of 12-O-tetradecanoyl-phorbol and sodium lauryl sulfate on the production and expression of cytokines and proto-oncogenes in photoaged and intrinsically aged human keratinocytes. *J. Invest. Dermatol.* **117**, 1225–1233 (2001).

272. Ettehadi, P., Greaves, M. W., Wallach, D., Aderka, D. & Camp, R. D. Elevated tumour necrosis factor-alpha (TNF-alpha) biological activity in psoriatic skin lesions. *Clin. Exp. Immunol.* **96**, 146–51 (1994).

273. Becke, F. M., Hehlgans, T., Brockhoff, G. & Männel, D. N. Development of allergic contact dermatitis requires activation of both tumor necrosis factor-receptors. *Eur. Cytokine Netw.* **12**, 45–50 (2001).

274. Teraki, Y., Moriya, N. & Shiohara, T. Drug-induced expression of intercellular adhesion molecule-1 on lesional keratinocytes in fixed drug eruption. *Am. J. Pathol.* **145**, 550–60 (1994).

275. Yıldırım Baş, F. *et al.* Effect of alpha lipoic acid on smoking-induced skin damage. *Cutan. Ocul. Toxicol.* **36**, 67–73 (2017).

276. Kennedy-Feitosa, E. *et al.* Eucalyptol attenuates CS-induced acute lung inflammation and oxidative stress in the mouse. *Pulm. Pharmacol. Ther.* **41**, 11–18 (2016).

277. Turner, M. D., Nedjai, B., Hurst, T. & Pennington, D. J. Cytokines and chemokines: At the crossroads of cell signalling and inflammatory disease. *Biochim. Biophys. Acta - Mol. Cell Res.* **1843**, 2563–2582 (2014).

278. Duan, H. *et al.* Interleukin-8-positive neutrophils in psoriasis. *J. Dermatol. Sci.* **26**, 119–24 (2001).

279. Anttila, H. S. I. *et al.* Interleukin-8 Immunoreactivity in the Skin of Healthy Subjects and Patients with Palmoplantar Pustulosis and Psoriasis. *J. Invest. Dermatol.* **98**, 96–101 (1992).

280. Lyte, P., Sur, R., Nigam, A. & Southall, M. D. Heat-killed *Propionibacterium acnes* is capable of inducing inflammatory responses in skin. *Exp. Dermatol.* **18**, 1070–1072 (2009).

281. Chen, Q. *et al.* Propionibacterium acnes-induced IL-8 production may be mediated by NF-kappaB activation in human monocytes. *J. Dermatol. Sci.* **29**, 97–103 (2002).

282. Tsuji, G. *et al.* An environmental contaminant, benzo(a)pyrene, induces oxidative stress-mediated interleukin-8 production in human keratinocytes via the aryl hydrocarbon receptor signaling pathway. *J. Dermatol. Sci.* **62**, 42–49 (2011).

283. Ursini, F., Maiorino, M. & Forman, H. J. Redox homeostasis: The Golden Mean of healthy living. *Redox Biol.* **8**, 205–215 (2016).

284. Bickers, D. R. & Athar, M. Oxidative stress in the pathogenesis of skin disease. *J. Invest. Dermatol.* **126**, 2565–2575 (2006).

285. L. Danoux, S. Cadau, S. Leoty-Okombi, C. Jeanmaire, P. Moussou, V. André-Frei. Synergistic Effect of UV and Pollutants on Human Skin, IFSCC Journal 2017 , Volume 20, Number 3. *International Journal of Cosmetic Science* **20**, (2017).

286. Burcham, P. C. Genotoxic lipid peroxidation products: their DNA damaging properties and role in formation of endogenous DNA adducts. *Mutagenesis* **13**, 287–305 (1998).

287. Sticozzi, C. *et al.* CS affects keratinocytes SRB1 expression and localization via H_2O_2 production and HNE protein adducts formation. *PLoS One* **7**, (2012).

288. Magnani, N. D. *et al.* Skin damage mechanisms related to airborne particulate matter exposure. *Toxicol. Sci.* **149**, 227–236 (2016).

289. Romani, A. *et al.* Keratinocytes oxidative damage mechanisms related to airbone particle matter exposure. *Mech. Ageing Dev.* **172**, 86–95 (2018).

290. Verdin, A. *et al.* An *in vitro* model to evaluate the impact of environmental fine particles (PM 0.3-2.5) on skin damage. *Toxicol. Lett.* **305**, 94–102 (2019).

291. Negre-Salvayre, A., Coatrieux, C., Ingueneau, C. & Salvayre, R. Advanced lipid peroxidation end products in oxidative damage to proteins. Potential role in diseases and therapeutic prospects for the inhibitors. *Br. J. Pharmacol.* **153**, 6–20 (2008).

292. Baglole, C. J., Sime, P. J. & Phipps, R. P. CS-induced expression of heme oxygenase-1 in human lung fibroblasts is regulated by intracellular glutathione. *Am. J. Physiol. Lung Cell. Mol. Physiol.* **295**, L624-36 (2008).

293. Pecorelli, A., Cervellati, C., Hayek, J. & Valacchi, G. OxInflammation in Rett syndrome. *Int. J. Biochem. Cell Biol.* **81**, 246–253 (2016).

294. Jux, B. *et al.* The aryl hydrocarbon receptor mediates UVB radiation-induced skin tanning. *J. Invest. Dermatol.* **131**, 203–210 (2011).

295. Uchi, H., Yasumatsu, M., Morino-Koga, S., Mitoma, C. & Furue, M. Inhibition of aryl hydrocarbon receptor signaling and induction of NRF2-mediated antioxidant activity by cinnamaldehyde in human keratinocytes. *J. Dermatol. Sci.* **85**, 36–43 (2017).

296. Costa, C. *et al.* Exposure of human skin to benzo[a]pyrene: Role of CYP1A1 and aryl hydrocarbon receptor in oxidative stress generation. *Toxicology* **271**, 83–86 (2010).

297. Di Meglio, P. *et al.* Activation of the aryl hydrocarbon receptor dampens the severity of inflammatory skin conditions. *Immunity* **40**, 989–1001 (2014).

298. Van Den Bogaard, E. H. *et al.* Genetic and pharmacological analysis identifies a physiological role for the AHR in epidermal differentiation. *J. Invest. Dermatol.* **135**, 1320–1328 (2015).

299. O'Driscoll, C. A. *et al.* Polycyclic aromatic hydrocarbons (PAHs) present in ambient urban dust drive proinflammatory T cell and dendritic cell responses via the aryl hydrocarbon receptor (AHR) *in vitro*. *PLoS One* **13**, e0209690 (2018).

300. Poligone, B. *et al.* A Role for NF-κB Activity in Skin Hyperplasia and the Development of Keratoacanthomata in Mice. *PLoS One* **8**, e71887 (2013).

301. Klement, J. F. *et al.* IkappaBalpha deficiency results in a sustained NF-kappaB response and severe widespread dermatitis in mice. *Mol. Cell. Biol.* **16**, 2341–9 (1996).

302. Kim, C. & Pasparakis, M. Epidermal p65/NF-κB signalling is essential for skin carcinogenesis. *EMBO Mol. Med.* **6**, 970–83 (2014).

303. Grinberg-Bleyer, Y. *et al.* Cutting Edge: NF-κB p65 and c-Rel Control Epidermal Development and Immune Homeostasis in the Skin. *J. Immunol.* **194**, 2472–2476 (2015).

304. Rebholz, B. *et al.* Crosstalk between Keratinocytes and Adaptive Immune Cells in an IκBα Protein-Mediated Inflammatory Disease of the Skin. *Immunity* **27**, 296–307 (2007).

305. Sur, I., Ulvmar, M. & Toftgård, R. The Two-Faced NF-κB in the Skin. *Int. Rev. Immunol.* **27**, 205–223 (2008).

306. Pasparakis, M. Regulation of tissue homeostasis by NF-κB signalling: implications for inflammatory diseases. *Nat. Rev. Immunol.* **9**, 778–788 (2009).

307. Fu, X.-J. *et al.* NADPH oxidase 1 and its derived reactive oxygen species mediated tissue injury and repair. *Oxid. Med. Cell. Longev.* **2014**, 282854 (2014).

308. Panday, A., Sahoo, M. K., Osorio, D. & Batra, S. NADPH oxidases: an overview from structure to innate immunity-associated pathologies. *Cell. Mol. Immunol.* **12**, 5–23 (2015).

309. Ning, W. *et al.* CS Stimulates Matrix Metalloproteinase-2 Activity via EGR-1 in Human Lung Fibroblasts. *Am. J. Respir. Cell Mol. Biol.* **36**, 480–490 (2007).

310. Ma, Q. Role of nrf2 in oxidative stress and toxicity. *Annu. Rev. Pharmacol. Toxicol.* **53**, 401–26 (2013).

311. Schäfer, M. & Werner, S. Nrf2—A regulator of keratinocyte redox signaling. *Free Radic. Biol. Med.* **88**, 243–252 (2015).

312. Pinkus, R., Weiner, L. M. & Daniel, V. *Role of Oxidants and Antioxidants in the Induction of AP-1, NF-B, and Glutathione S-Transferase Gene Expression**. (1996).

313. Eckert, R. L. *et al.* AP1 Transcription Factors in Epidermal Differentiation and Skin Cancer. *J. Skin Cancer* **2013**, 1–9 (2013).

314. Zhong, C.-Y., Zhou, Y.-M., Douglas, G. C., Witschi, H. & Pinkerton, K. E. MAPK/AP-1 signal pathway in tobacco smoke-induced cell proliferation and squamous metaplasia in the lungs of rats. doi:10.1093/carcin/bgi189

315. Müller, T. & Hengstermann, A. Nrf2: Friend *and* Foe in Preventing Cigarette Smoking-Dependent Lung Disease. *Chem. Res. Toxicol.* **25**, 1805–1824 (2012).

316. Lin, L. *et al.* Ursolic acid attenuates CS-induced emphysema in rats by regulating PERK and Nrf2 pathways. *Pulm. Pharmacol. Ther.* **44**, 111–121 (2017).

317. Gao, W., Guo, Y. & Yang, H. Platycodin D protects against CS-induced lung inflammation in mice. *Int. Immunopharmacol.* **47**, 53–58 (2017).

318. Nrf2 Signaling is Activated After CS Extract Exposure in Rpe Cells *in vitro* and *in vivo* | IOVS | ARVO Journals. Available at: https://iovs.arvojournals.org/article.aspx?articleid=2372730. (Accessed: 13th November 2020)

319. From Cellular Genotype to CS-Induced Phenotype: The Case of Nrf2 | PMI Science. Available at: https://www.pmiscience.com/library/publication/from-cellular-genotype-to-cigarette-smoke-induced-phenotype-the-case-of-nrf2. (Accessed: 13th November 2020)

320. Sekine, T. *et al.* Regulation of NRF2, AP-1 and NF-κB by CS exposure in three-dimensional human bronchial epithelial cells. *J. Appl. Toxicol.* **39**, 717–725 (2019).

321. Cano, M. *et al.* Cigarette smoking, oxidative stress, the anti-oxidant response through Nrf2 signaling, and Age-related Macular Degeneration. *Vision Res.* **50**, 652–664 (2010).

322. Müller, T. & Hengstermann, A. Nrf2: Friend and Foe in preventing cigarette smoking-dependent lung disease. *Chemical Research in Toxicology* **25**, 1805–1824 (2012).

323. Han, S. H., Jerome, J. A., Gregory, A. D. & Mallampalli, R. K. CS destabilizes NLRP3 protein by promoting its ubiquitination. *Respir. Res.* **18**, (2017).

324. Buscetta, M. *et al.* CS inhibits the NLRP3 inflammasome and leads to caspase-1 activation via the TLR4-TRIF-caspase-8 axis in human macrophages. *FASEB J.* **34**, 1819–1832 (2020).

325. Eltom, S. *et al.* Role of the inflammasome-caspase1/11-IL-1/18 axis in CS driven airway inflammation: An insight into the pathogenesis of COPD. *PLoS One* **9**, e112829 (2014).

326. Ye, P. *et al.* Long-term cigarette smoking suppresses NLRP3 inflammasome activation in oral mucosal epithelium and attenuates host defense against Candida albicans in a rat model. *Biomed. Pharmacother.* **113**, 108597 (2019).

327. Ayala-Fontánez, N., Soler, D. C. & McCormick, T. S. Current knowledge on psoriasis and autoimmune diseases. *Psoriasis (Auckland, N.Z.)* **6**, 7–32 (2016).

328. Albanesi, C., Madonna, S., Gisondi, P. & Girolomoni, G. The Interplay Between Keratinocytes and Immune Cells in the Pathogenesis of Psoriasis. *Front. Immunol.* **9**, 1549 (2018).

329. Lowes, M. A., Suárez-Fariñas, M. & Krueger, J. G. Immunology of Psoriasis. (2014). doi:10.1146/annurev-immunol-032713-120225

330. Calautti, E., Avalle, L. & Poli, V. Psoriasis: A STAT3-Centric View. *Int. J. Mol. Sci.*

19, 171 (2018).

331. Schön, M. P. & Erpenbeck, L. The Interleukin-23/Interleukin-17 Axis Links Adaptive and Innate Immunity in Psoriasis. *Front. Immunol.* **9**, 1323 (2018).

332. Zheng, Y. *et al.* Interleukin-22, a TH17 cytokine, mediates IL-23-induced dermal inflammation and acanthosis. *Nature* **445**, 648–651 (2007).

333. Sano, S. Psoriasis as a barrier disease. *Dermatologica Sin.* **33**, 64–69 (2015).

334. Iizuka, H., Takahashi, H., Honma, M. & Ishida-Yamamoto, A. Unique Keratinization Process in Psoriasis: Late Differentiation Markers Are Abolished Because of the Premature Cell Death. *J. Dermatol.* **31**, 271–276 (2004).

335. Roberson, E. D. O. & Bowcock, A. M. Psoriasis genetics: breaking the barrier Psoriasis: a common inflammatory skin disease with a genetic component. doi:10.1016/j.tig.2010.06.006

336. Bergboer, J. G. M., Zeeuwen, P. L. J. M. & Schalkwijk, J. *Pathogenesis of Atopic Dermatitis and Psoriasis: Focus on the Epidermal Differentiation Complex GENETIC STUDIES ON SKIN DISEASES: INVOLVE-MENT OF THE EPIDERMAL DIFFERENTIATION COMPLEX. The Open Dermatology Journal* **4**, (2010).

337. Bergstresser, P. R. & Taylor, J. R. Epidermal 'turnover time'--a new examination. *Br. J. Dermatol.* **96**, 503–9 (1977).

338. Dika, E., Bardazzi, F., Balestri, R. & Maibach, H. I. Environmental Factors and Psoriasis1. in *Environmental Factors in Skin Diseases* **35**, 118–135 (KARGER, 2007).

339. Barrea, L. *et al.* Environmental Risk Factors in Psoriasis: The Point of View of the Nutritionist. doi:10.3390/ijerph13070743

340. Nestle, F. O., Kaplan, D. H. & Barker, J. Psoriasis. *N. Engl. J. Med.* **361**, 496–509 (2009).

341. Zeng, J., Luo, S., Huang, Y. & Lu, Q. Critical role of environmental factors in the pathogenesis of psoriasis. *J. Dermatol.* **44**, 863–872 (2017).

342. K., K., G., J., A., B., O., E. & Yildirim, A. O. The dynamics of Th17 cells in a CS induced COPD mouse model. (2012).

343. Duan, M.-C., Tang, H.-J., Zhong, X.-N. & Huang, Y. Persistence of Th17/Tc17 Cell Expression upon Smoking Cessation in Mice with CS-Induced Emphysema. *Clin. Dev. Immunol.* **2013**, 1–11 (2013).

344. Zhou, H. *et al.* Tc17 cells are associated with CS-induced lung inflammation and emphysema. *Respirology* **20**, 426–433 (2015).

345. Wang, H. *et al.* Imbalance of Th17/Treg cells in mice with chronic CS exposure. *Int. Immunopharmacol.* **14**, 504–512 (2012).

346. Torii, K. *et al.* Tobacco smoke is related to Th17 generation with clinical implications for psoriasis patients. *Exp. Dermatol.* **20**, 371–373 (2011).

347. Naldi, L. Psoriasis and smoking: links and risks. *Psoriasis (Auckland, N.Z.)* **6**, 65–71 (2016).

348. CAROLINE ROBERT, M.D., AND THOMAS S. KUPPER, M. D. INFLAMMATORY SKIN DISEASES, T CELLS, AND IMMUNE SURVEILLANCE. 1817–1828 (1999).

349. Bergboer, J. G. M., Zeeuwen, P. L. J. M. & Schalkwijk, J. Pathogenesis of Atopic Dermatitis and Psoriasis: Focus on the Epidermal Differentiation Complex. *Open Dermatol. J.* **4**, 48–51 (2010).

350. Howell, M. D. *et al.* Cytokine modulation of atopic dermatitis filaggrin skin expression. *J. Allergy Clin. Immunol.* **124**, R7–R12 (2009).

351. Osawa, R., Akiyama, M. & Shimizu, H. Filaggrin Gene Defects and the Risk of Developing Allergic Disorders. *Allergol. Int.* **60**, 1–9 (2011).

352. Pellerin, L. *et al.* Defects of filaggrin-like proteins in both lesional and nonlesional atopic skin. *J. Allergy Clin. Immunol.* **131**, 1094–1102 (2013).

353. Gao, P.-S. *et al.* Filaggrin mutations that confer risk of atopic dermatitis confer greater risk for eczema herpeticum. *J. Allergy Clin. Immunol.* **124**, 507–13, 513.e1–7 (2009).

354. O'Regan, G. M. *et al.* Raman profiles of the stratum corneum define 3 filaggrin genotype-determined atopic dermatitis endophenotypes. *J. Allergy Clin. Immunol.* **126**, 574–80.e1 (2010).

355. Kezic, S., Kammeyer, A., Calkoen, F., Fluhr, J. W. & Bos, J. D. Natural moisturizing factor components in the stratum corneum as biomarkers of filaggrin genotype: evaluation of minimally invasive methods. *Br. J. Dermatol.* **161**, 1098–1104 (2009).

356. Leung, D. Y. Role of IgE in atopic dermatitis. *Curr. Opin. Immunol.* **5**, 956–62 (1993).

357. Murota, H. & Katayama, I. Exacerbating factors of itch in atopic dermatitis. *Allergol. Int.* **66**, 8–13 (2017).

358. Wilson, S. R. *et al.* The epithelial cell-derived atopic dermatitis cytokine TSLP activates neurons to induce itch. *Cell* **155**, 285–95 (2013).

359. Wahlgren, C. F. Itch and atopic dermatitis: an overview. *J. Dermatol.* **26**, 770–9 (1999).

360. Dainichi, T. *et al.* The epithelial immune microenvironment (EIME) in atopic dermatitis and psoriasis. *Nat. Immunol.* **19**, 1286–1298 (2018).

361. Kaufman, B. P., Guttman-Yassky, E. & Alexis, A. F. Atopic dermatitis in diverse racial and ethnic groups-Variations in epidemiology, genetics, clinical presentation and treatment. *Exp. Dermatol.* **27**, 340–357 (2018).

362. Choy, D. F. *et al.* Comparative transcriptomic analyses of atopic dermatitis and psoriasis reveal shared neutrophilic inflammation. *J. Allergy Clin. Immunol.* **130**, 1335–43.e5 (2012).

363. Shirinde, J., Wichmann, J. & Voyi, K. Environmental tobacco smoke and the risk of eczema symptoms among school children in South Africa: a cross-sectional study. *BMJ Open* **5**, e008234 (2015).

364. Kim, S. Y., Sim, S. & Choi, H. G. Atopic dermatitis is associated with active and passive cigarette smoking in adolescents. *PLoS One* **12**, e0187453 (2017).

365. Kantor, R., Kim, A., Thyssen, J. P. & Silverberg, J. I. Association of atopic dermatitis with smoking: A systematic review and meta-analysis. *J. Am. Acad. Dermatol.* **75**, 1119-1125.e1 (2016).

366. Ka, D. *et al.* Association between passive smoking and atopic dermatitis in dogs. *Food Chem. Toxicol.* **66**, 329–333 (2014).

367. Yi, O. *et al.* Effect of environmental tobacco smoke on atopic dermatitis among children in Korea. *Environ. Res.* **113**, 40–45 (2012).

368. Vitiligo Update - SCMS. Available at: http://scmsjournal.com/article/buy_now/?id=243. (Accessed: 19th March 2019)

369. Jain, A., Mal, J., Mehndiratta, V., Chander, R. & Patra, S. K. Study of oxidative stress in vitiligo. *Indian J. Clin. Biochem.* **26**, 78–81 (2011).

370. Karsli, N., Akcali, C., Ozgoztasi, O., Kirtak, N. & Inaloz, S. Role of oxidative stress in the pathogenesis of vitiligo with special emphasis on the antioxidant action of narrowband ultraviolet B phototherapy. *J. Int. Med. Res.* **42**, 799–805 (2014).

371. Slap, G. B. & Zucker, M. L. Acne. *Adolesc. Med.* 97–103 (2008). doi:10.1016/B978-032304073-0.10015-9

372. Capitanio, B. *et al.* Acne and smoking. *Dermatoendocrinol.* **1**, 129–35 (2009).

373. Silverstein, P. Smoking and wound healing. *Am. J. Med.* **93**, 22–24 (1992).

374. Kishibe, M., Griffin, T. M. & Radek, K. A. Keratinocyte nicotinic acetylcholine receptor activation modulates early TLR2-mediated wound healing responses. *Int. Immunopharmacol.* **29**, 63–70 (2015).

375. Morimoto, N., Takemoto, S., Kawazoe, T. & Suzuki, S. Nicotine at a Low Concentration Promotes Wound Healing. *J. Surg. Res.* **145**, 199–204 (2008).

376. Jacobi, J. *et al.* Nicotine accelerates angiogenesis and wound healing in genetically diabetic mice. *Am. J. Pathol.* **161**, 97–104 (2002).

377. Sørensen, L. T. *et al.* Acute Effects of Nicotine and Smoking on Blood Flow, Tissue Oxygen, and Aerobe Metabolism of the Skin and Subcutis. *J. Surg. Res.* **152**, 224–230 (2009).

378. Sakamoto, K., Lochhead, R. Y., Maibach, H. I. & Yamashita, Y. *Cosmetic science and technology : theoretical principles and applications*.

379. Okada, H. C., Alleyne, B., Varghai, K., Kinder, K. & Guyuron, B. Facial Changes Caused by Smoking. *Plast. Reconstr. Surg.* **132**, 1085–1092 (2013).

380. Srinivasan, B. *et al.* TEER Measurement Techniques for *In vitro* Barrier Model Systems. *J. Lab. Autom.* **20**, 107–126 (2015).

381. Characterisation, B., The, O. F. & Skin, R. Basic Characterisation of the Reconstructed Skin Models. 76–89

382. Blume, L.-F., Denker, M., Gieseler, F. & Kunze, T. Temperature corrected transepithelial electrical resistance (TEER) measurement to quantify rapid changes in paracellular permeability. *Pharmazie* **65**, 19–24 (2010).

383. Ponec, M., Boelsma, E., Gibbs, S. & Mommaas, M. Characterization of Reconstructed Skin Models. *Skin Pharmacol. Physiol.* **15**, 4–17 (2002).

384. Monteiro-Riviere, N. A., Inman, A. O., Snider, T. H., Blank, J. A. & Hobson, D. W. Comparison of an *in vitro* skin model to normal human skin for dermatological research. *Microsc. Res. Tech.* **37**, 172–179 (1997).

385. Tfayli, A., Piot, O., Draux, F., Pitre, F. & Manfait, M. Molecular characterization of reconstructed skin model by Raman microspectroscopy: Comparison with excised human skin. *Biopolymers* **87**, 261–274 (2007).

386. Sylvestre, J.-P., Bouissou, C. C., Guy, R. H. & Delgado-Charro, M. B. Extraction and quantification of amino acids in human stratum corneum *in vivo*. *Br. J. Dermatol.* **163**, 458–465 (2010).

387. Carvalho, B. G., Raniero, L. J., Martin, A. A. & Favero, P. P. Phenylalanine ab initio models for the simulation of skin natural moisturizing factor. *Spectrochim. Acta Part A Mol. Biomol. Spectrosc.* **106**, 73–79 (2013).

388. AARON BUNSEN LERNER AND THOMAS B. FITZPATRICK. Biochemistry of melanin formation. *Physiol. Rev.* **30**, (1950).

389. Zane Arp, §, Daniel Autrey, §, Jaan Laane, §, Stacy A. Overman, ‖ and & George J. Thomas, J. *,. Tyrosine Raman Signatures of the Filamentous Virus Ff Are Diagnostic of Non-Hydrogen-Bonded Phenoxyls: Demonstration by Raman and Infrared Spectroscopy of p-Cresol Vapor†,‡. (2001). doi:10.1021/BI0023753

390. Siamwiza, M. N. *et al.* Interpretation of the doublet at 850 and 830 cm $^{-1}$ in the Raman spectra of tyrosyl residues in proteins and certain model compounds. *Biochemistry* **14**, 4870–4876 (1975).

391. Schneider, F. W. Frank S. Parker: *Applications of Infrared, Raman, and Resonance Raman Spectroscopy in Biochemistry* , Plenum Press, New York and London 1983. 550 Seiten, Preis: $ 78,-. *Berichte der Bunsengesellschaft für Phys. Chemie* **88**, 1167B – 1168 (1984).

392. Yu, J. *et al.* A tryptophan metabolite of the skin microbiota attenuates inflammation in patients with atopic dermatitis through the aryl hydrocarbon receptor. *J. Allergy Clin. Immunol.* **143**, 2108-2119.e12 (2019).

393. Binazzi, M. & Calandra, P. Tryptophan metabolism in skin diseases. *Acta Vitaminol. Enzymol.* **29**, 161–3 (1975).

394. Clemente Plaza, N., Reig García-Galbis, M. & Martínez-Espinosa, R. M. Effects of the Usage of l-Cysteine (l-Cys) on Human Health. *Molecules* **23**, (2018).

395. Smit, N. P. M. *et al.* Melanogenesis in Cultured Melanocytes can be Substantially Influenced by L-Tyrosine and L-Cysteine. *J. Invest. Dermatol.* **109**, 796–800 (1997).

396. Baumruk, V. *Spectral Techniques for Rapid Quantification of Protein Structure in Solution*.

397. Williams, R. W. [14] Protein secondary structure analysis using Raman amide I and amide III spectra. *Methods Enzymol.* **130**, 311–331 (1986).

398. Wertz, P. Epidermal lipids. *Semin. Dermatol.* **11**, 106–113 (1992).

399. Gniadecka, M., Faurskov Nielsen, O., Christensen, D. H. & Wulf, H. C. *Structure of Water, Proteins, and Lipids in Intact Human Skin, Hair, and Nail*. *Journal of Investigative Dermatology* **110**, (1998).

400. Downing, D. T. Lipid and protein structures in the permeability barrier of mammalian epidermis. *J. Lipid Res.* **33**, 301–13 (1992).

401. Mao-Qiang, M., Feingold, K. R., Jain, M. & Elias, P. M. Extracellular processing of phospholipids is required for permeability barrier homeostasis. *J. Lipid Res.* **36**, 1925–35 (1995).

402. Stone, N., Kendall, C., Smith, J., Crow, P. & Barr, H. Raman spectroscopy for identification of epithelial cancers. *Faraday Discuss.* **126**, 141 (2004).

403. Tfayli, A., Piot, O., Draux, F., Pitre, F. & Manfait, M. Molecular characterization of reconstructed skin model by Raman microspectroscopy: Comparison with excised human skin. *Biopolymers* **87**, 261–274 (2007).

404. K.Czamara, K.Majzner, M.Z. Pacia, K.Kochan, A. K. and M. B. Raman spectroscopy of lipids: a review. *J. Raman Spectrosc.* (2014).

405. Ali, S. M. *et al.* Raman spectroscopic mapping for the analysis of solar radiation induced skin damage. *Analyst* **138**, 3946 (2013).

406. Anigbogu, A. N. C., Williams, A. C., Barry, B. W. & Edwards, H. G. M. Fourier transform raman spectroscopy of interactions between the penetration enhancer dimethyl sulfoxide and human stratum corneum. *Int. J. Pharm.* **125**, 265–282 (1995).

407. Barry, B. W., Edwards, H. G. M. & Williams, A. C. Fourier transform Raman and infrared vibrational study of human skin: Assignment of spectral bands. *J. Raman Spectrosc.* **23**, 641–645 (1992).

408. Chrit, L. *et al. In vivo* chemical investigation of human skin using a confocal Raman fiber optic microprobe. *J. Biomed. Opt.* **10**, 044007 (2005).

409. Tfaili, S. *et al.* Confocal Raman microspectroscopy for skin characterization: a comparative study between human skin and pig skin. *Analyst* **137**, 3673 (2012).

410. Huang, Z. *et al.* <title>Evaluation of variations of biomolecular constituents in human skin *in vivo* by near-infrared Raman spectroscopy</title> in (eds. Chiou, A. E. T., Podbielska, H. & Jacques, S. L.) 109–114 (2001). doi:10.1117/12.446645

411. Zhao, J., Lui, H., I., D. & Zeng, H. Real-Time Raman Spectroscopy for Noninvasive *in vivo* Skin Analysis and Diagnosis. in *New Developments in Biomedical Engineering* (InTech, 2010). doi:10.5772/7603

412. Flach, C. R. & Moore, D. J. Infrared and Raman imaging spectroscopy of *ex vivo* skin. *Int. J. Cosmet. Sci.* **35**, 125–135 (2013).

413. Yu, G., Zhang, G., Flach, C. R. & Mendelsohn, R. Vibrational spectroscopy and microscopic imaging: novel approaches for comparing barrier physical properties in native and human skin equivalents. *J. Biomed. Opt.* **18**, 061207 (2012).

414. Lo, W.-L. *et al.* Raman spectroscopy monitoring of the cellular activities of a tissue-

engineered *ex vivo* produced oral mucosal equivalent. *J. Raman Spectrosc.* **42**, 174–178 (2011).

415. Caspers, P. J., Lucassen, G. W., Wolthuis, R., Bruining, H. A. & Puppels, G. J. *In vitro* and *in vivo* Raman spectroscopy of human skin. *Biospectroscopy* **4**, S31-9 (1998).

416. Ali, S. M. *et al.* Raman spectroscopic analysis of human skin tissue sections *ex-vivo* : evaluation of the effects of tissue processing and dewaxing. *J. Biomed. Opt.* **18**, 061202 (2012).

417. Tfayli, A., Guillard, E., Manfait, M. & Baillet-Guffroy, A. Thermal dependence of Raman descriptors of ceramides. Part I: effect of double bonds in hydrocarbon chains. *Anal. Bioanal. Chem.* **397**, 1281–1296 (2010).

418. Krimm, S. & Bandekar, J. Vibrational Spectroscopy and Conformation of Peptides, Polypeptides, and Proteins. *Adv. Protein Chem.* **38**, 181–364 (1986).

419. Mahadevan-Jansen, A. & Richards-Kortum, R. R. Raman spectroscopy for the detection of cancers and precancers. *J. Biomed. Opt.* **1**, 31 (1996).

420. Nguyen, T. T. *et al.* Characterization of Type I and IV Collagens by Raman Microspectroscopy: Identification of Spectral Markers of the Dermo-Epidermal Junction. *Spectrosc. An Int. J.* **27**, 421–427 (2012).

421. Kemény, L., Rózicka, T., Dobozy, A. & Michel, G. Role of lnterleukin-8 receptor in skin. *Int. Arch. Allergy Immunol.* **104**, 317–322 (1994).

422. Zhou, G. *et al.* Chemical constituents of tobacco smoke induce the production of interleukin-8 in human bronchial epithelium, 16HBE cells. *Tob. Induc. Dis.* **14**, (2016).

423. Mortaz, E. *et al.* CS attenuates the production of cytokines by human plasmacytoid dendritic cells and enhances the release of IL-8 in response to TLR-9 stimulation. *Respir. Res.* **10**, 47 (2009).

424. Xu, L. *et al.* CS triggers inflammation mediated by autophagy in BEAS-2B cells. *Ecotoxicol. Environ. Saf.* **184**, (2019).

425. Czekala, L. *et al.* Toxicological comparison of CS and e-cigarette aerosol using a 3D *in vitro* human respiratory model. *Regul. Toxicol. Pharmacol.* **103**, 314–324 (2019).

426. Rikken, G., Niehues, H. & van den Bogaard, E. H. Organotypic 3D Skin Models: Human Epidermal Equivalent Cultures from Primary Keratinocytes and Immortalized Keratinocyte Cell Lines. in *Methods in Molecular Biology* **2154**, 45–61 (Humana Press Inc., 2020).

427. Armstrong, H., Bording-Jorgensen, M., Chan, R. & Wine, E. Nigericin Promotes NLRP3-Independent Bacterial Killing in Macrophages. *Front. Immunol.* **10**, 2296 (2019).

428. Zhang, L. Keratins in Skin Epidermal Development and Diseases. in *Keratin* (IntechOpen, 2018). doi:10.5772/intechopen.79050

429. Nithya, S., Radhika, T. & Jeddy, N. Loricrin - an overview. *J. Oral Maxillofac. Pathol.* **19**, 64–8 (2015).

430. Candi, E., Schmidt, R. & Melino, G. The cornified envelope: a model of cell death in

the skin. *Nat. Rev. Mol. Cell Biol.* **6**, 328–340 (2005).

431. Poumay, Y. Atopic Dermatitis Studies through *In vitro* Models. **4**, (2017).

432. Desmet, E., Ramadhas, A., Lambert, J. & Van Gele, M. *In vitro* psoriasis models with focus on reconstructed skin models as promising tools in psoriasis research. *Exp. Biol. Med.* **242**, 1158–1169 (2017).

433. Poli, G., Biasi, F. & Leonarduzzi, G. 4-Hydroxynonenal-protein adducts: A reliable biomarker of lipid oxidation in liver diseases. *Molecular Aspects of Medicine* **29**, 67–71 (2008).

434. Poli, G., Schaur, R. J., Siems, W. G. & Leonarduzzi, G. 4-Hydroxynonenal: A membrane lipid oxidation product of medicinal interest. *Medicinal Research Reviews* **28**, 569–631 (2008).

435. Sguizzato, M. *et al.* Ethosomes for coenzyme Q10 cutaneous administration: From design to 3D skin tissue evaluation. *Antioxidants* **9**, (2020).

436. Frankart, A. *et al.* Epidermal morphogenesis during progressive *in vitro* 3D reconstruction at the air-liquid interface. *Exp. Dermatol.* **21**, 871–875 (2012).

437. Barel, André, PAye, Marc, Maibach, H. *Cosmetic Science and Technology*. (1970). doi:10.1016/B978-1-85617-943-0.10041-3

438. Dinkova-Kostova, A. T. *et al.* Direct evidence that sulfhydryl groups of Keap1 are the sensors regulating induction of phase 2 enzymes that protect against carcinogens and oxidants. *Proc. Natl. Acad. Sci. U. S. A.* **99**, 11908–11913 (2002).

439. Dubinina, E. E. & Dadali, V. A. Role of 4-hydroxy-trans-2-nonenal in cell functions. *Biochemistry (Moscow)* **75**, 1069–1087 (2010).

440. Pecorelli, A., Woodby, B., Prieux, R. & Valacchi, G. Involvement of 4-hydroxy-2-nonenal in pollution-induced skin damage. *BioFactors* **45**, 536–547 (2019).

441. POOT, M., VERKERK, A., KOSTER, J. F., ESTERBAUER, H. & JONGKIND, J. F. Influence of cumene hydroperoxide and 4-hydroxynonenal on the glutathione metabolism during *in vitro* ageing of human skin fibroblasts. *Eur. J. Biochem.* **162**, 287–291 (1987).

442. Jørgensen, P., Milkovic, L., Zarkovic, N., Waeg, G. & Rattan, S. I. S. Lipid peroxidation-derived 4-hydroxynonenal-modified proteins accumulate in human facial skin fibroblasts during ageing *in vitro*. *Biogerontology* **15**, 105–110 (2014).

443. Ogura, Y. *et al.* Dermal carbonyl modification is related to the yellowish color change of photo-aged Japanese facial skin. *J. Dermatol. Sci.* **64**, 45–52 (2011).

444. Helou, D. G., Martin, S. F., Pallardy, M., Chollet-Martin, S. & Kerdine-Römer, S. Nrf2 involvement in chemical-induced skin innate immunity. *Frontiers in Immunology* **10**, 1004 (2019).

445. Hennig, P. *et al.* The crosstalk between Nrf2 and inflammasomes. *Int. J. Mol. Sci.* **19**, (2018).

446. Kezic, S. & Jakasa, I. Filaggrin and Skin Barrier Function. in *Current problems in dermatology* **49**, 1–7 (2016).

447. Roth, W. *et al.* Keratin 1 maintains skin integrity and participates in an inflammatory network in skin through interleukin-18. *J. Cell Sci.* **125**, 5269–5279 (2012).

448. RAMAN, C. V. & KRISHNAN, K. S. A New Type of Secondary Radiation. *Nature* **121**, 501–502 (1928).

449. Darvin, M. E. *et al. In vivo* distribution of carotenoids in different anatomical locations of human skin: comparative assessment with two different Raman spectroscopy methods. *Exp. Dermatol.* **18**, 1060–1063 (2009).

450. Richters, R. J. H. *et al.* Sensitive Skin: Assessment of the Skin Barrier Using Confocal Raman Microspectroscopy. *Skin Pharmacol. Physiol.* **30**, 1–12 (2017).

451. Bunaciu, A. A., Aboul-Enein, H. Y. & Hoang, V. D. Raman Spectroscopy for Protein Analysis. *Appl. Spectrosc. Rev.* **50**, 377–386 (2015).

452. Tfayli, A. *et al.* Comparison of structure and organization of cutaneous lipids in a reconstructed skin model and human skin: spectroscopic imaging and chromatographic profiling. *Exp. Dermatol.* **23**, 441–443 (2014).

453. Choe, C., Lademann, J. & Darvin, M. E. Lipid organization and stratum corneum thickness determined *in vivo* in human skin analyzing lipid-keratin peak (2820-3030 cm $^{-1}$) using confocal Raman microscopy. *J. Raman Spectrosc.* **47**, 1327–1331 (2016).

454. Jung, N., Vukosavljevic, B. & Windbergs, M. Raman Spectroscopy in Skin Research and Dermal Drug Delivery. in 421–448 (2018). doi:10.1007/978-3-319-75380-5_17

455. Rangel, A. P. *et al.* Confocal Raman spectroscopy: determination of natural moisturizing factor profile related to skin hydration. *Rev. Bras. Eng. Biomédica* **30**, 11–16 (2014).

456. Tippavajhala, V. K. *et al. In vivo* Determination of Moisturizers Efficacy on Human Skin Hydration by Confocal Raman Spectroscopy. *AAPS PharmSciTech* **19**, 3177–3186 (2018).

457. Franzen, L. & Windbergs, M. Applications of Raman spectroscopy in skin research — From skin physiology and diagnosis up to risk assessment and dermal drug delivery. *Adv. Drug Deliv. Rev.* **89**, 91–104 (2015).